DEPARTMENT OF THE INTERIOR

U.S. Geological Survey

Summary of Geotechnical and Hydrologic Data Collected From May 1, 1990 Through April 30, 1991, for the Alani-Paty Landslide, Manoa Valley, Honolulu, Hawaii

by

Rex L. Baum[1], Mark E. Reid[2], Cynthia A. Wilburn[2], and Jill D. Torikai[2]

Open-File Report 91-598

Prepared in Cooperation with
the City and County of Honolulu,
Department of Public Works

[1]Denver, CO [2]Honolulu, HI

1991

INTRODUCTION

Following mapping of slow-moving landslides on the east side of Manoa Valley (Baum and others, 1989) we began a detailed investigation of the Alani-Paty landslide (fig. 1) in order to understand the physical processes active in it and similar landslides on Oahu. In order to make basic data available to all interested parties, we have compiled the observations and measurements collected during the period from May 1, 1990 to April 30, 1991. Data collected from September 1989 through April 1990 were published previously (Baum and others, 1990). The following summary highlights our observations of the physical properties of the landslide material, behavior of the Alani-Paty landslide, and the behavior of subsurface water. Five appendices containing laboratory test results, subsurface water conditions, daily precipitation, displacement, and results of field permeability tests follow the summary. Each appendix includes a description of the methods used to obtain the data.

SUMMARY OF MEASUREMENTS AND OBSERVATIONS

Laboratory testing -- The landslide material, as observed in samples taken from borings, consists of boulder-, cobble- and gravel-sized clasts of weathered basalt in a fine-grained matrix. The matrix is brown to gray, sandy to slightly sandy, highly plastic, clayey silt interlayered with dark brown to gray, highly plastic silty clay (Baum and others, 1990).

Laboratory testing of remolded specimens of clayey silt and silty clay, chosen to represent the range of materials sampled, indicates that the matrix material has high plasticity and low to moderate residual shear strength (Appendix A, also Baum and others, 1990). Plastic limits range from 29 to 61, and Liquid limits range from 59 to 137. The matrix contains roughly 50-80 percent clay, 10-30 percent silt, and 5-25 percent sand. Specimens that are clay rich and have high Liquid limits (from about 95 to 137) have low strengths characterized by friction angles from 6 to 11°, with cohesion intercepts from 0 to 220 lbf/ft^2. Specimens having relatively low Liquid limits (from about 59 to 75) generally have higher residual strengths, characterized by friction angles ranging from 20 to 25° and cohesion intercepts ranging from 150 to 230 lbf/ft^2.

Instrumentation -- Instrumentation was installed at the surface of the landslide and in borings in order to measure rainfall, displacement, depth of the landslide, and ground-water levels and pressures. Surface instrumentation (figs. 2 and 3) consisted of rain gauges and extensometers (for measuring displacement). Bore-hole instrumentation consisted of cables anchored below the failure surface for measuring displacement, open-tube piezometers for measuring water levels, and pore-pressure transducers for monitoring subsurface water pressure. A few borings were cased for inclinometer measurements. The pore-pressure transducers, several piezometers, one inclinometer and an anchored cable were added to the previous instrumentation between June 1990 and September 1990. The instrumentation has been described by Baum and others (1990) and in appendices B, C, and D of this report. The piezometer, pore-pressure transducer, and inclinometer measurements are compiled in Appendix B. Rainfall observations are compiled in Appendix C. Measurements of

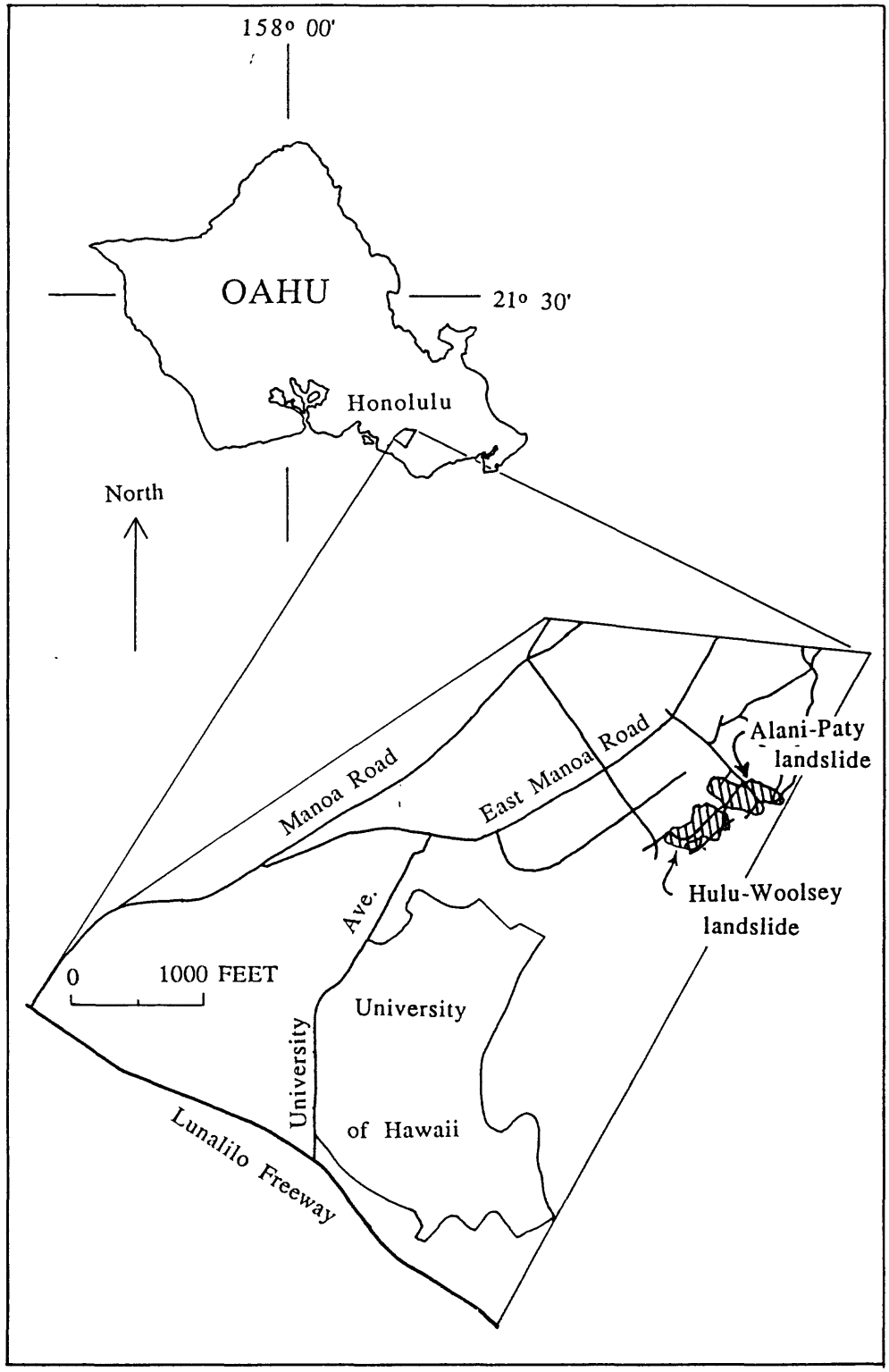

Figure 1. Map showing location of landslides in the Woodlawn area, Manoa Valley, Honolulu, Hawaii.

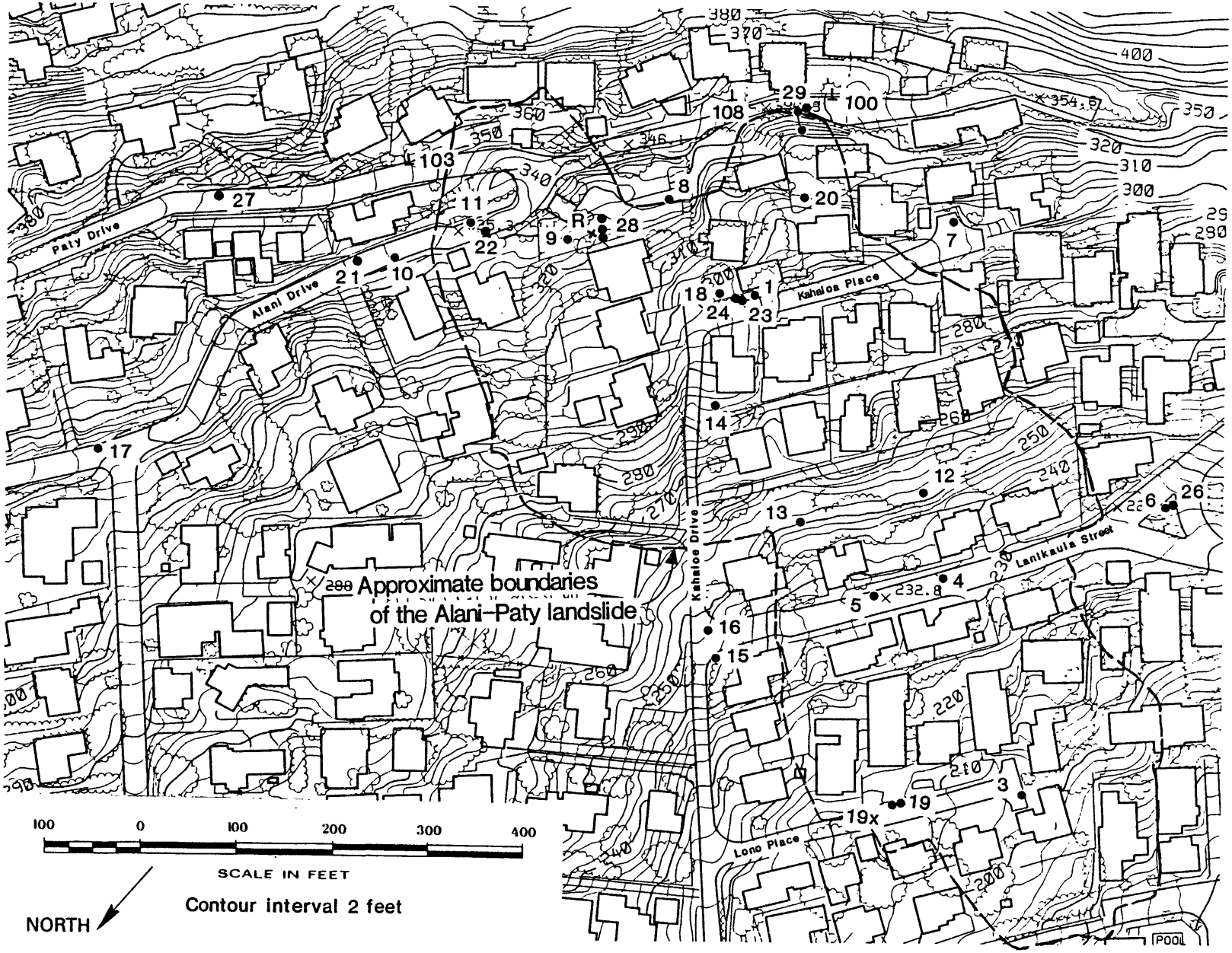

Figure 2. Map showing locations of borings, rain gauge and extensometer on the Alani-Paty landslide. Base from *Topographic Map of Portion of Manoa Valley, Honolulu, Oahu, Hawaii*, by R.M. Towill Corporation for STV/Lyon Associates, Inc. under contract with the City and County of Honolulu, Department of Public Works, 1989.

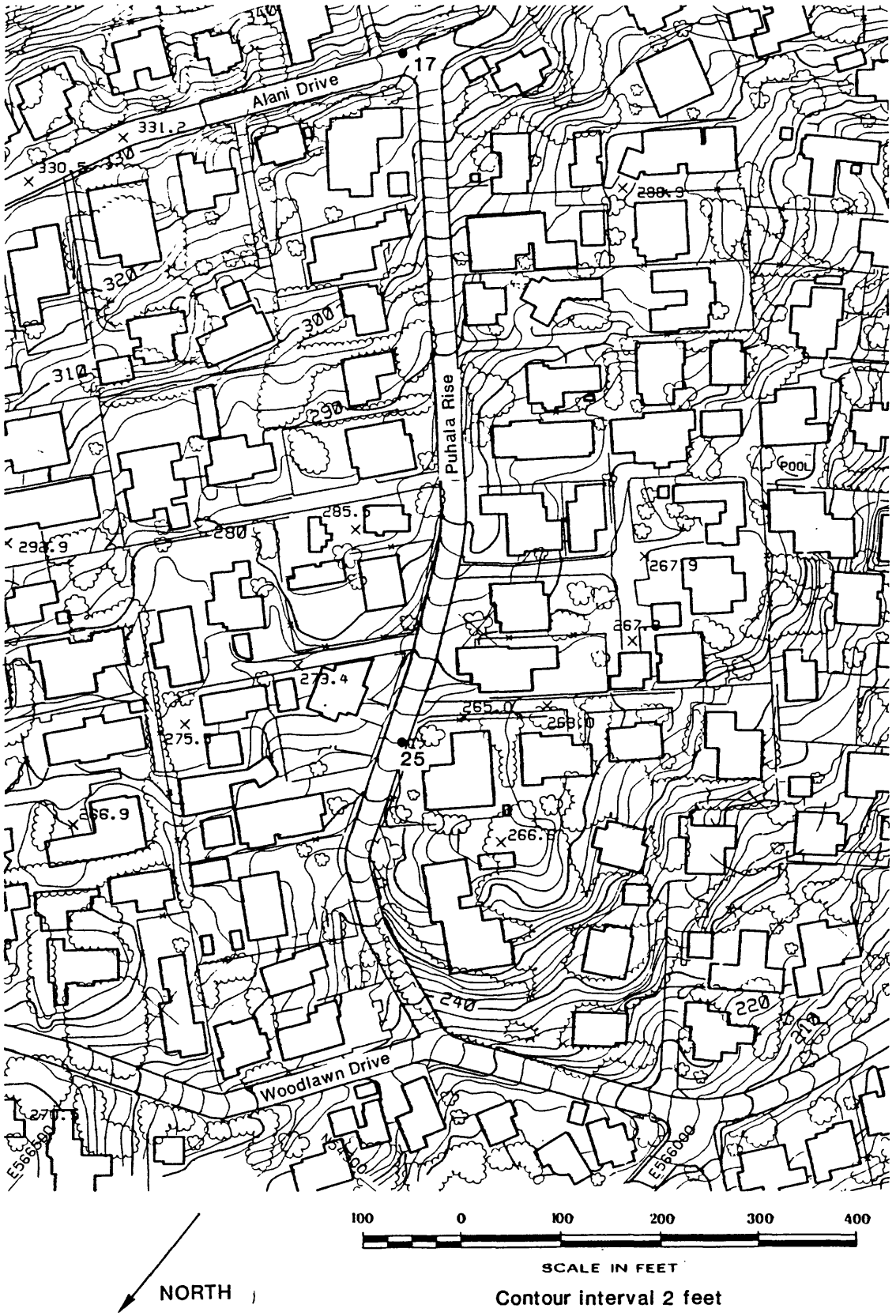

Figure 3. Map showing locations of borings 17 and 25 (solid circles), north of the Alani-Paty landslide. Base from *Topographic Map of Portion of Manoa Valley, Honolulu, Oahu, Hawaii*, by R.M. Towill Corporation for STV/Lyon Associates, Inc. under contract with the City and County of Honolulu, Department of Public Works, 1989.

displacement are compiled in Appendix D. Field permeability tests are described in Appendix E. All are summarized below.

Ground-water conditions -- Several trends are present in the ground-water observations (Appendix B). Water levels in several piezometers and pressure at several pore-pressure transducers (in borings 1, 8, 9, 20, 22, 24, 100, and 103) upslope from Kahaloa Place increased within a few days following rainy periods and then gradually returned to pre-storm levels (figs. 2 and 4, and Appendix B). Water levels in borings 1 and 100 increase much more than water levels in other borings Pressure transducers in borings 22 and 24 indicate that the pressures peak within a short period, ranging from a few hours to approximately two days, following a storm (appendix B). Increases in water levels/pressure heads ranged from 1 to 10 ft. Water levels in most piezometers downslope from Kahaloa Place changed insignificantly during and after storms. Water levels in piezometers at shallow and intermediate depths downslope from Kahaloa Place (borings 3, 4, 5, 14, 16, 19, and 19x) have generally been steady since shortly after installation. Deep piezometers in borings 3 and 9 and the intermediate piezometer in boring 16 showed steadily declining or steadily increasing water levels, indicating that water levels in these piezometers required several months following their installation to reach equilibrium with their surroundings. Deep (30-40 ft) piezometers in borings 4, 5, 8, 13, 14, 16, 20, and 21 are usually dry (appendix B). Deep piezometers in borings 12 and 19 were initially dry, but became flooded when water at the ground surface flowed into the piezometer tubes.

Rainfall -- Rainfall for the period from May 1, 1990, to April 30, 1991, totaled 91.52 in. at the head of the landslide (Appendix C). Most of this fell during November and December 1990, and March 1991. Comparison of rainfall for a one-year period on Waahila ridge with rainfall for the same period at the head of the Alani-Paty landslide (3102 Alani Dr.) indicates that rainfall is greater at the head of the landslide than on the ridge. Rainfall at the ridge crest immediately upslope from the Alani-Paty landslide is about 90 percent of rainfall at the head, and rainfall on the ridge crest upslope from the Hulu-Woolsey landslide is about 75 percent of rainfall at the head of the Alani-Paty landslide (Appendix C).

Movement of the landslide -- Surface displacement recorded at the headscarp (fig. 2) from May 1990 through April 1991 totaled approximately 0.15 ft (Appendix D). About half of this was due to gradual movements (approximately 0.02 ft/month) of uncertain origin between mid April and mid July 1990 (possibly related to construction near the extensometer during the summer of 1990). About 0.05 ft of displacement occurred during a rainy period in November 1990. Increments of displacement of about 0.01 ft each also may have occurred during rainy periods in December 1990 and March 1991 (Appendix D). Total verifiable displacement at the head of the landslide for the entire period of monitoring (from September 1989 to April 1991) is approximately 0.35 ft. Displacement of the main body of the landslide since installation of the anchored cables has been insufficient (less than the diameter of a boring) to pull the cables down the hole a measurable amount. Measurements of lateral offset of curbs and walls at the boundaries of the landslide show insignificant changes since April 1990 (Appendix D).

Figure 4. Graph showing response of selected piezometers to rainfall.

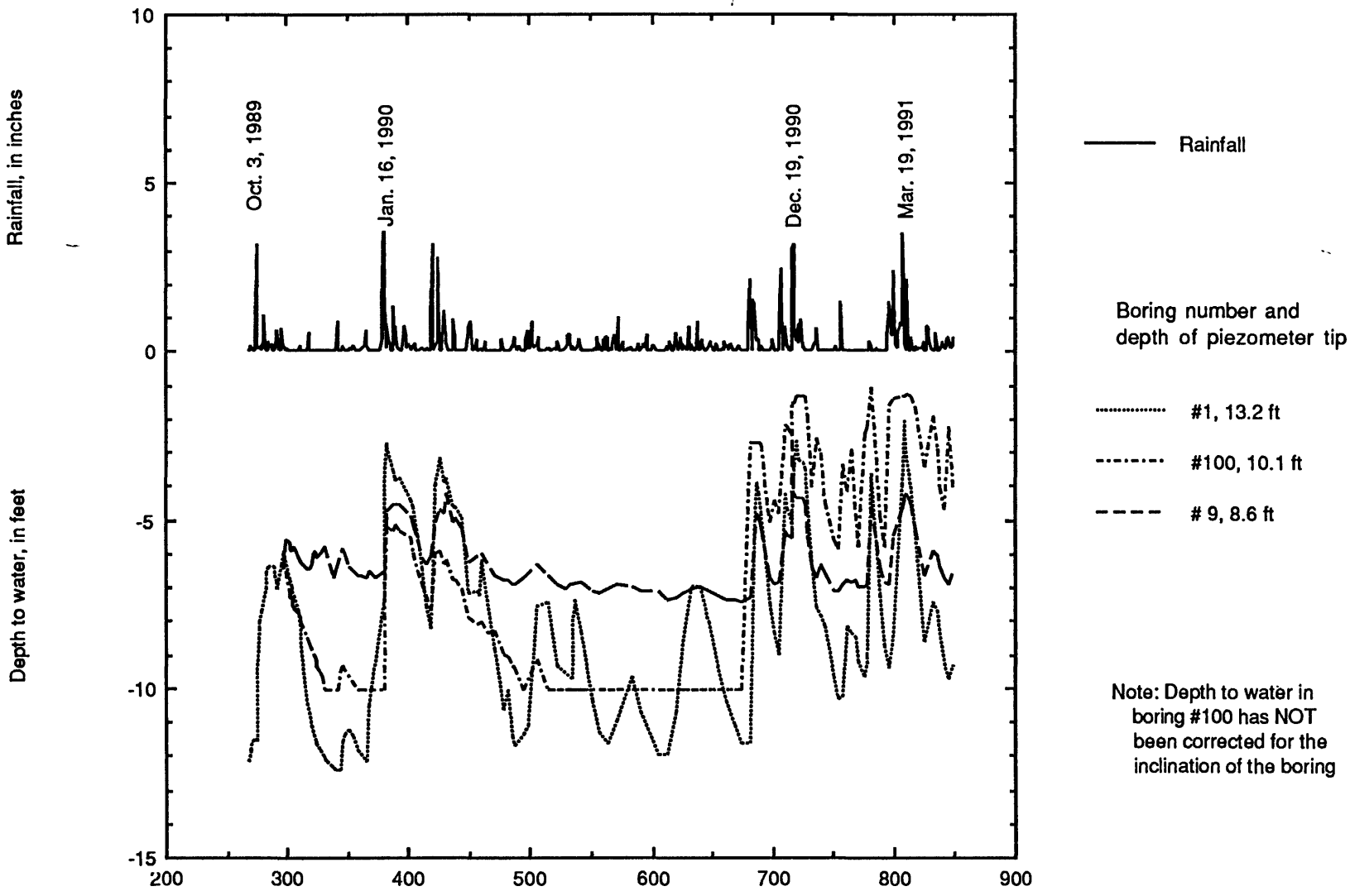

Field permeability tests -- We performed "slug" tests (Bouwer and Rice, 1976; Freeze and Cherry, 1979; and Bouwer, 1989) in several piezometers to determine the hydraulic conductivity of various saturated materials in the landslide. The tests are described and the data are compiled in Appendix E. The tests indicate that the hydraulic conductivity varies widely throughout the landslide. The conductivity ranges from 7.1×10^{-2} ft/day at a shallow piezometer near mid length of the landslide to 1.1×10^{-5} ft/day at a deep piezometer in the toe. With only one exception (the piezometer at 25.5 ft in boring 1), the hydraulic conductivities measured in piezometers from 20 to 30 ft below the ground surface (near the basal failure surface of the landslide) are less than the conductivities measured in shallow piezometers, from 0 to 20 ft below the ground surface.

Displacement in areas outside the mapped boundaries of the landslide -- Inclinometer measurements were made in three locations (borings 10, 15, and 25, see figs. 2, 3, and Appendix B) where incipient movement was suspected (Baum and others, 1989; Robert Fleming, pers. comm., 1990) and in one place (boring 6) that appears to be stable ground between the Hulu-Woolsey and Alani-Paty landslides. The inclinometer measurements in boring 15 indicate sliding occurred at a depth of 26 ft during January 1990. Measurements since then mainly show random deflections of the casing, but may also indicate less than 0.03 ft of downslope movement on the 26-ft-deep slip surface. Thus far, borings 6 and 10 have shown only small random deflections but no unequivocal evidence of sliding. Negligible deflection has been observed in boring 25 on Puhala Rise.

ACKNOWLEDGEMENTS

We thank Sam Callejo and his staff of the Department of Public Works, City and County of Honolulu, for coordinating access to sites for drilling and instrumentation. We also thank residents and owners of property in the landslide area for their cooperation in providing access to sites for drilling and instrumentation of the landslide. Sue Cannon performed particle-size analyses, Coyn Criley determined Atterberg Limits, and William McArthur performed the direct-shear tests reported in Appendix A. The University of Hawaii provided rainfall measurements for the month of February 1991.

REFERENCES

ASTM, 1990, Annual Book of ASTM Standards: Philadelphia, American Society for Testing and Materials, v. 4.08, 1089 p.

Baum, R.L., Fleming, R.W., and Ellen, S.D., 1989, Maps showing landslide features and related ground deformation in the Woodlawn area of the Manoa Valley, City and County of Honolulu, Hawaii: U.S. Geological Survey Open-File Report 89-290, 16 p. + 2 oversize plates.

Baum, R.L., Spengler, S.R., Torikai, J.D., and Liu, L.A.S.M., 1990, Summary of Geotechnical and Hydrologic Data Collected Through April 30, 1990, for the Alani-Paty Landslide, Manoa Valley, Honolulu, Hawaii: U.S. Geological Survey Open-File Report 90-531, 67 p.

Bouwer, H., 1989, The Bouwer and Rice slug test--An update: Groundwater, v. 27, no. 3, p. 304-309.

Bouwer, H. and Rice, R.C., 1976, A slug test for determining hydraulic conductivity of unconfined aquifers with completely or partially penetrating wells: Water Resources Research, v. 12, p. 423-428.

Freeze, R.A. and Cherry, J.A., 1979, Groundwater: Englewood Cliffs, New Jersey, Prentice-Hall, 604 p.

APPENDIX A

Laboratory test results

This appendix contains physical properties determined for samples tested at USGS laboratories in Denver, Colorado, Menlo Park, California, and Palo Alto, California (table A1). A soil plasticity chart summarizes the Atterberg limits (fig. A1), and graphs show results of direct-shear tests on some remolded samples (figs. A2 and A3). Particle-size distributions were determined by standard methods of sieving and hydrometer analysis (D 422-63, ASTM, 1990). Atterberg limits were determined by standard methods on materials that were air-dried prior to testing (D 4318-84, ASTM, 1990). The plasticity chart (figure A1) includes data from previous tests (Baum and others, 1990).

Residual strength tests were performed in a direct-shear device using remolded samples having pre-cut shear surfaces. Each sample was tested at normal loads of 720, 1440, and 3600 lbf/ft^2. Before testing, the samples were sieved to remove particles coarser than medium sand. Sufficient moisture was added to the material to bring it to the plastic limit, and it was compacted into a 2.5-in.-diameter frame. Each sample was consolidated at twice the normal load used to measure the shear strength. After consolidation was complete, the shear plane was cut with a wire while the sample was under the normal load. Each sample was sheared in forward and reverse cycles to a total displacement of 2.4 in. in order to develop the shear surface and reduce the strength to its residual value. Each sample was then sheared at a rate of 0.00094 in./min for a distance of 0.35 in. to determine the residual strength. The rate of shear was increased by a factor of three and then reduced by a factor of 10 to check for the development of pore pressures during the test.

Table A1. Soil Sample Test Results

Boring Number	Sample[2] Number	Depth[3] range (feet)	Particle Size Distribution[1] A.S.T.M. Classification: Gravel >4.76 (mm)	Sand <4.76->0.075 (mm)	Silt <0.075->0.005 (mm)	Clay <0.005 (mm)	Atterberg Limits[1] LL	PL	PI
1	TT-13	24.0-26.25					94	40	54
3	TT-32	26.5-28.6					107	44	63
4	TT-48C	39.0-41.0					76	61	15
6	TT-77	31.5-33.5	0	5	12	83			
11	RS-136	9.0-10.5	28	9	17	46	76	34	42
12	RS-153	10.5-12.0	1	5	15	79	116	42	74
13	RS-168	19.0-21.0	25	6	13	56			

[1]Percentage of dry sample weight

[2]"TT" prefix denotes samples taken by means of a triple-tube core barrel and diamond drill; RS prefix denotes 2.5-in. diameter ring samples

[3]Indicates approximate top and bottom of part of sample tested, including range of uncertainty imposed by incomplete sample recovery

Figure A1. Plasticity chart for samples from the Alani-Paty landslide

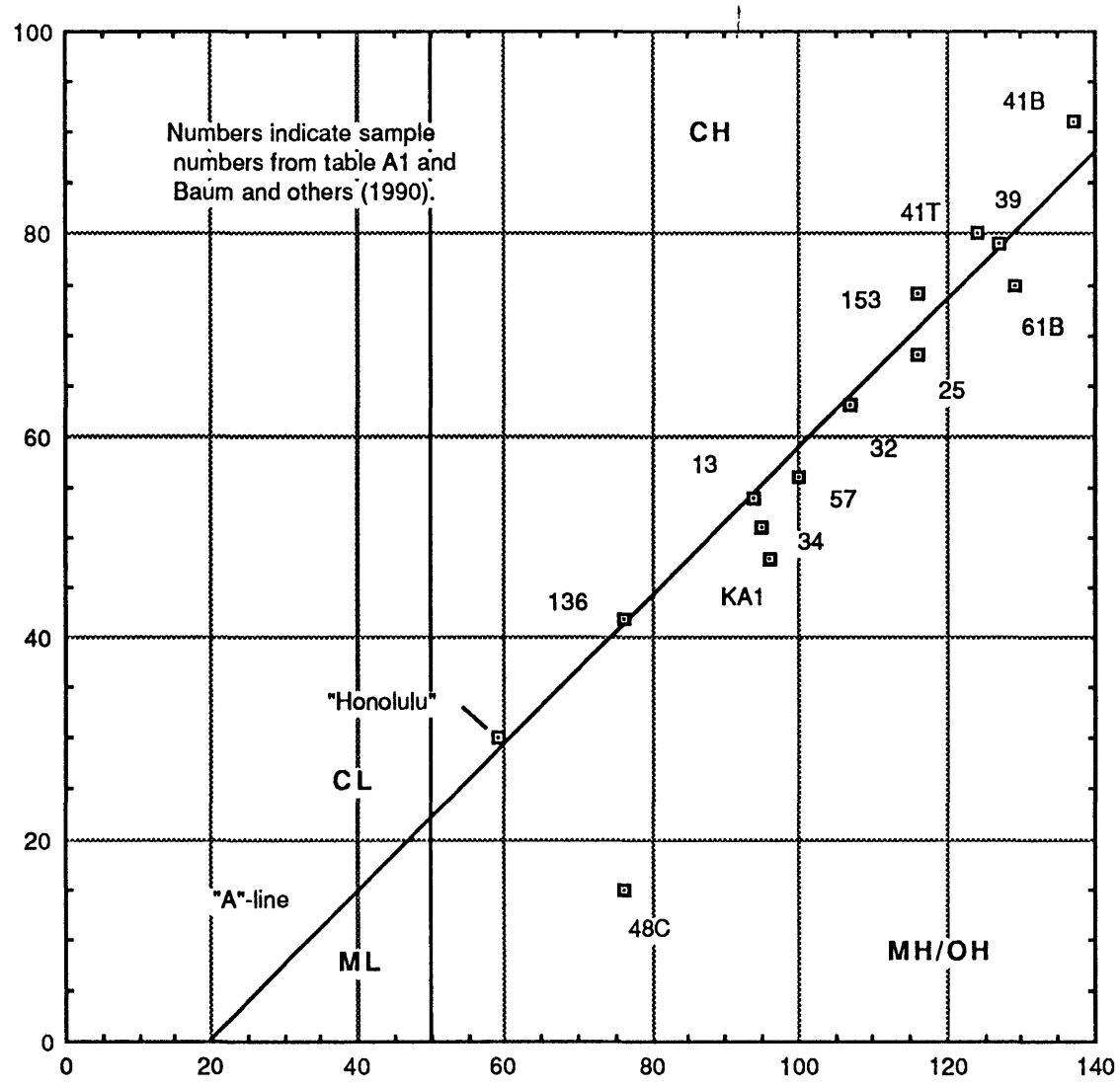

Figure A2. Graph showing residual shear strength of sample TT-32

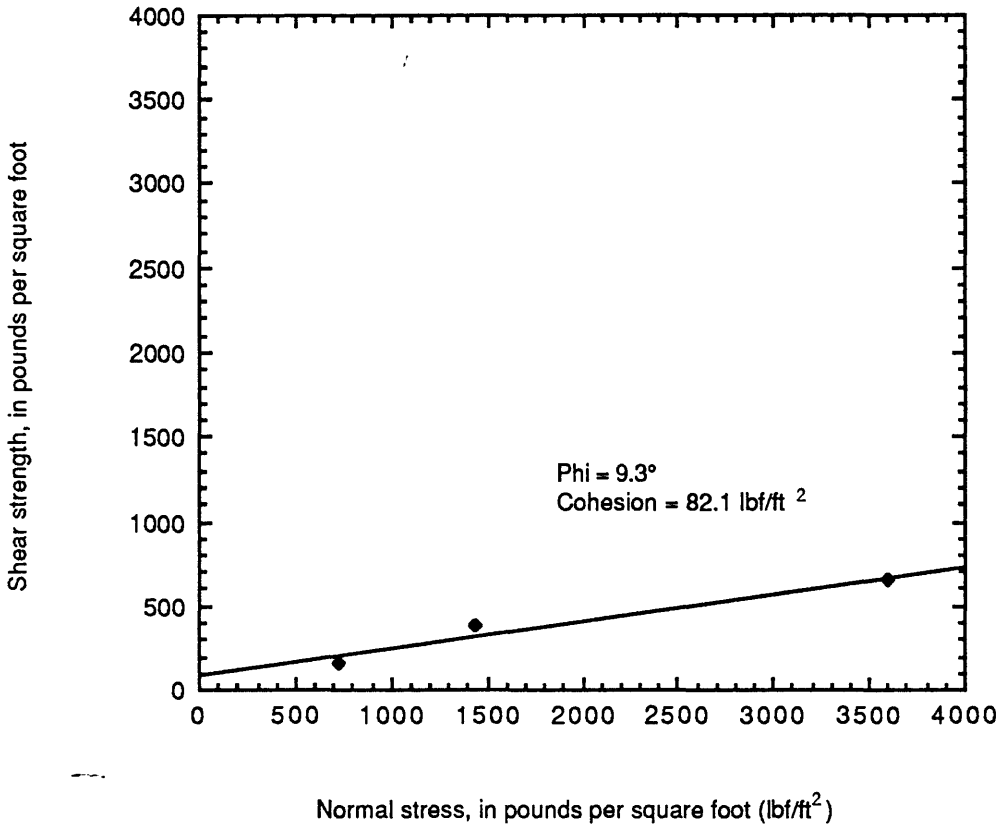

Figure A3. Graph showing residual shear strength of sample TT-48C

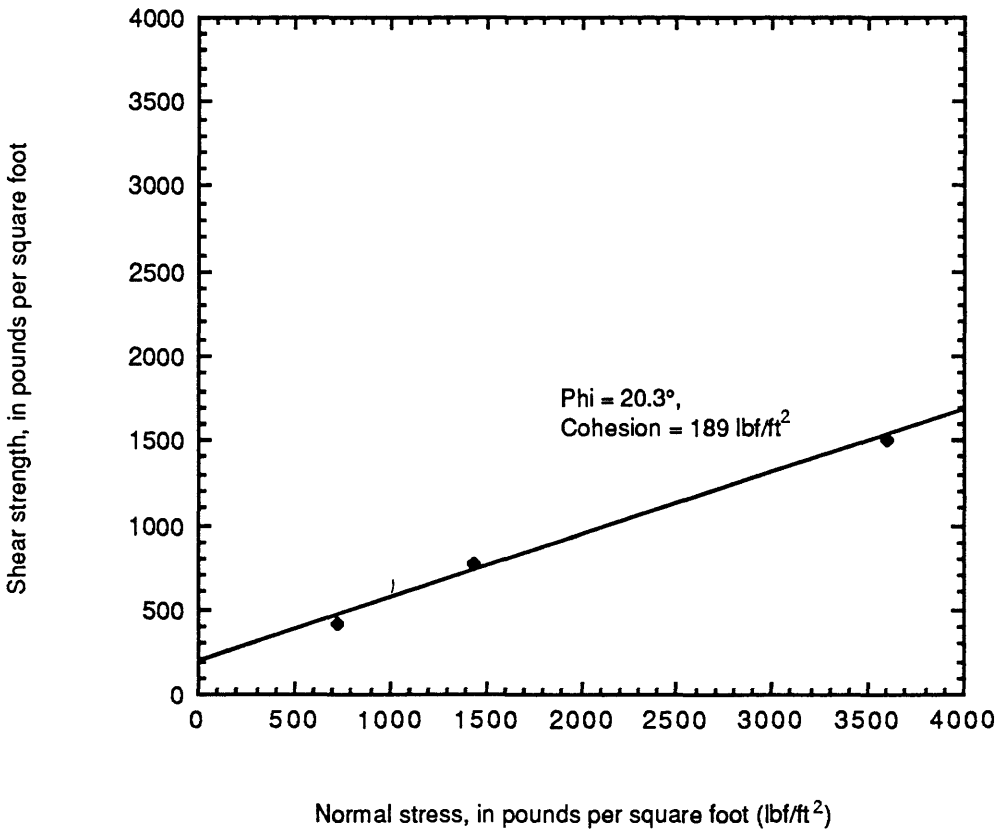

APPENDIX B

Subsurface Instrumentation

This appendix contains a listing of the instrumentation installed in borings (table B1), including instrumentation listed in the previous data report (Baum and others, 1990), graphs of piezometer measurements (figures B1, ..., B19) and pore-pressure transducer measurements (figures B20, ..., B45). Figures B46, B47, and B48 compare pore pressures to 15-minute rainfall increments during storms in November 1990, December 1990, and March 1991. Figure C16 in Appendix C shows daily rainfall from September 25, 1989 to April 30, 1990; it can be compared directly with figures B1, ..., B19 to study the response of individual piezometers to rainfall

Drilling operations were performed by Geolabs-Hawaii, under contract with the City and County of Honolulu, Department of Public Works. Instrumentation was installed by USGS personnel with assistance from Geolabs-Hawaii personnel. No samples were taken and no detailed logs were kept for borings 21-29 which were used primarily for installing instruments near locations of previous borings.

Personnel from the City and County of Honolulu determined the surface elevations of most borings by leveling. USGS personnel extended the City/County surveys to the remaining borings. The surveyed elevations reported here have been rounded to the nearest 0.1 ft.

Each piezometer consists of 1-in.-nominal-diameter PVC pipe with a 6-in.-long porous tip (piezometers in borings 21, 26, and 27 use 3/4-in.-diameter PVC). The tip is surrounded by a layer of coral sand backfill 2 to 3 ft thick and sealed above and below with layers of bentonite 2 to 3 ft high. The remainder of each hole was backfilled with cuttings left from the drilling operations. Water levels were measured using a probe lowered down the PVC pipe. Measurements were made approximately weekly during the dry seasons, and twice a week during the wet season.

The pore-pressure transducers (model PWS manufactured by the Irad Gage division of RocTest, Inc.) use vibrating-wire sensors, and have a pressure range from 0 to 50 lbf/in^2. The transducers were installed in a layer of coral sand, from 1 to 2 ft thick; the sand layer was sealed above and below with a layer of bentonite from 1 to 3 ft thick. Data loggers (model CR-10 by Campbell Scientific, Inc.) recorded pressure and temperature readings from the transducers at 30-minute intervals.

Anchored cables for monitoring displacement consist of 5/16-in.-diameter wire rope connected to a short section of steel pipe, capped at both ends and filled with lead shot. The pipe anchor was lowered to the bottom of the boring, which was several feet below the basal slip surface of the landslide. Back-fill materials placed in the boring hold the anchored end of the cable in place so that the cable is pulled down the hole as sliding occurs. A length of the cable was left protruding from the ground surface and movement is detected by repeatedly measuring the length of the protruding cable. Cables are measured weekly during the wet season and monthly during the dry season.

Table B1. Summary of instruments deployed in USGS borings in the Alani-Paty landslide

Boring #	Depth (feet)	Instrument	Depth (feet)	Surface Elevation (feet)
1	41.3			288.6
		piezometer	13.2	
		piezometer	25.5	
		anchor	27.8	
3	41.5			202.3
		piezometer	5.0	
		piezometer	30.0	
		anchor	36.3	
4	41.0			230.8
		piezometer	20.2	
		piezometer	39.5	
		anchor	39.9	
5	41.5			231.5
		piezometer	5.7	
		piezometer	34.4	
		anchor	38.0	
6	50.0			223.9
		inclinometer	47.6 (depth of lowest measurement)	
7	41.0			294.6
		piezometer	8.0	
		piezometer	37.3	
8	41.0			325.2
		piezometer	12.0	
		piezometer	35.1	
		anchor	40.2	
9	41.0			324.0
		piezometer	8.6	
		piezometer	25.1	
		anchor	41.0	
10	48.5			334.9
		inclinometer	47.6	
11	41.5			334.5
		neutron probe	40.0	
12	40.5			250.85
		piezometer	18.0	
		piezometer	35.8	
		anchor	39.9	

Table B1. (continued)

Boring #	Depth (feet)	Instrument	Depth (feet)	Surface Elevation (feet)
13	40.0			250.2
		piezometer	12.0	
		piezometer	32.1	
		anchor	37.5	
14	40.5			284.2
		piezometer	9.4	
		piezometer	21.9	
		piezometer	38.2	
15	50.8			245.4
		inclinometer	49.2	
16	40.5			247.5
		piezometer	15.4	
		piezometer	20.7	
		piezometer	36.7	
17	42.0			321
		neutron probe	40.0	(approx.)
18	44.3			297.5
		neutron probe	40.0	
19	35.3			207.8
		piezometer	14.4	
		piezometer	31.8	
		anchor	35.3	
19x	5.6			207.8
		piezometer	5.4	
20	50.0			313.0
		piezometer	9.5	
		piezometer	21.5	
		piezometer	30.0	
		anchor	40.0	
21	40.2			334.4
		piezometer	7.0	
		piezometer	23.4	
		piezometer	37.6	
22	22.0			334.1
		transducer	11.3	
		transducer	20.6	
23	35.5			289.7
		anchor	35.5	

Table B1. (continued)

Boring #	Depth (feet)	Instrument	Depth (feet)	Surface Elevation (feet)
24	21.0			289.6
		transducer	11.3	
		transducer	19.3	
25	51.0			approx. 264
		inclinometer	41.0	(depth of lowest measurement)
26	14.0			223.3
		obsevation well (3/4 -in. dia. slotted PVC)	3.5-13.5	
27	36.0			360.9
		piezometer	13.5	
		piezometer	22.4	
		piezometer	34.0	
28	10.5	(3 shallow borings 10.5 ft or less)		322.5--324.5
		tensiometers	1.0-5.0	(6 at various depths)
		transducer	9.0	
		transducer	10.2	
29	16.5			336.4
		transducer	9.0	

INCLINED BORINGS

These borings were made by PR Drilling Co., Inc., for STV/Lyon Associates, to determine the distance to bedrock. STV/Lyon had no plans to instrument the holes, so we plugged the holes at shallow or intermediate depths and installed open-tube piezometers. Depths in the table below indicate slope distances down the borings, which slope 40° from the horizontal.

Boring #	Depth (feet)	Instrument	Depth (feet)	Elevation (feet)
100	15.0			339.4
		piezometer	10.1	
103	80.0			351.0
		piezometer	5.8	
		piezometer	56.0	
108	19.8			343.2
		piezometer	19.4	

Figure B1. Piezometers in boring 1

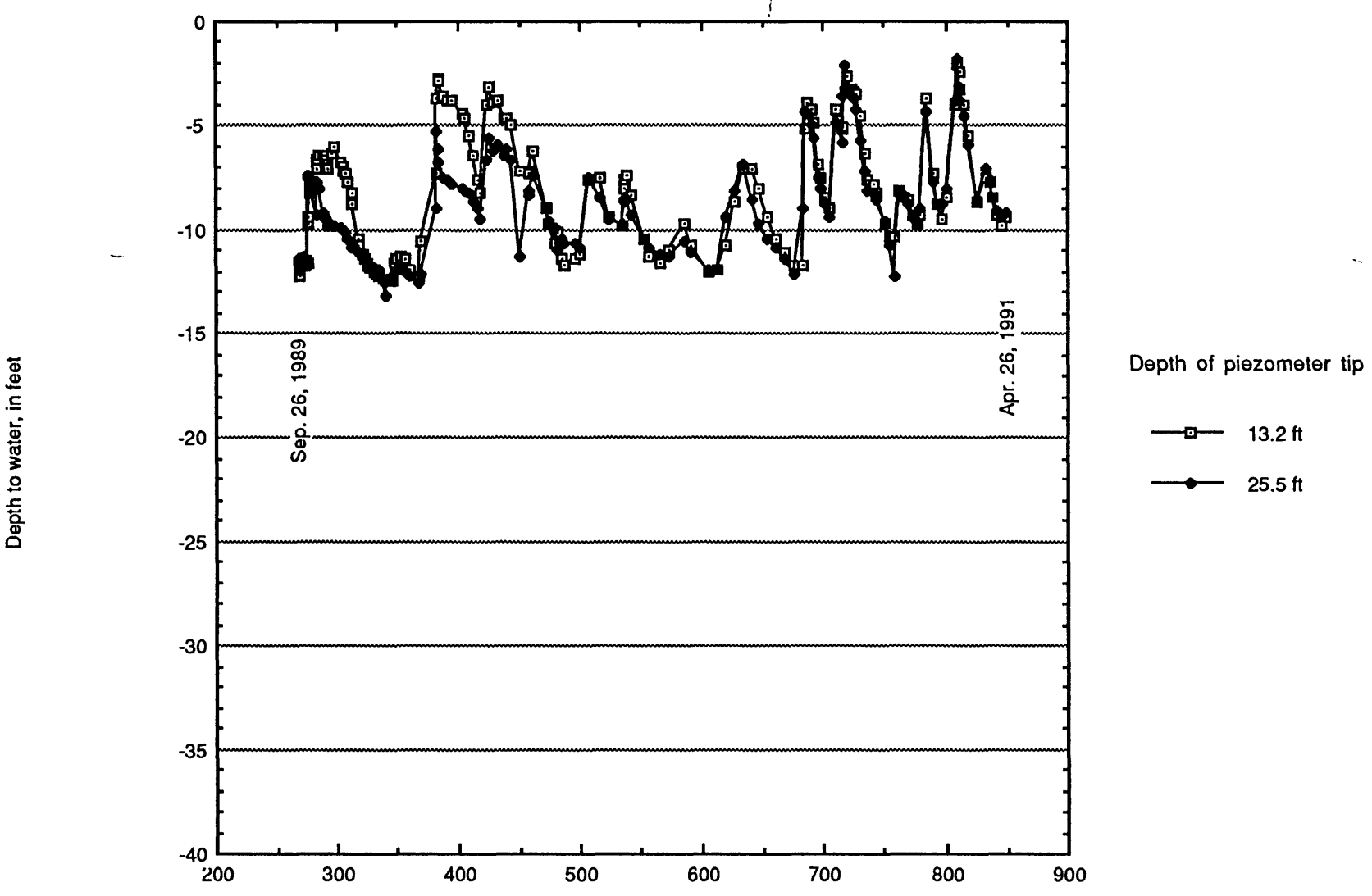

Figure B2. Piezometers in boring 3

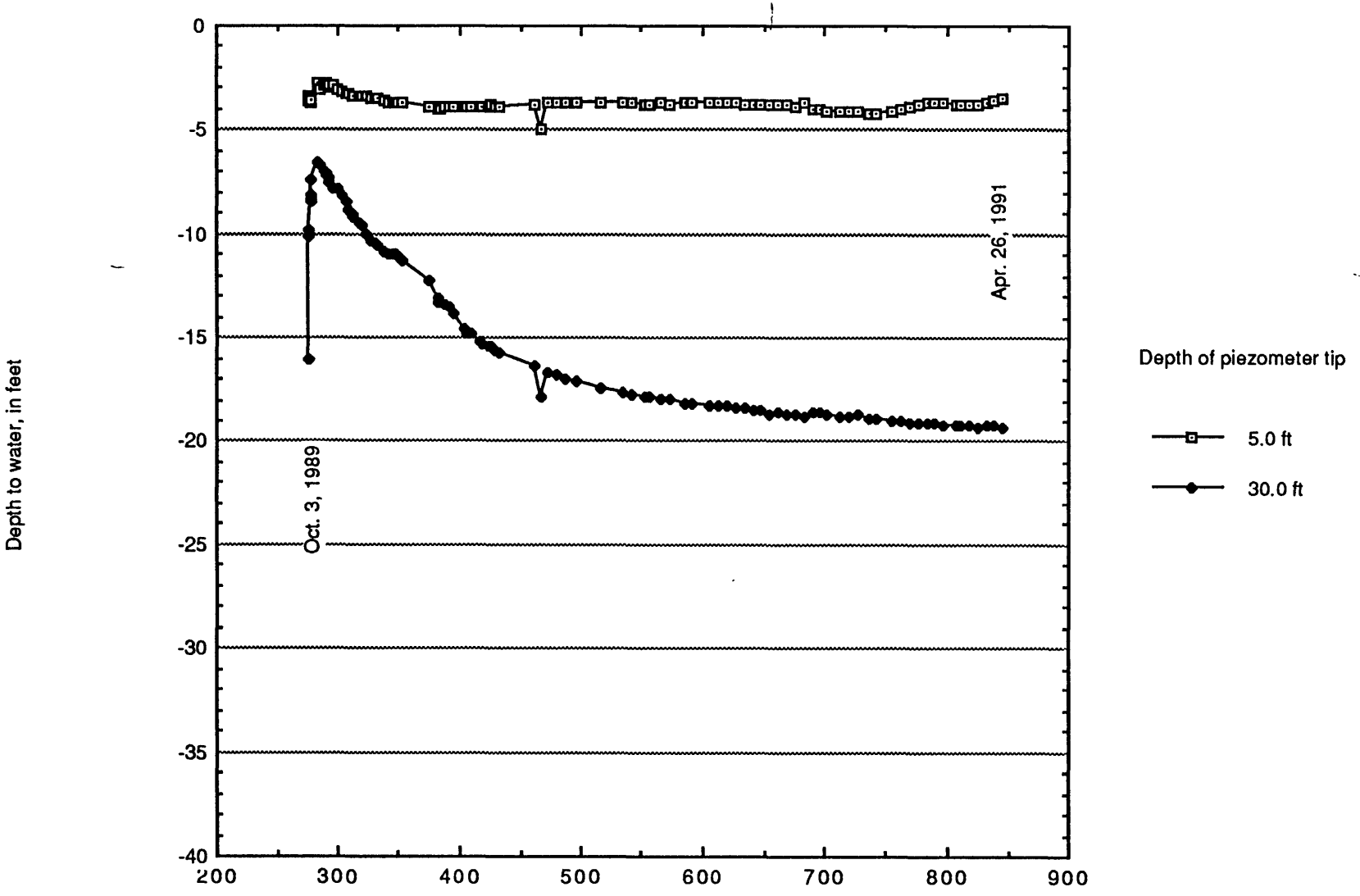

Figure B3. Piezometers in borings 4 and 5

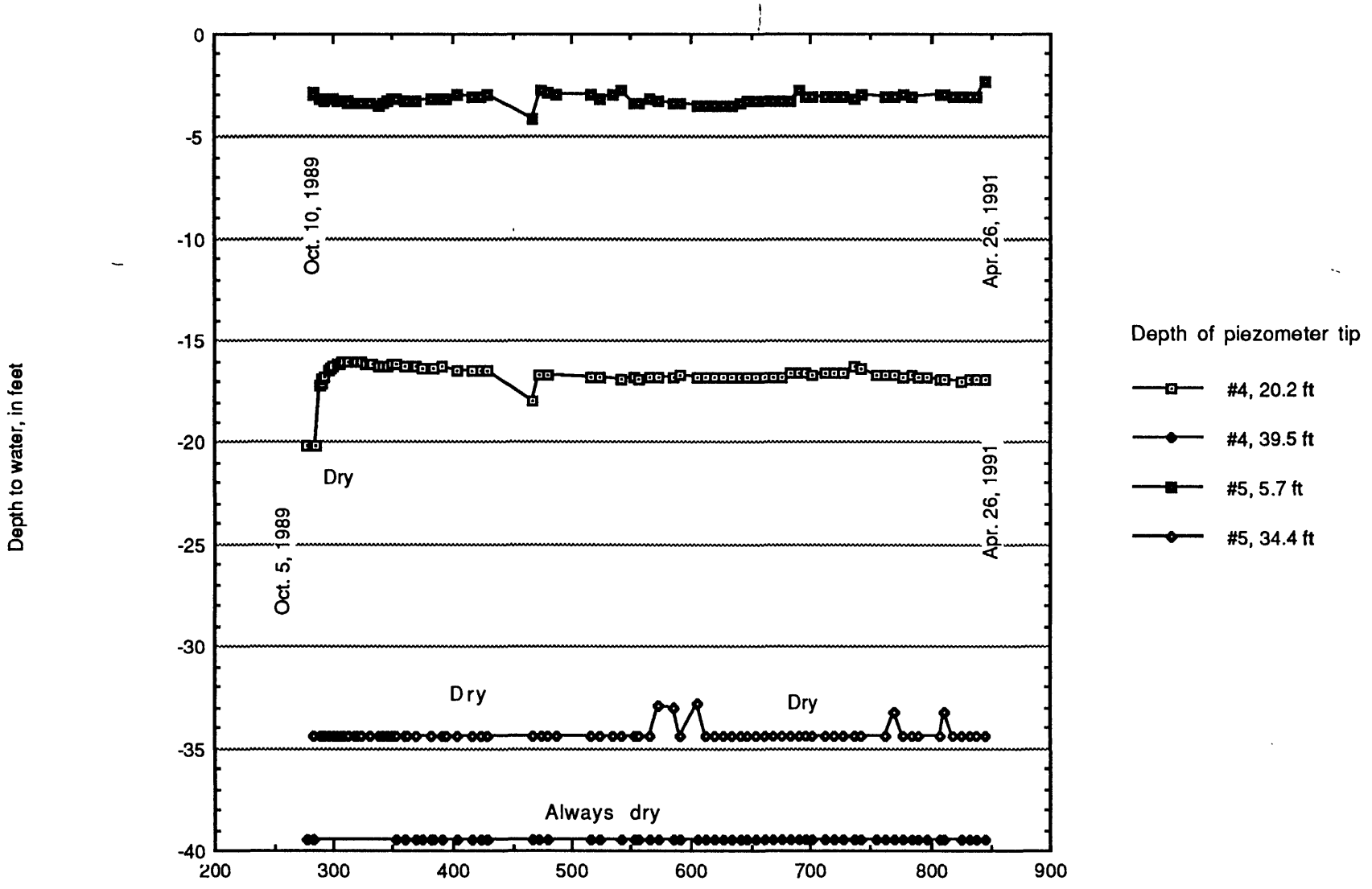

Figure B4. Piezometers in boring 7

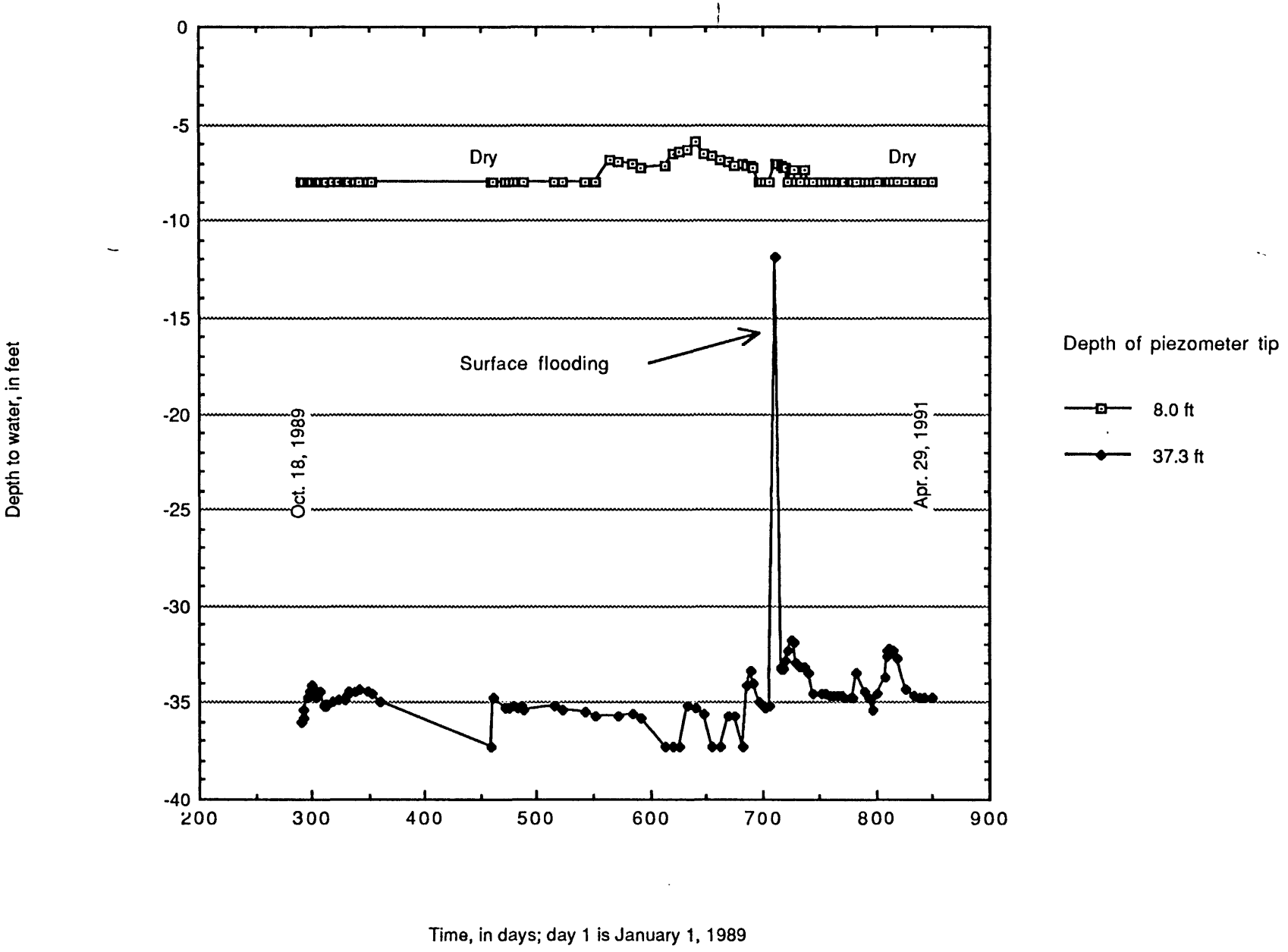

Figure B5. Piezometers in boring 8

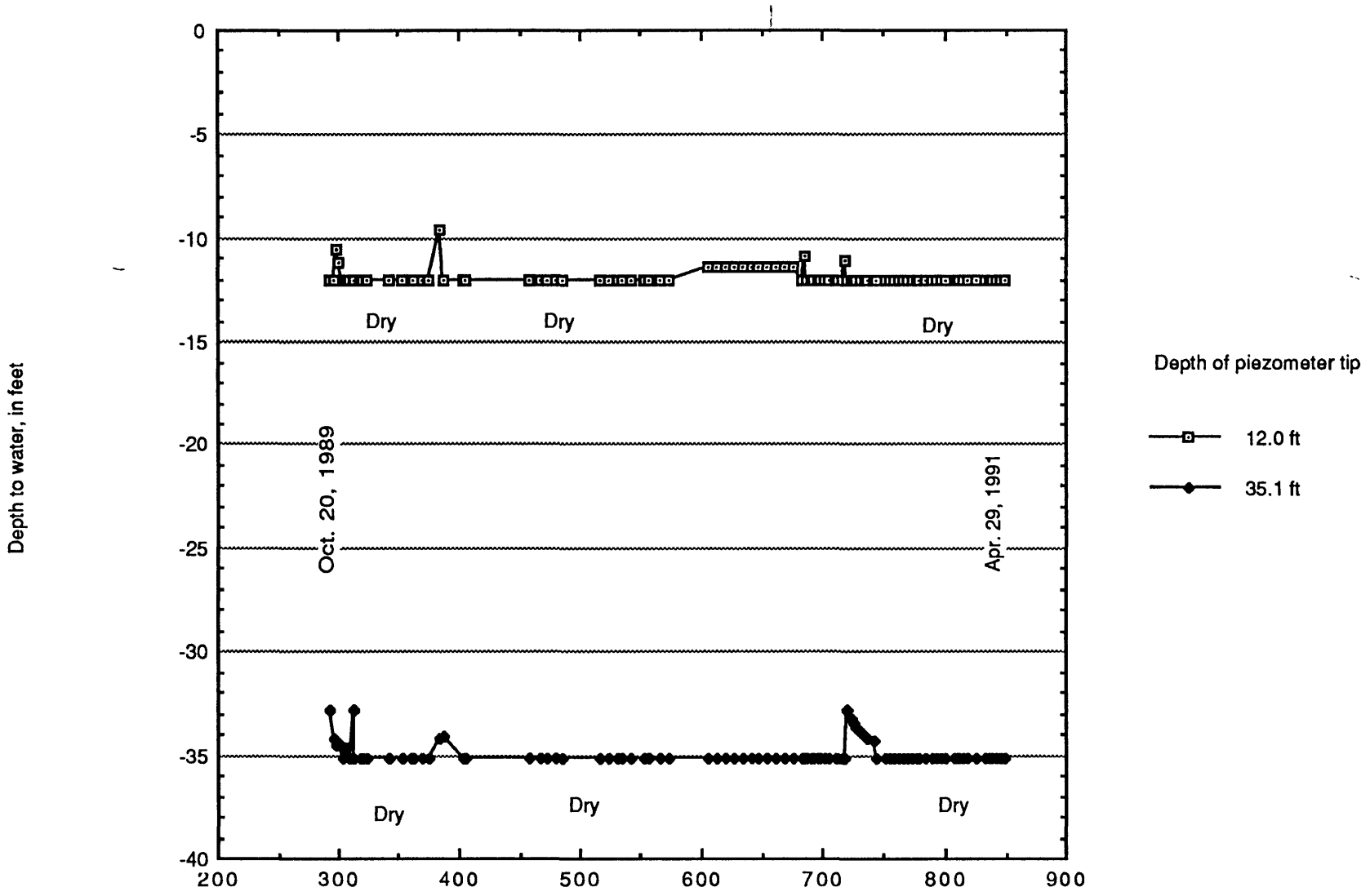

Figure B6. Piezometers in boring 9

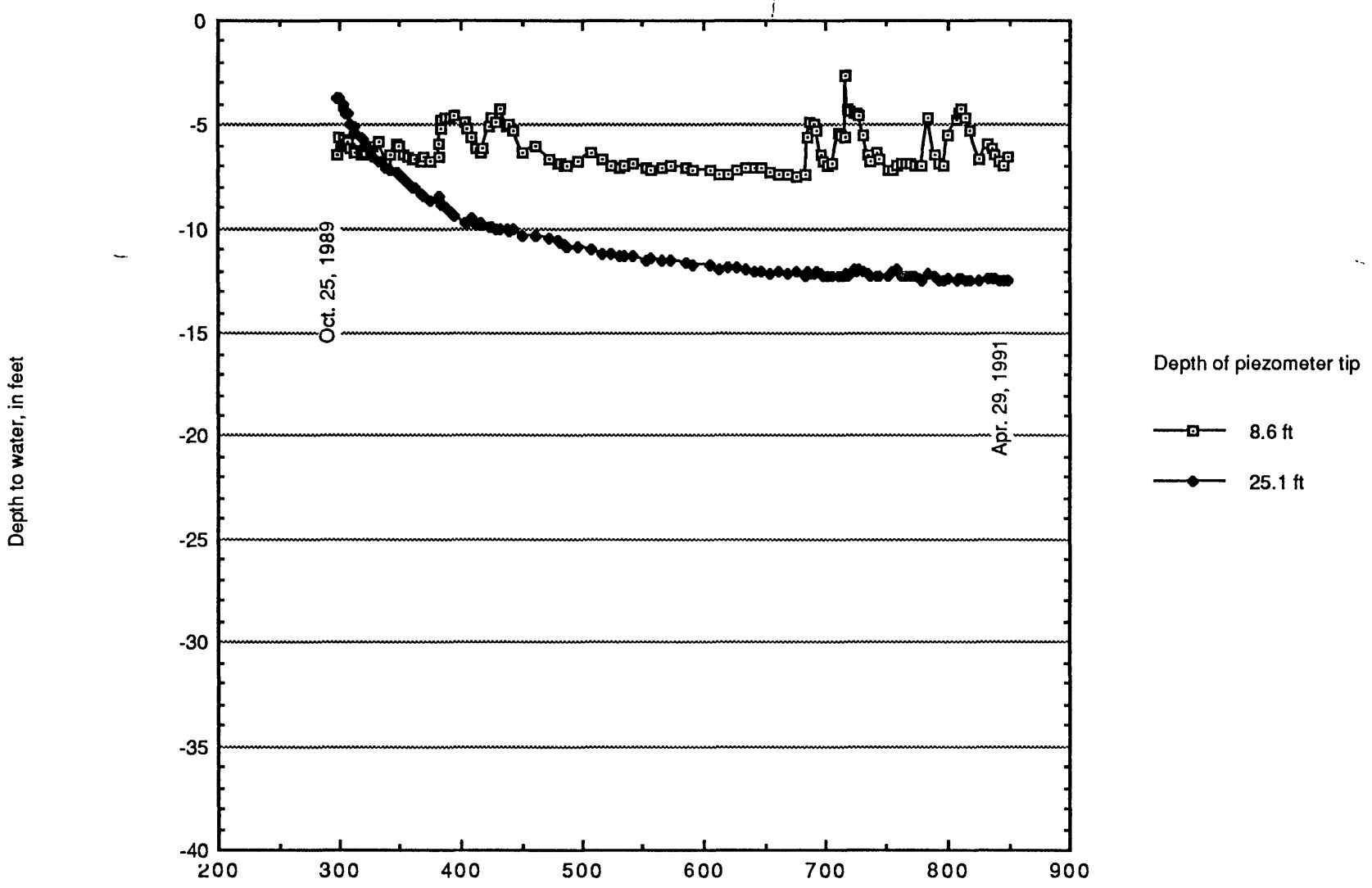

Figure B7. Piezometers in boring 12

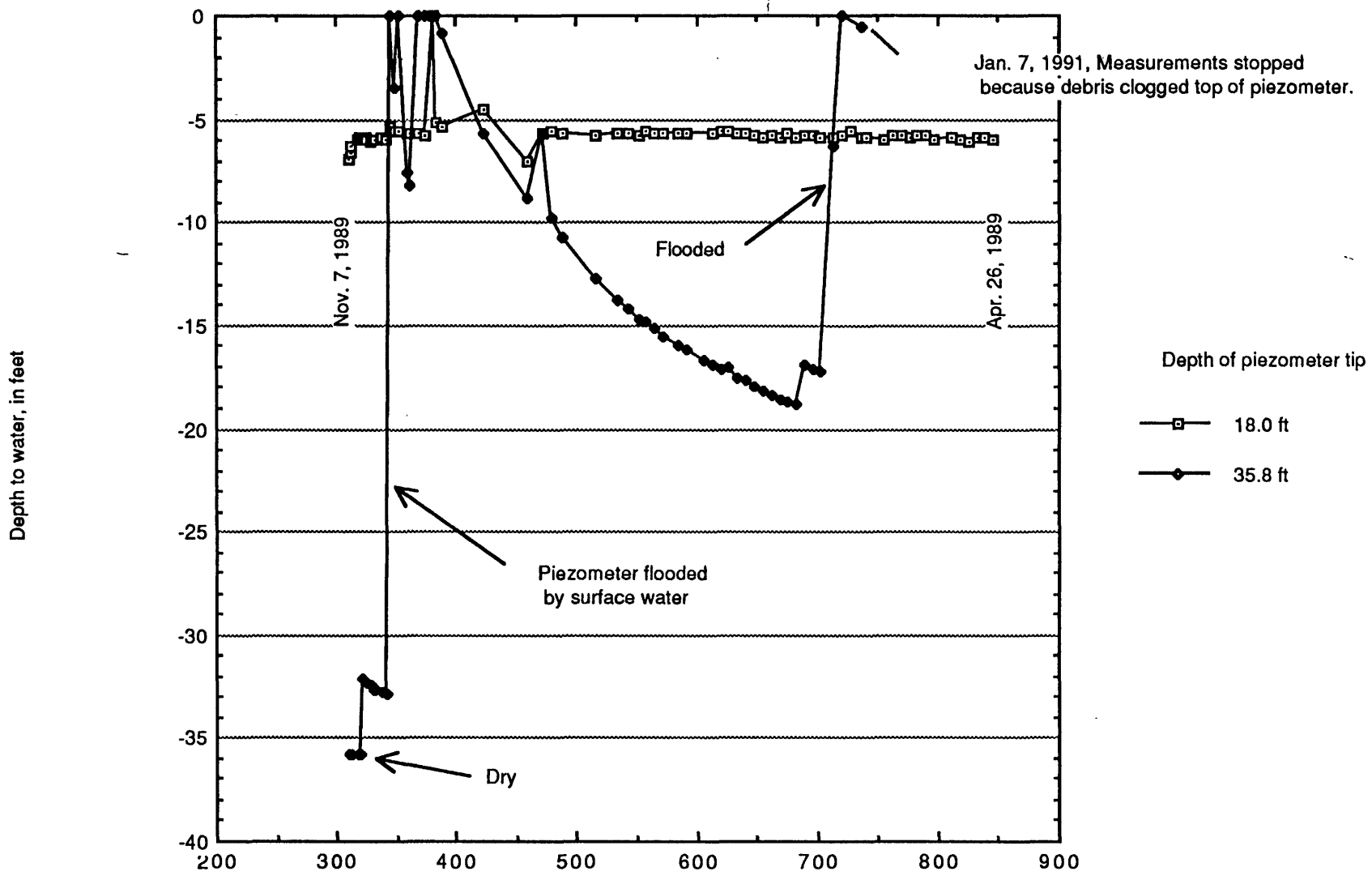

Figure B8. Piezometers in boring 13

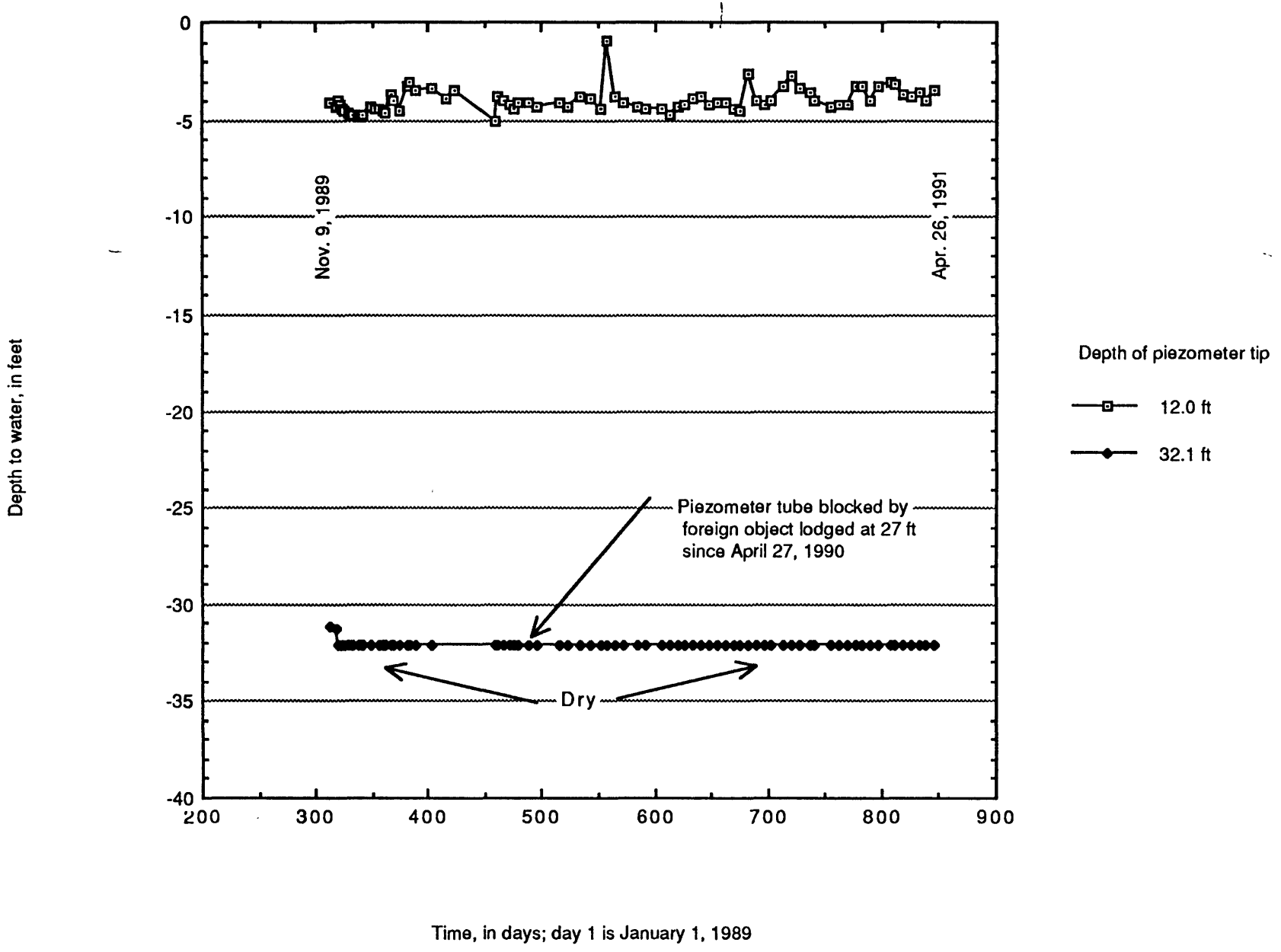

Figure B9. Piezometers in boring 14

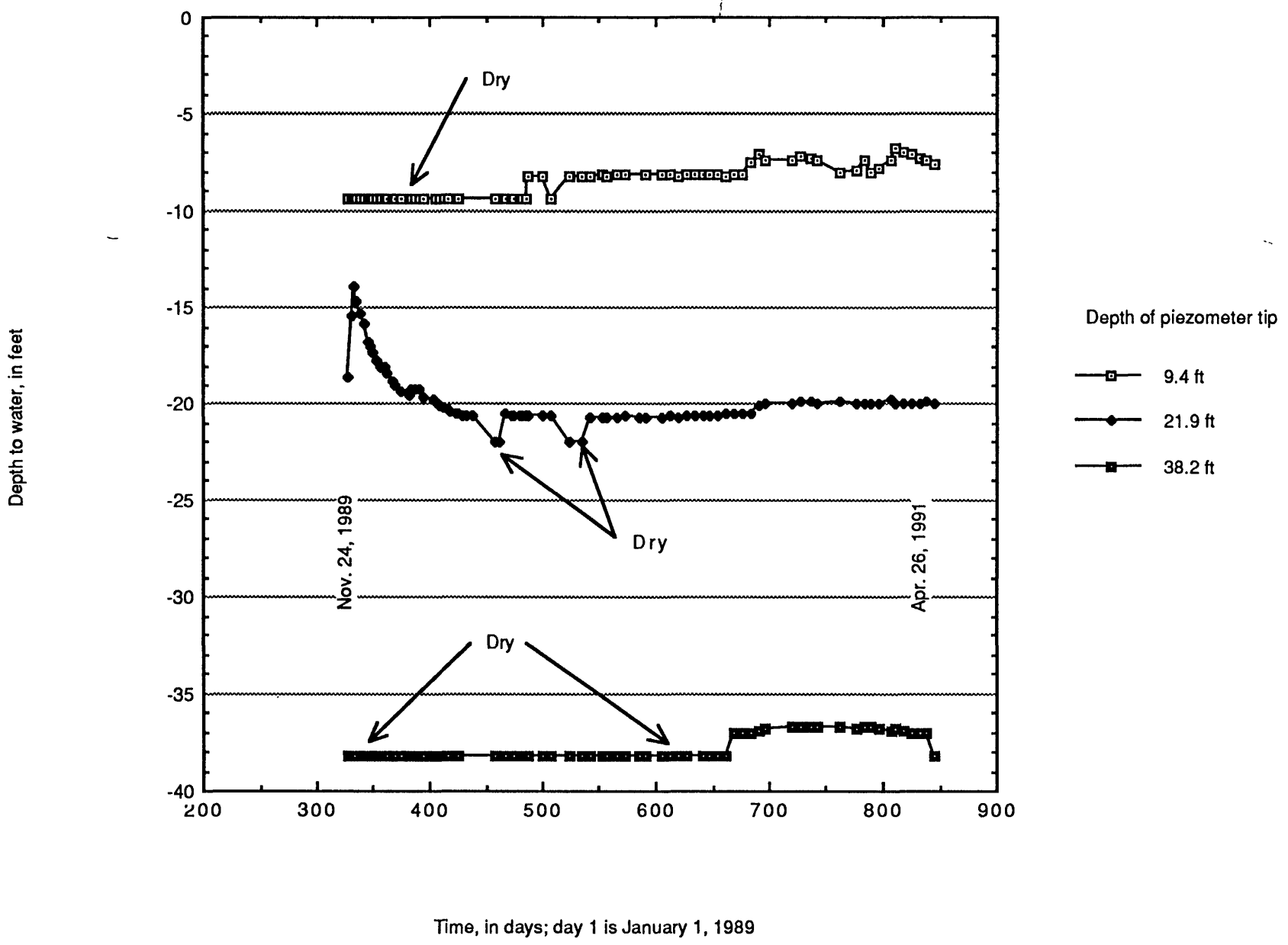

Figure B10. Piezometers in boring 16

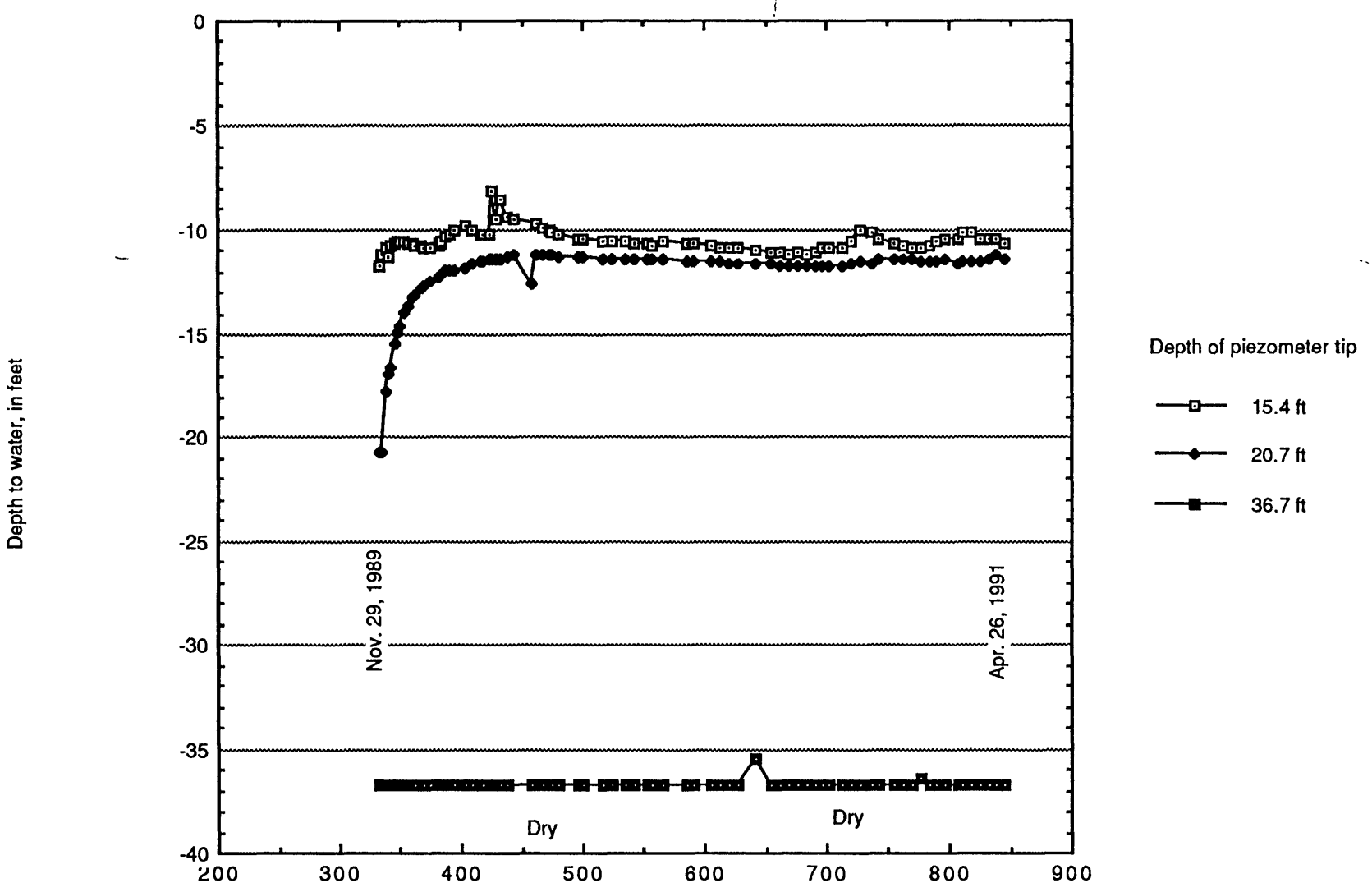

Figure B11. Piezometers in borings 19 and 19x

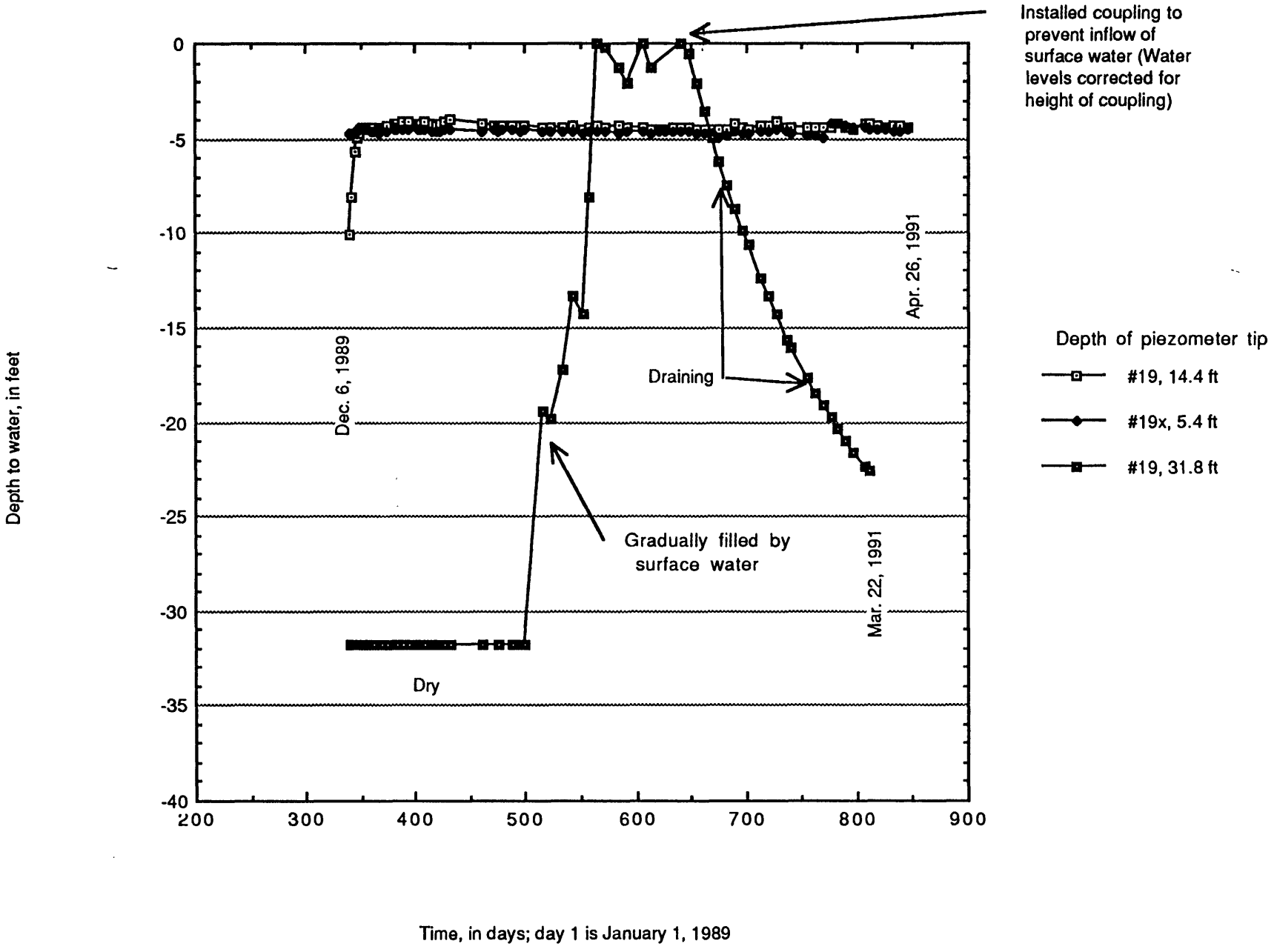

Figure B12. Piezometers in boring 20

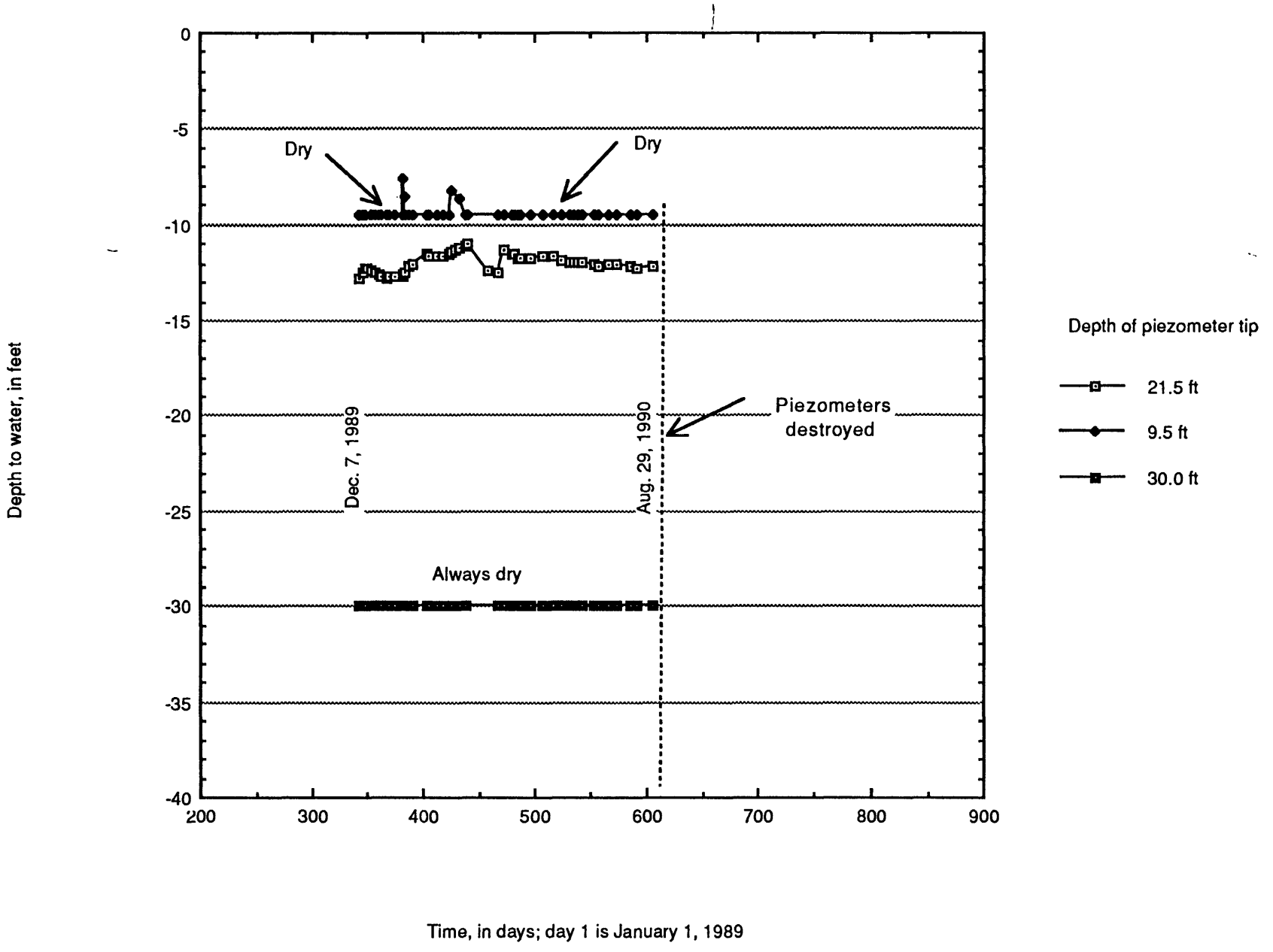

Figure B13. Piezometers in boring 21

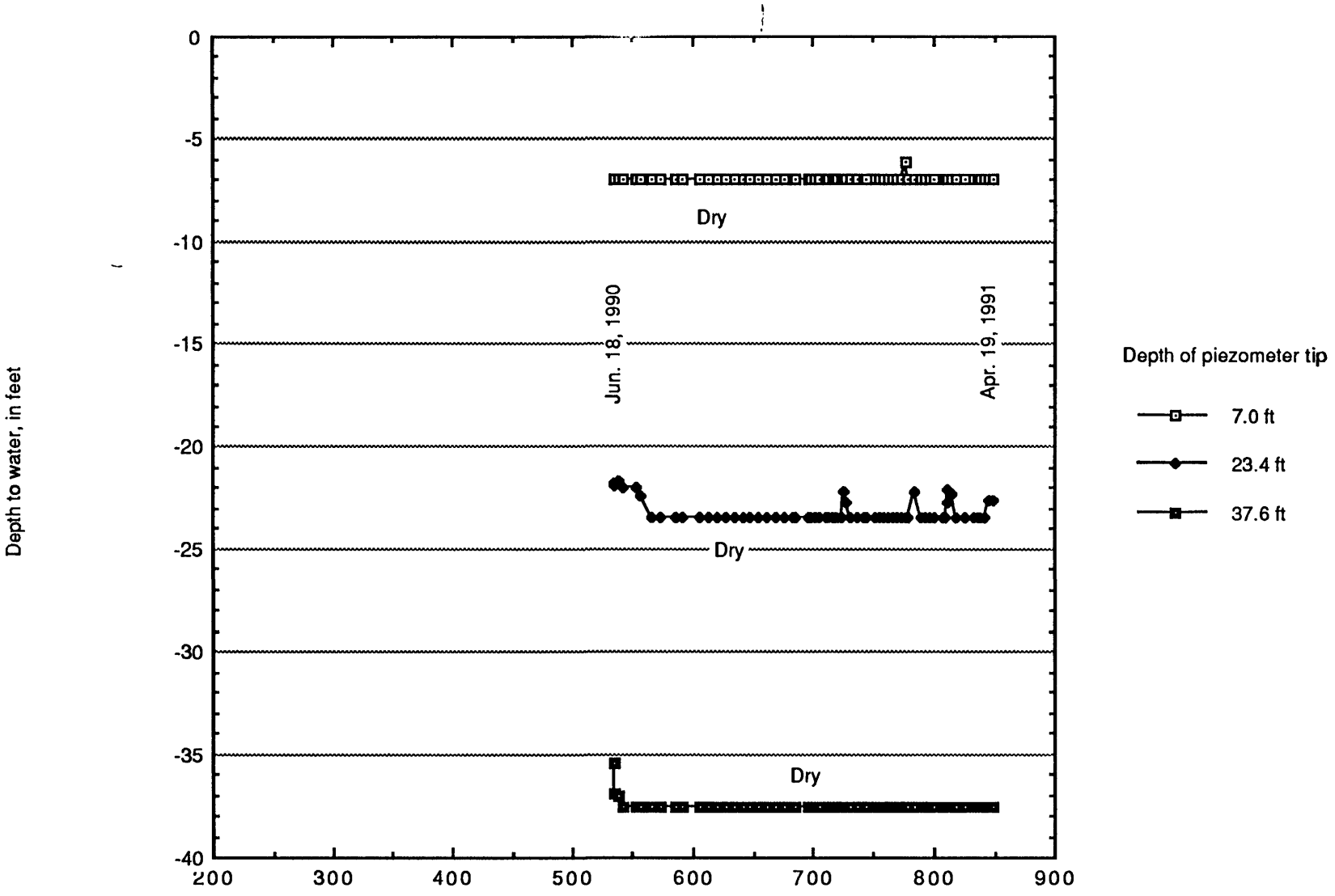

Figure B14. Water table in boring 26

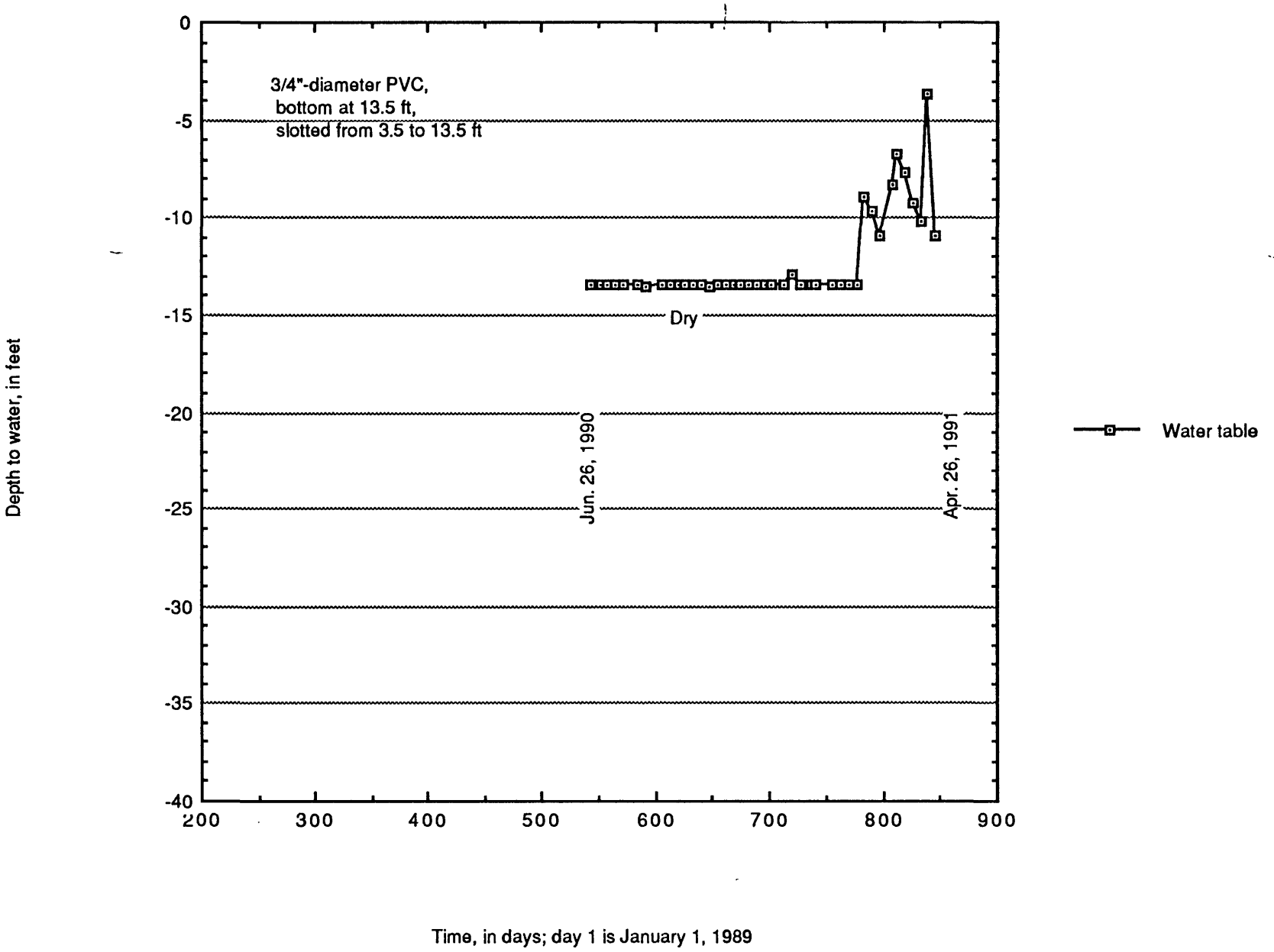

Figure B15. Piezometers in boring 27

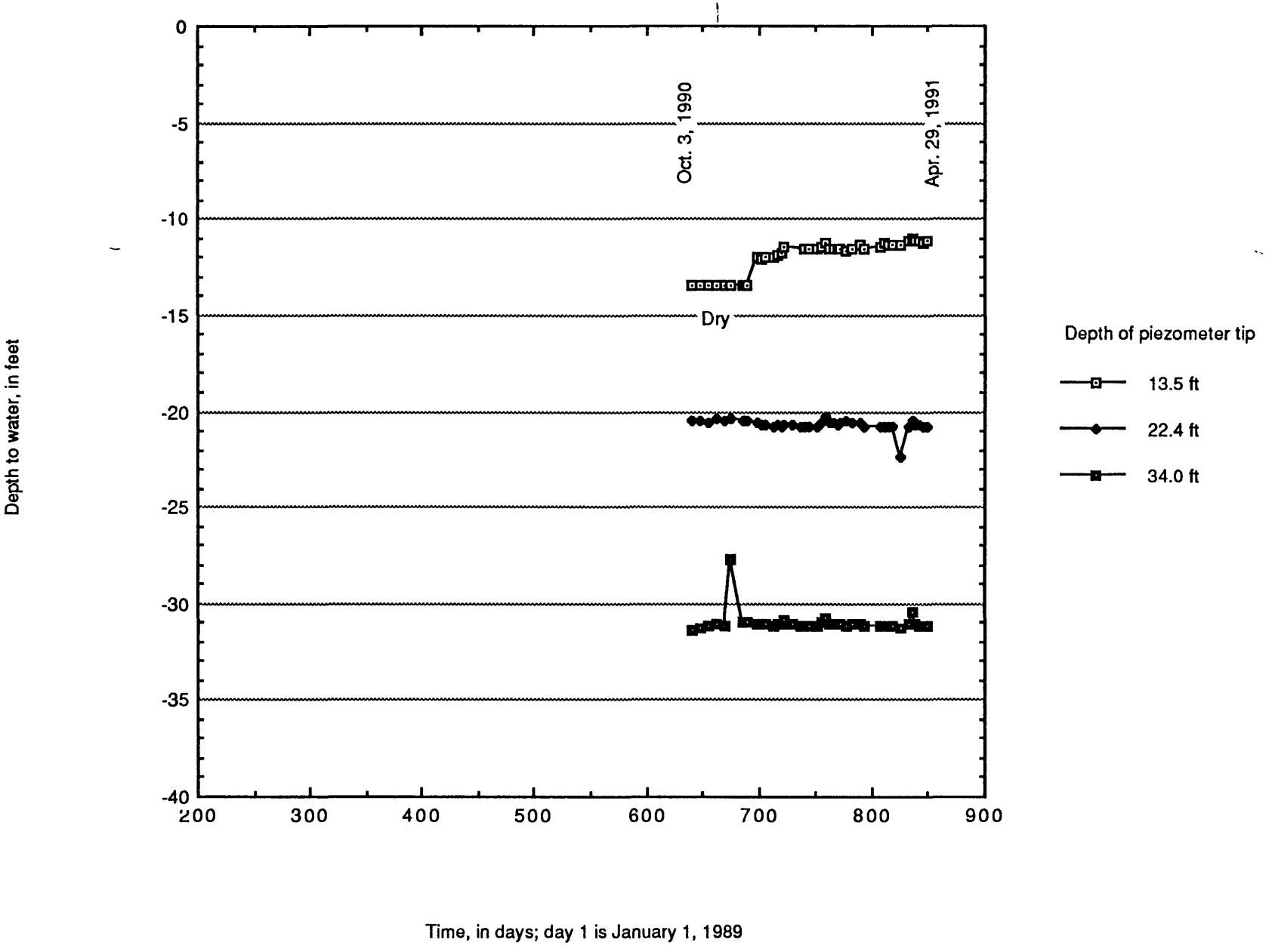

Figure B16. Piezometer in inclined boring 100

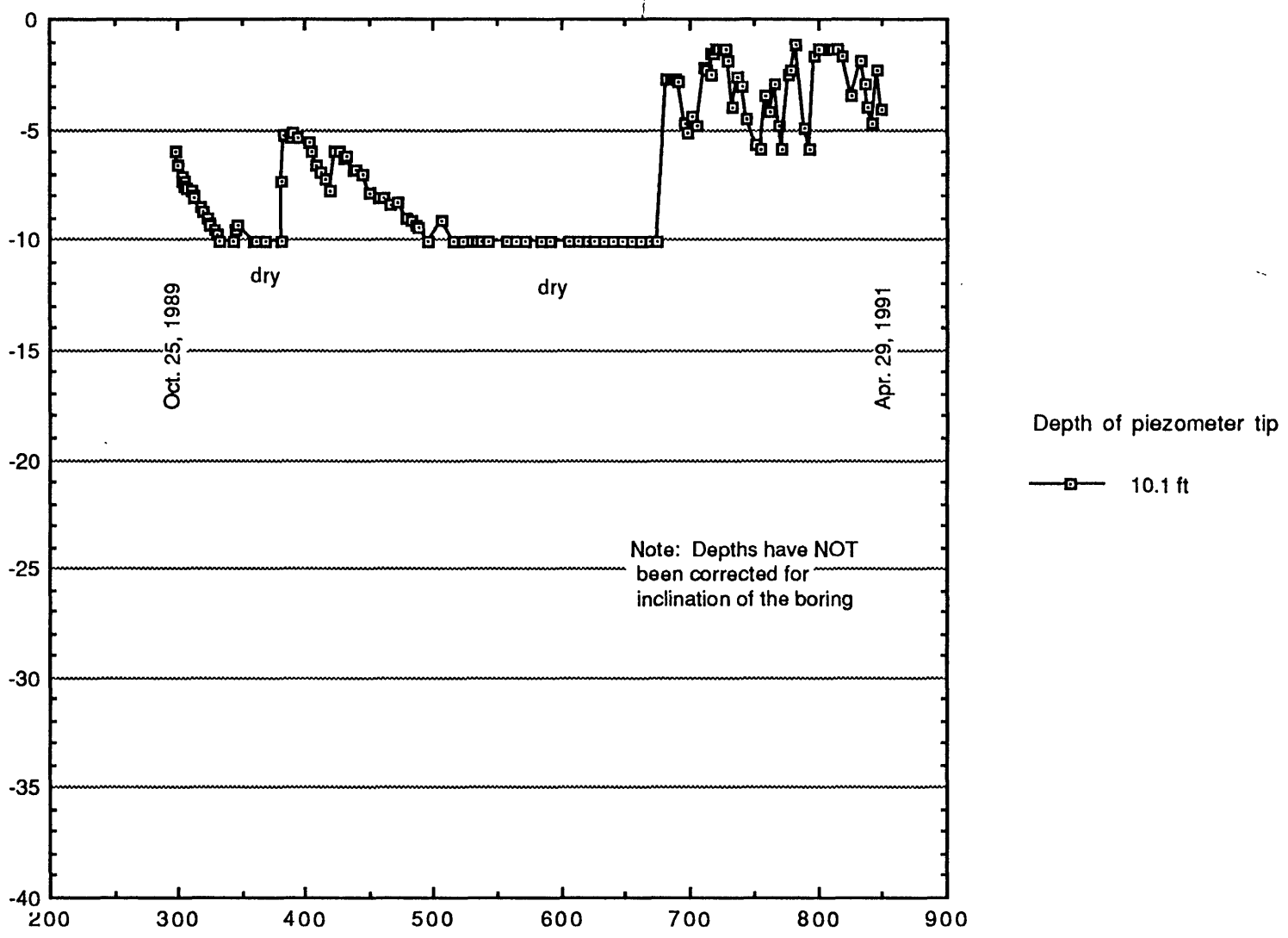

Figure B17. Shallow piezometer in inclined boring 103

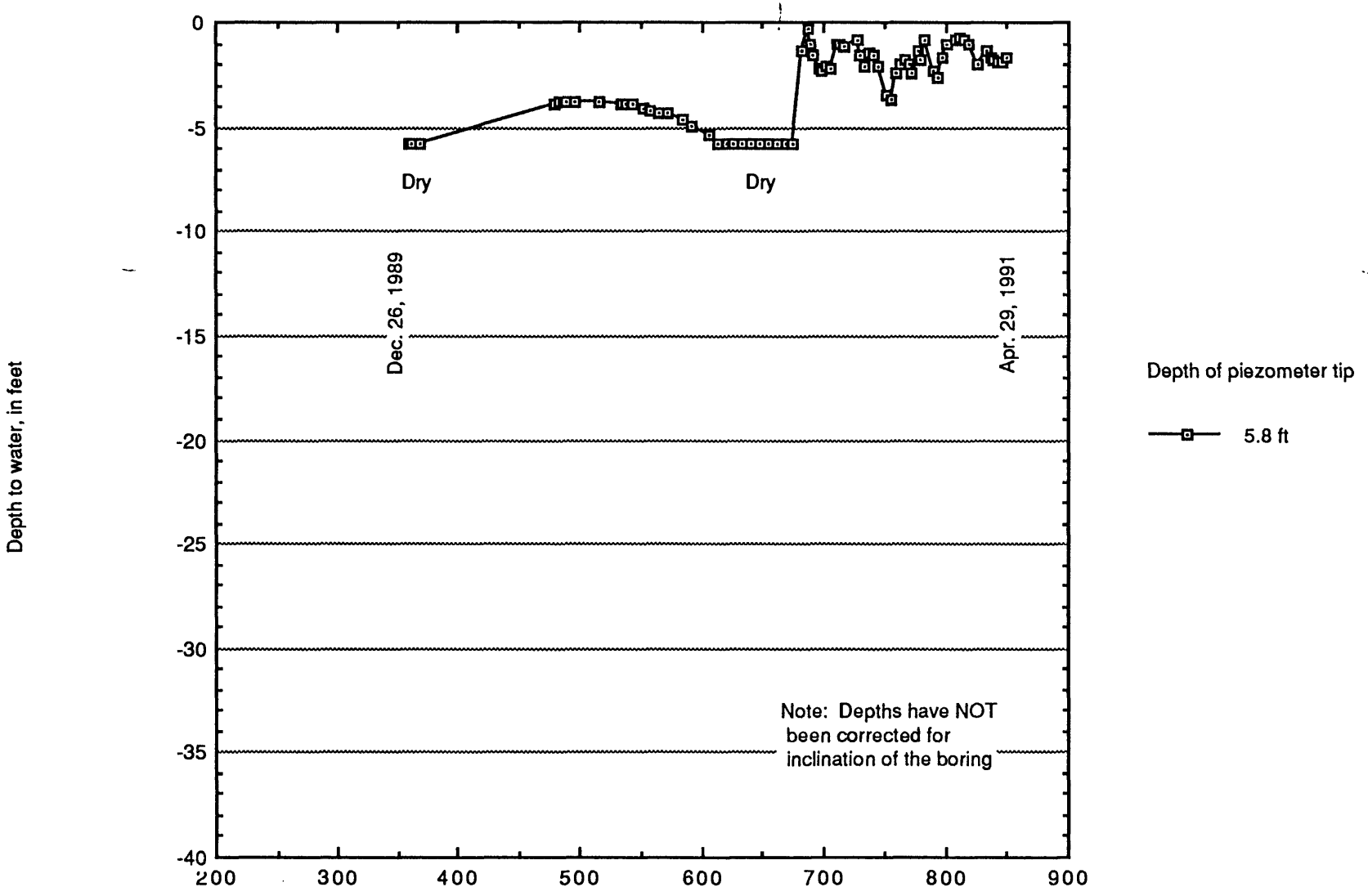

Figure B18. Deep piezometer in inclined boring 103

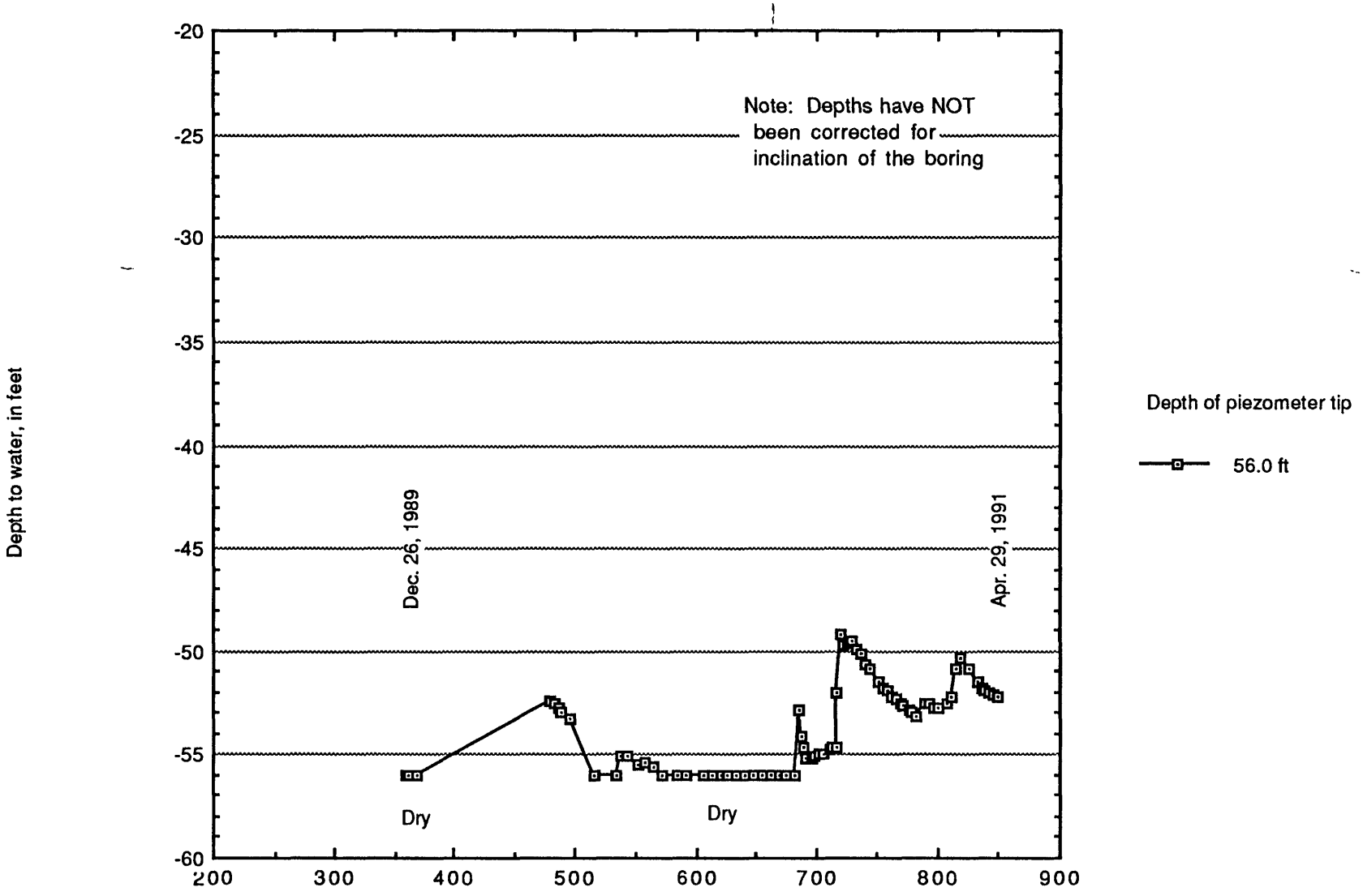

Figure B19. Piezometer in inclined boring 108

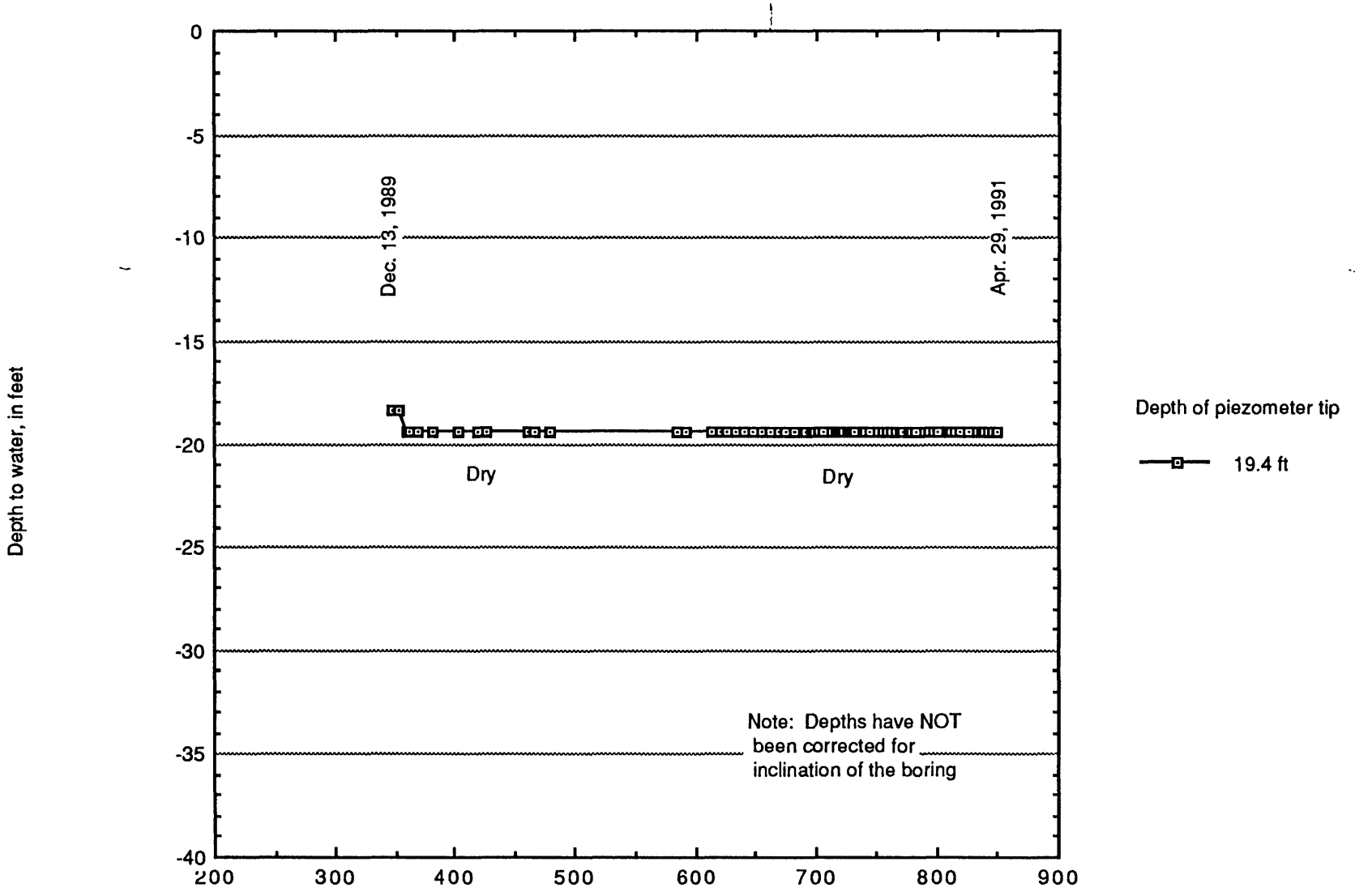

Figure B20. Pressure transducer in boring 22

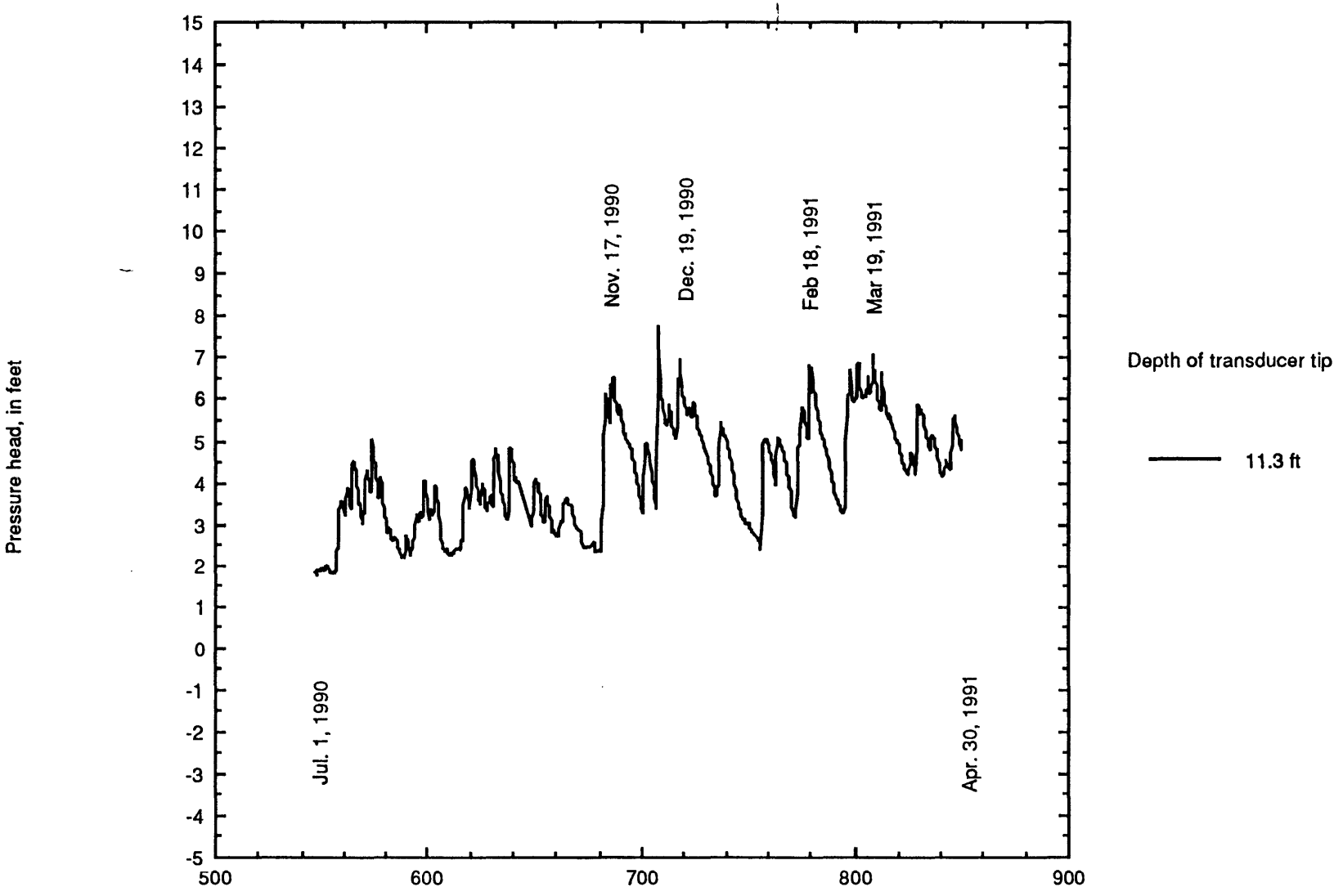

Figure B21. Pressure transducer in boring 22

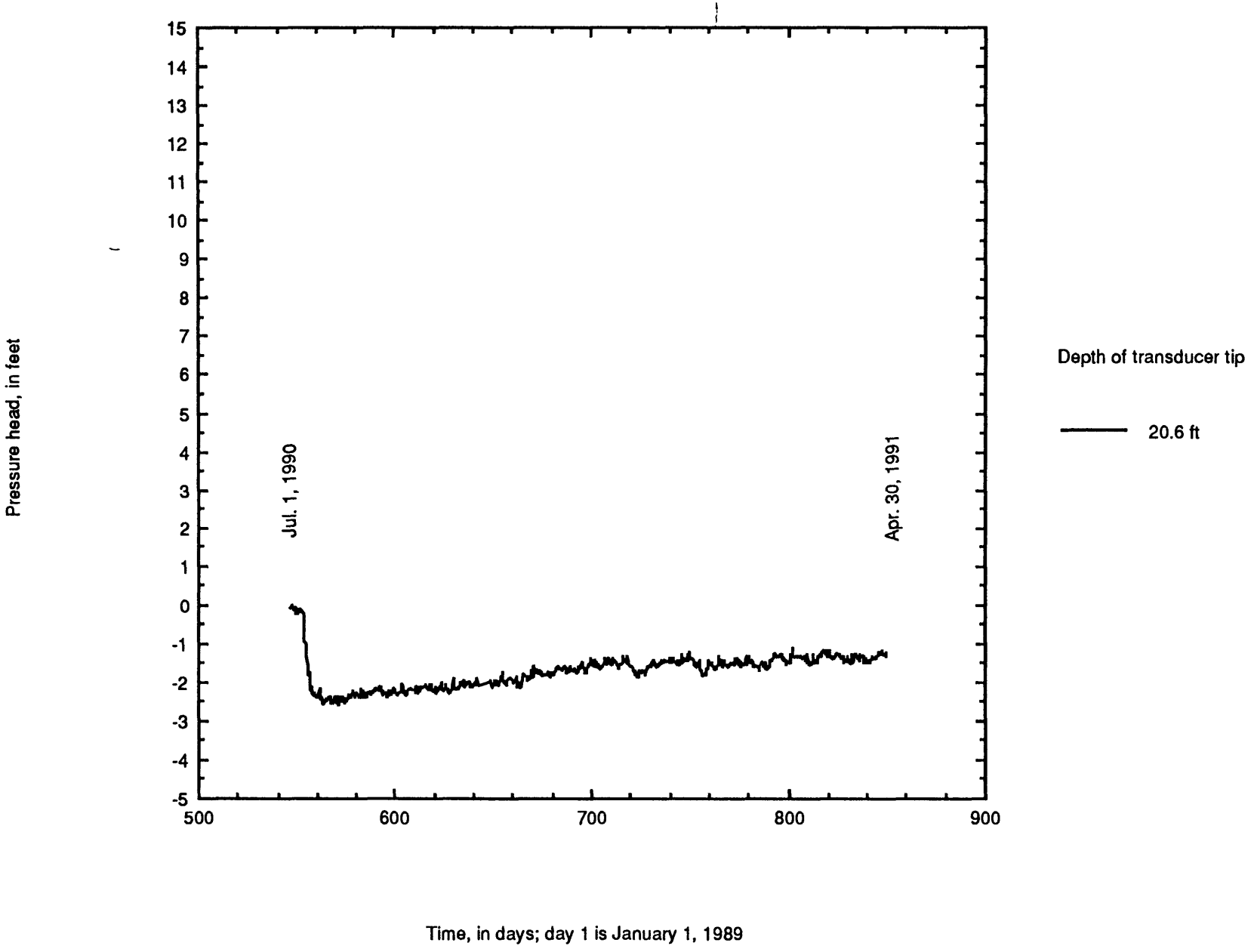

Figure B22. Pressure transducer in boring 24

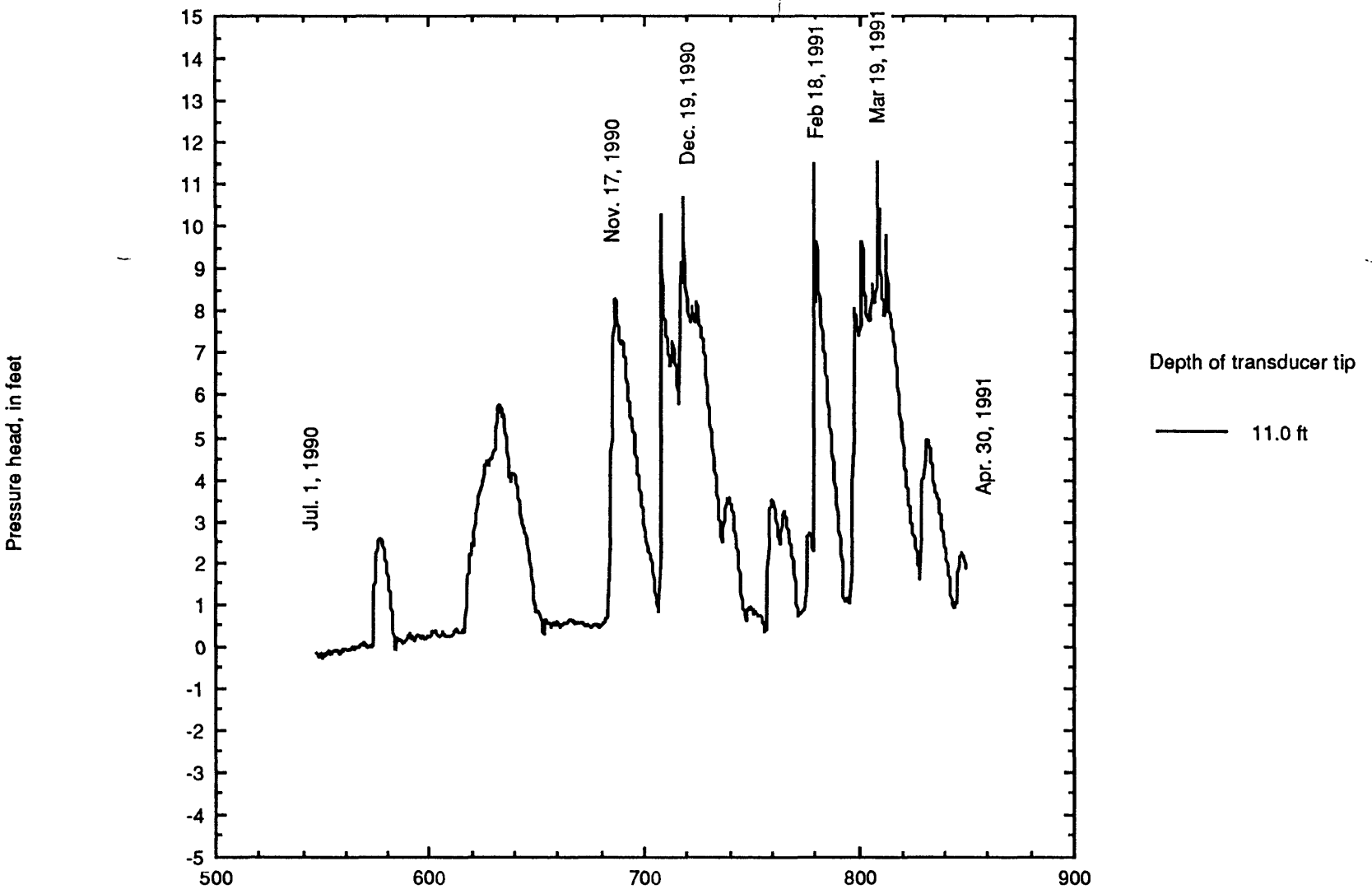

Figure B23. Pressure transducer in boring 24

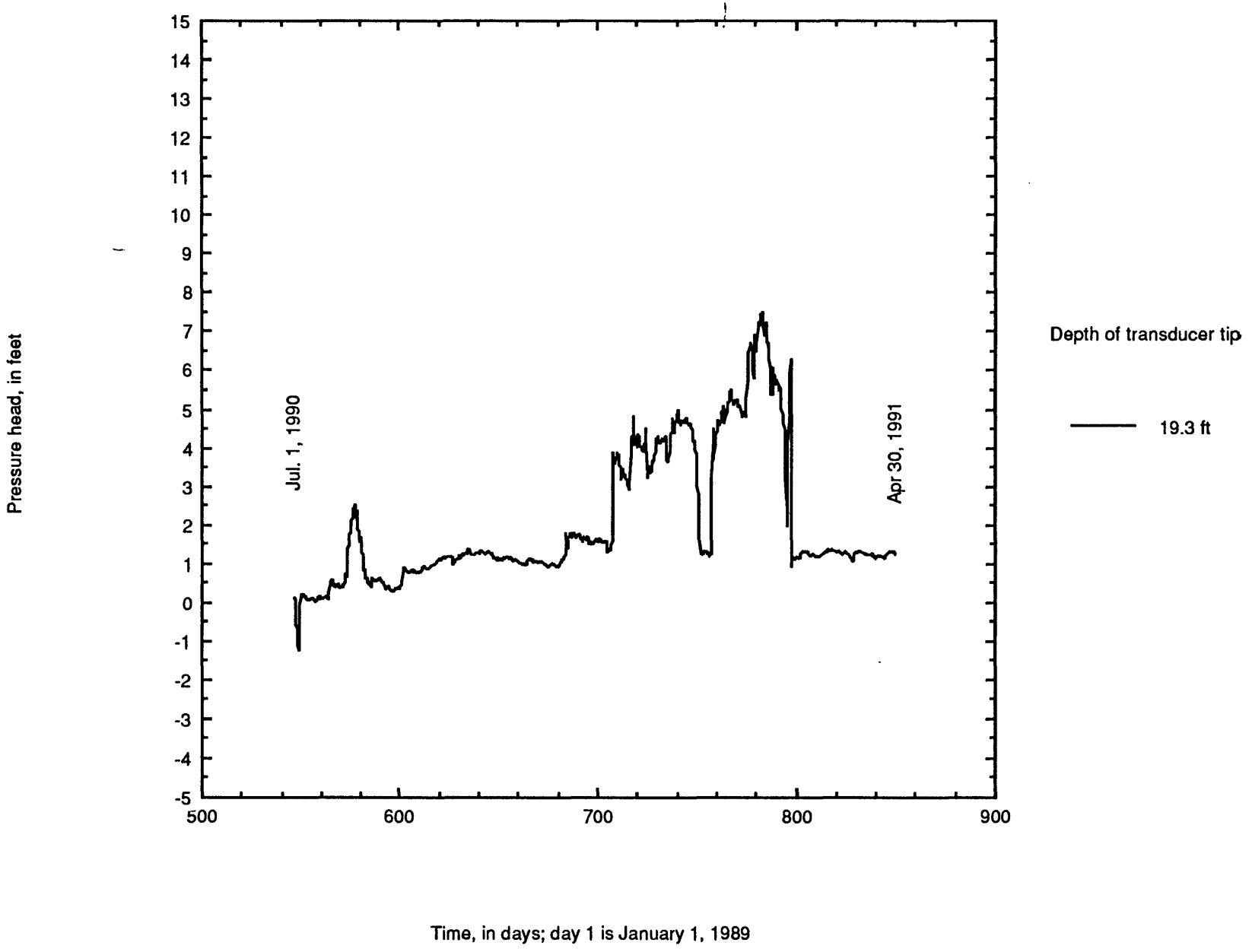

Figure B24. Transducers in boring 22, July 1990

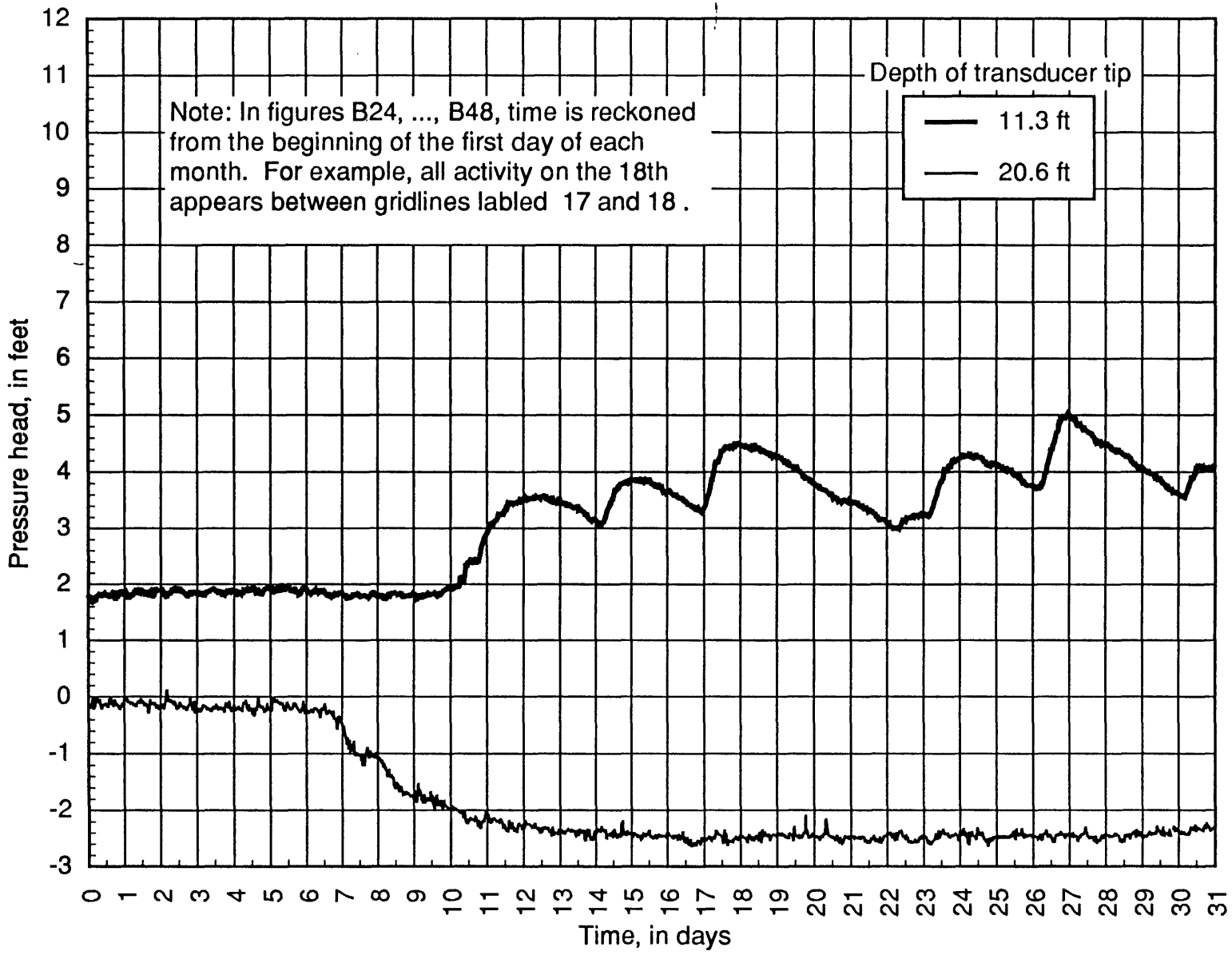

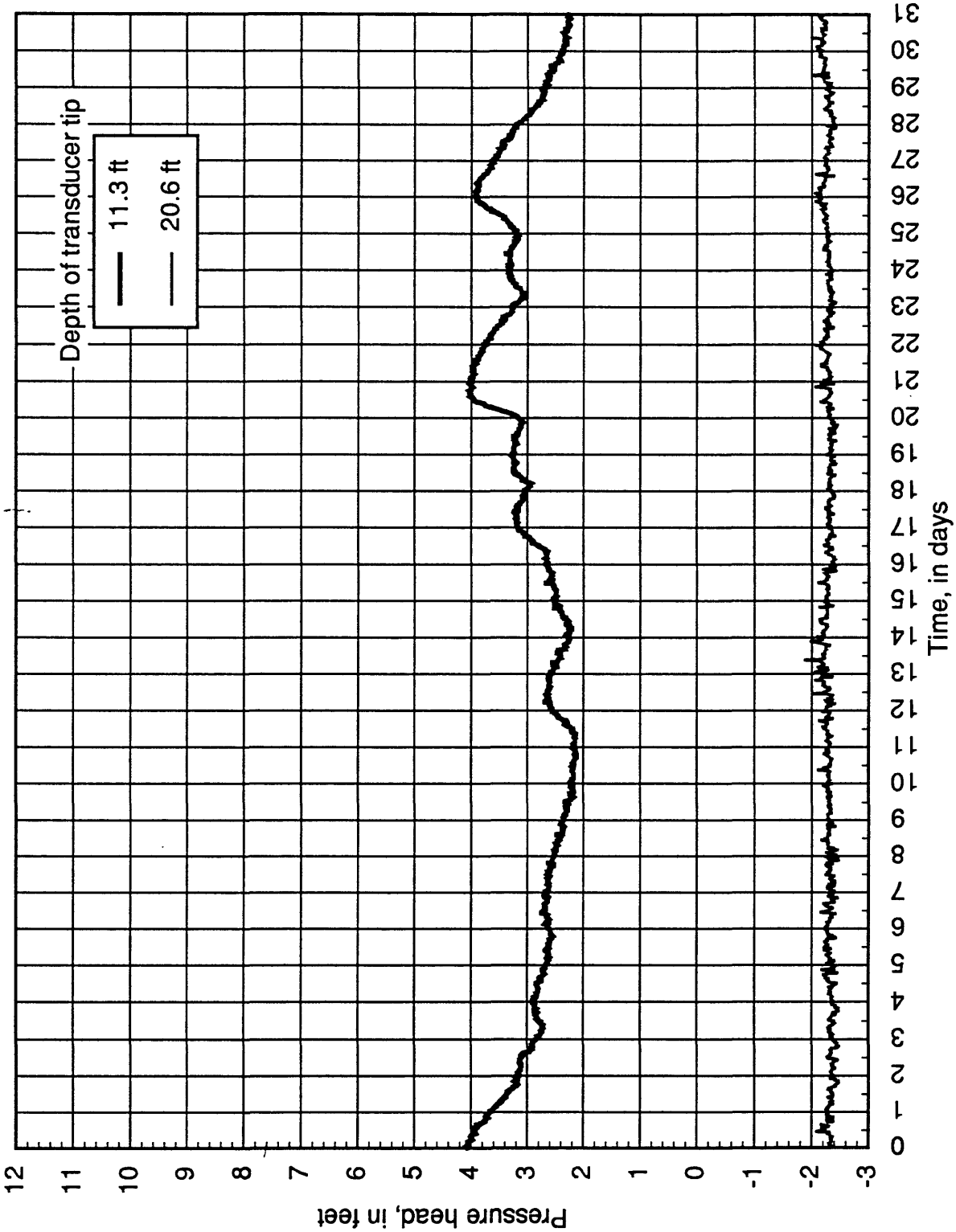

Figure B25. Transducers in boring 22, August 1990

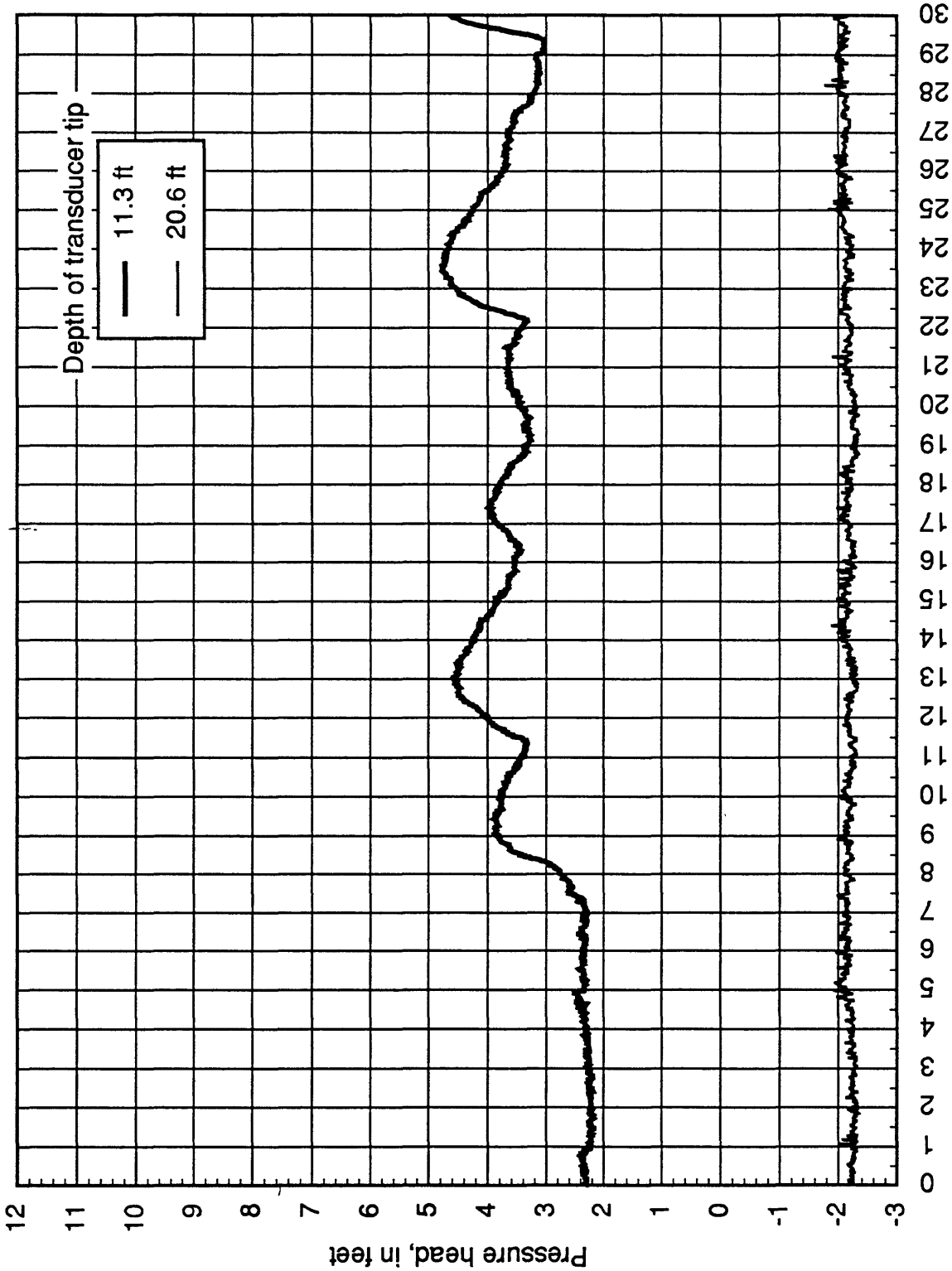

Figure B26. Transducers in boring 22, September 1990

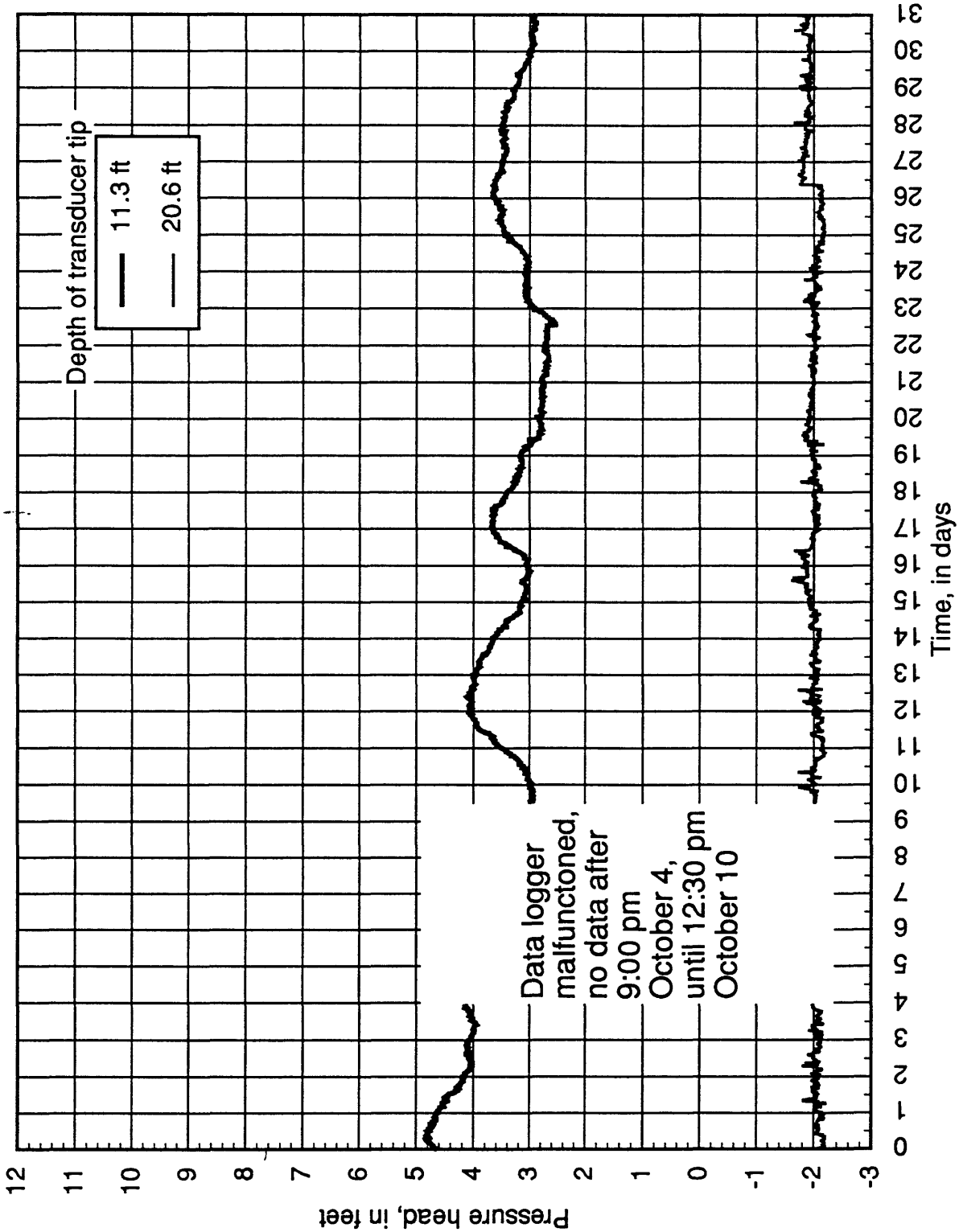

Figure B27. Transducers in boring 22, October 1990

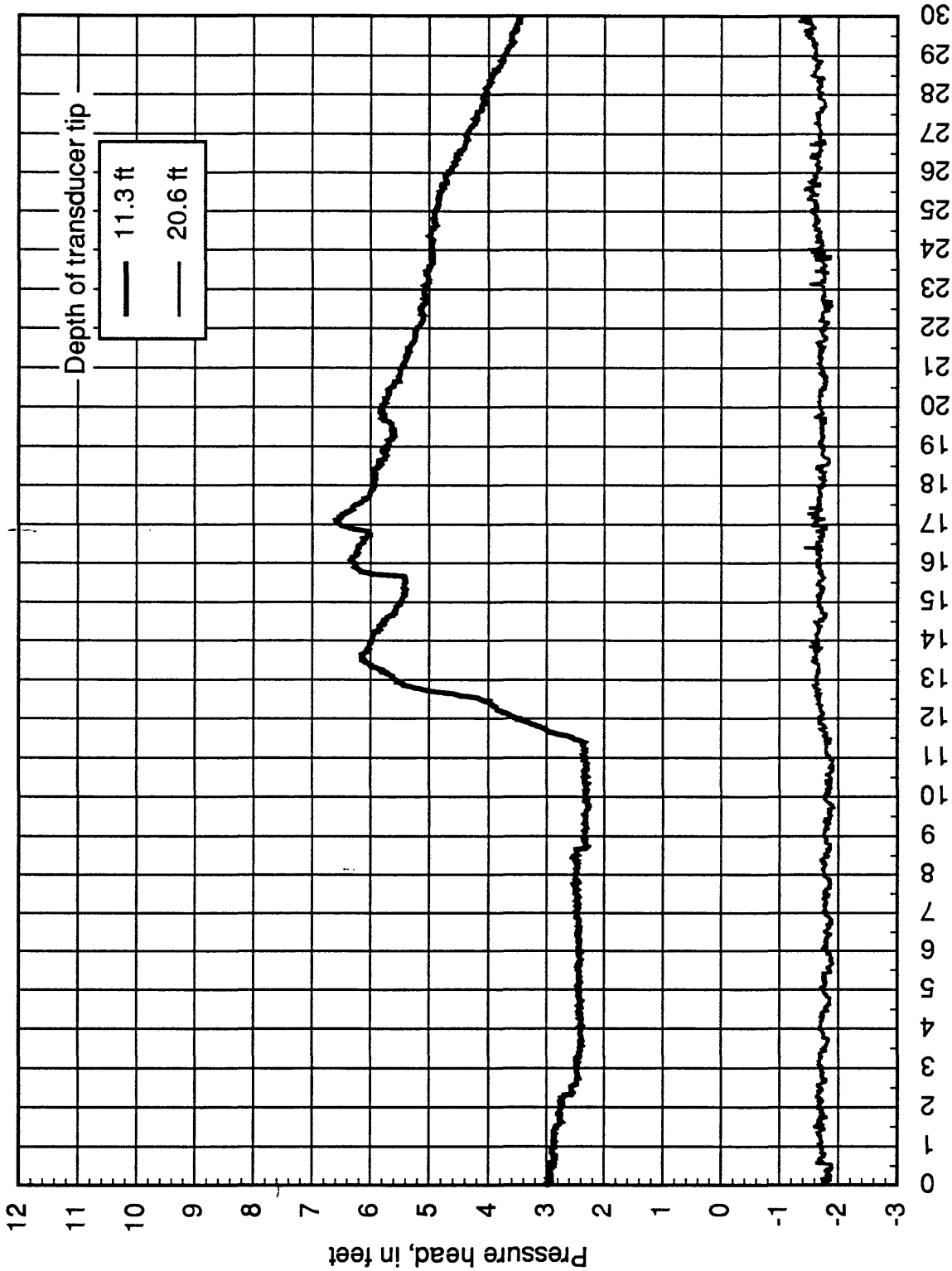

Figure B28. Transducers in boring 22, November 1990

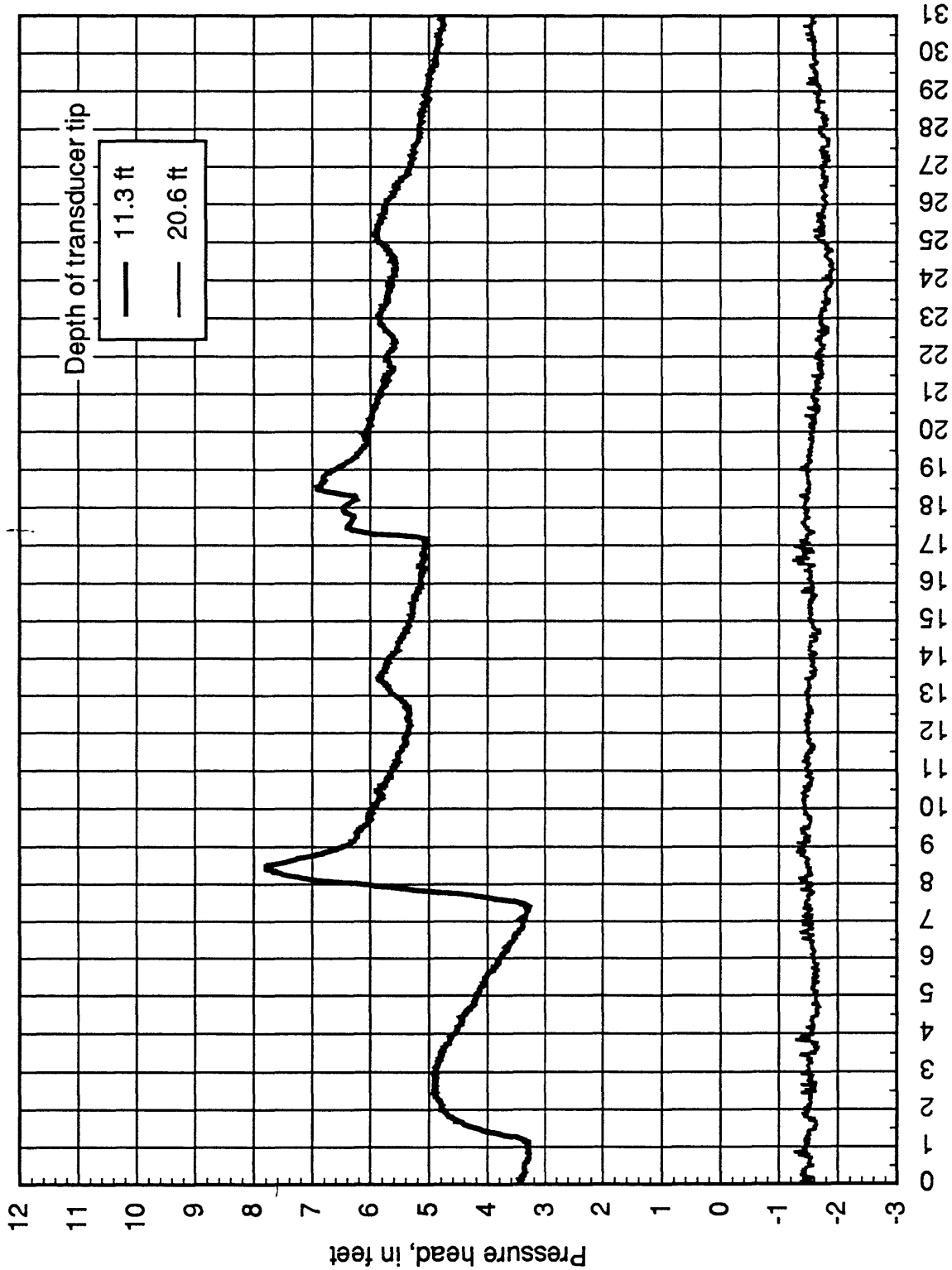

Figure B29. Transducers in boring 22, December 1990

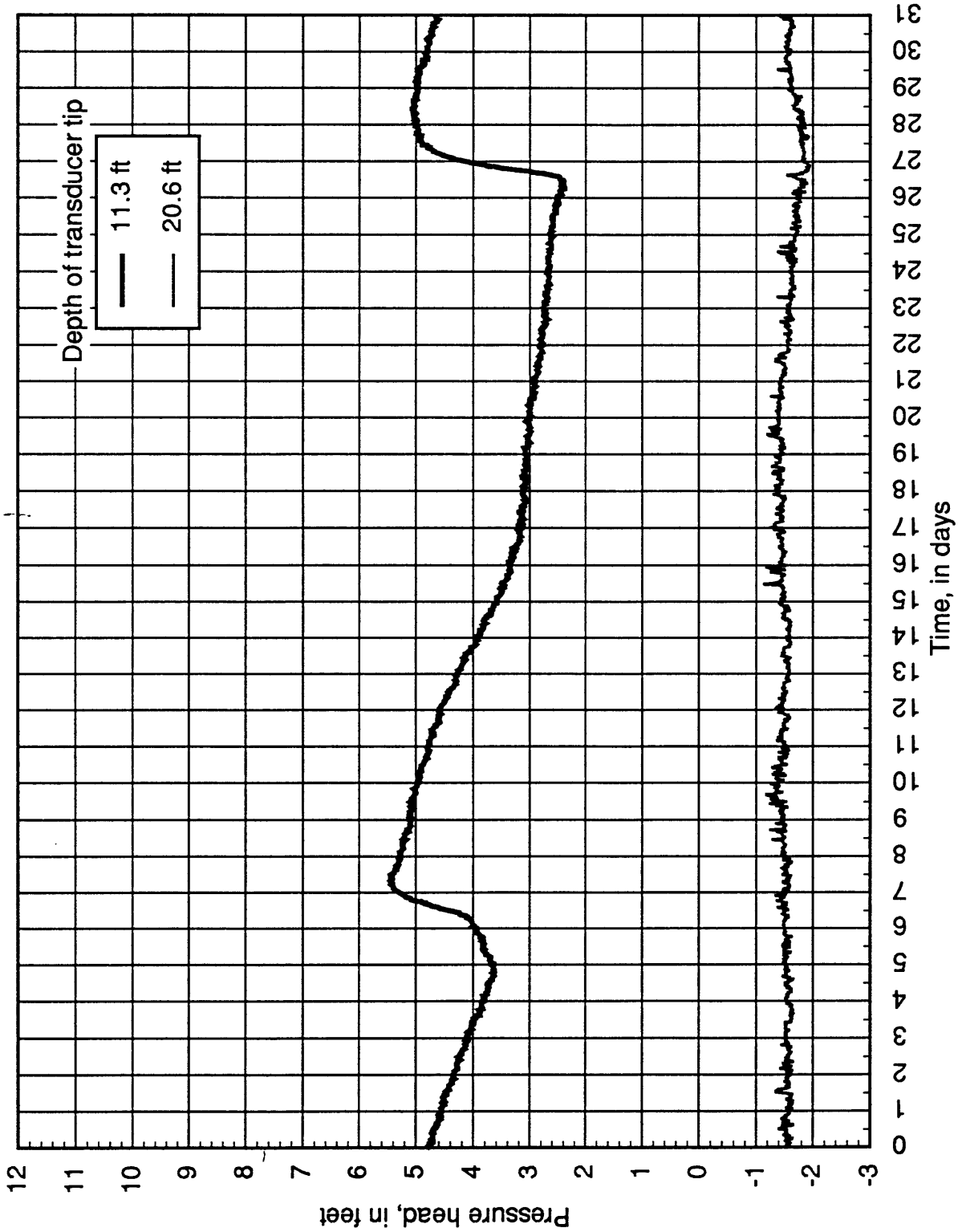

Figure B30. Transducers in boring 22, January 1991

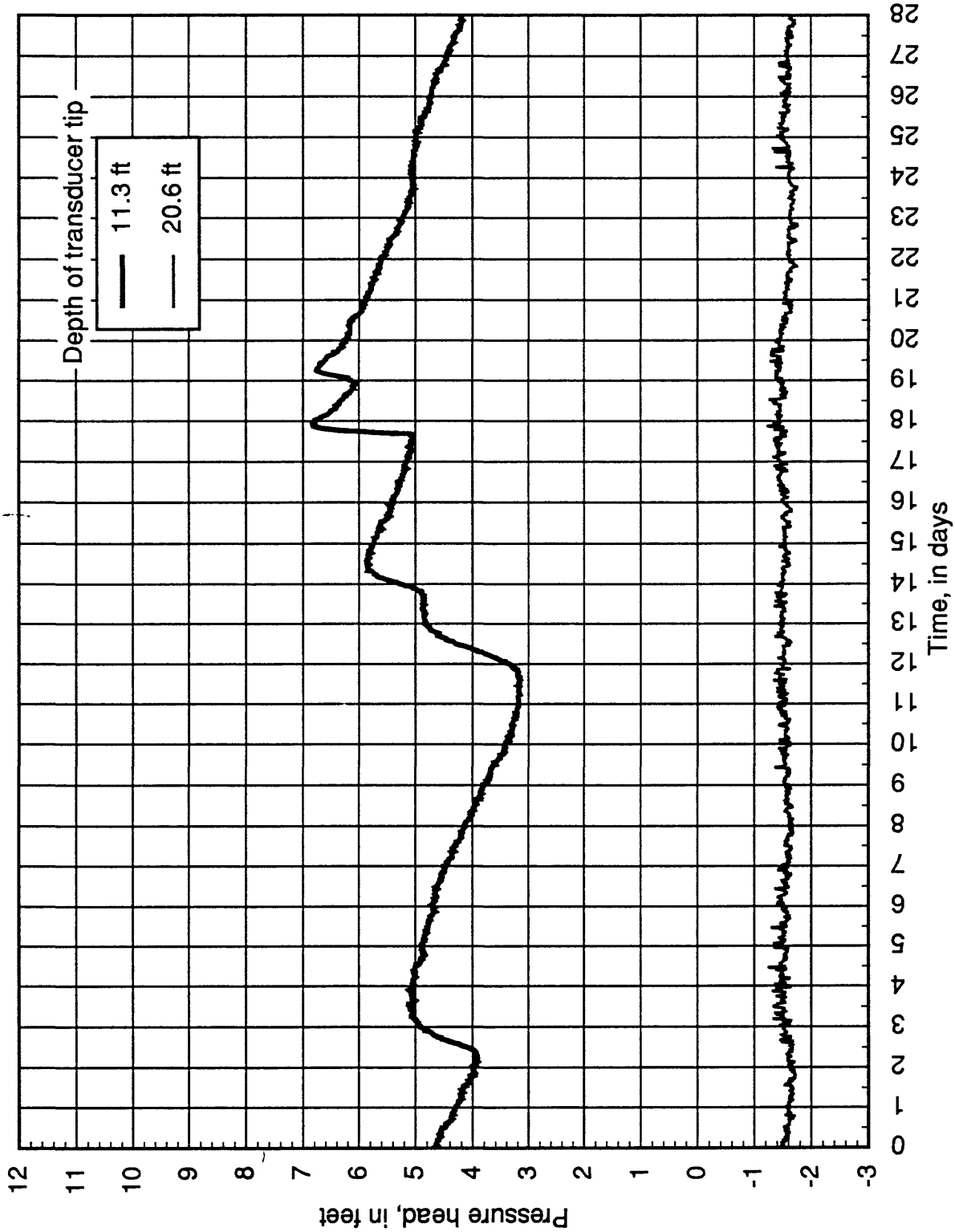

Figure B31. Transducers in boring 22, February 1991

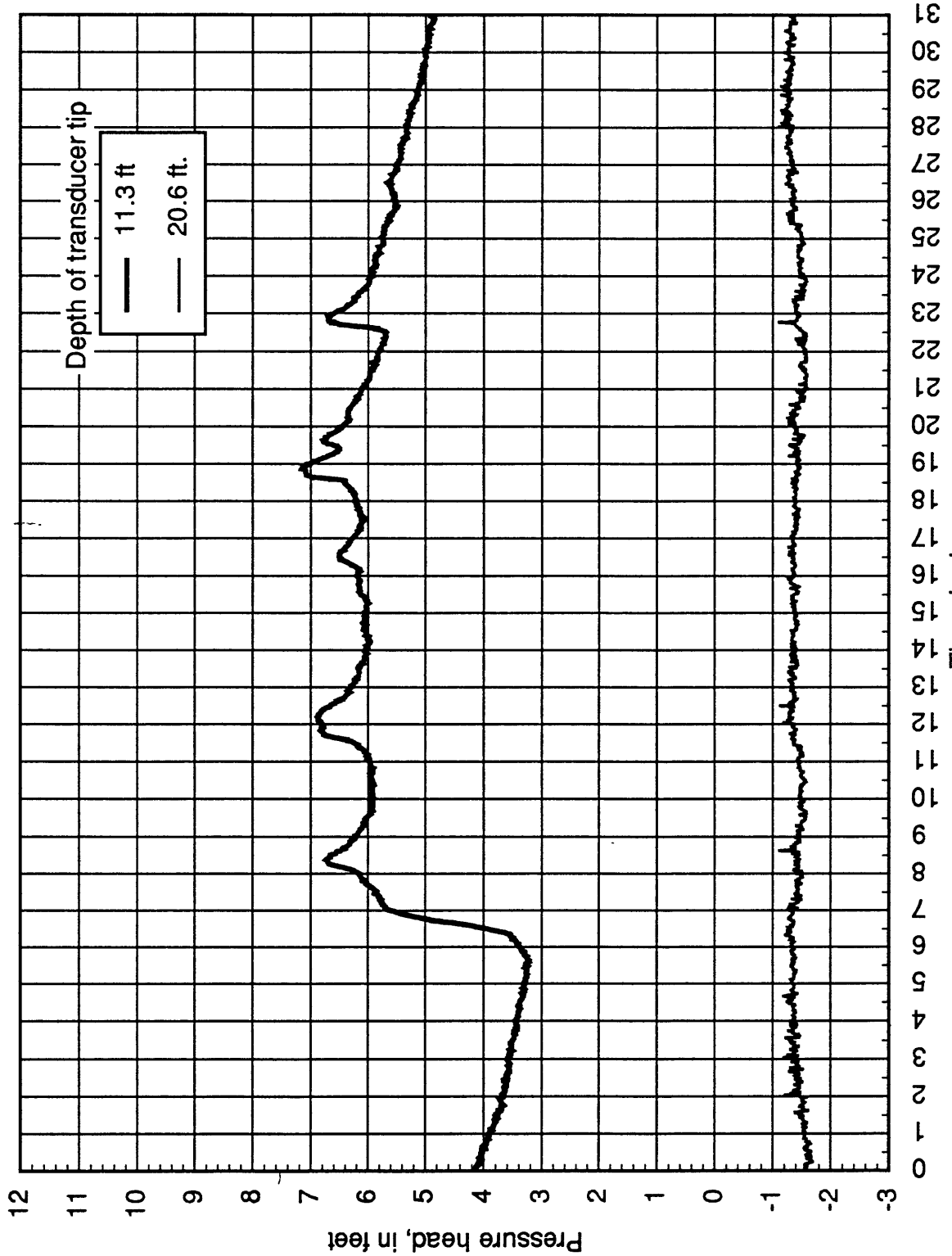

Figure B32. Transducers in boring 22, March 1991

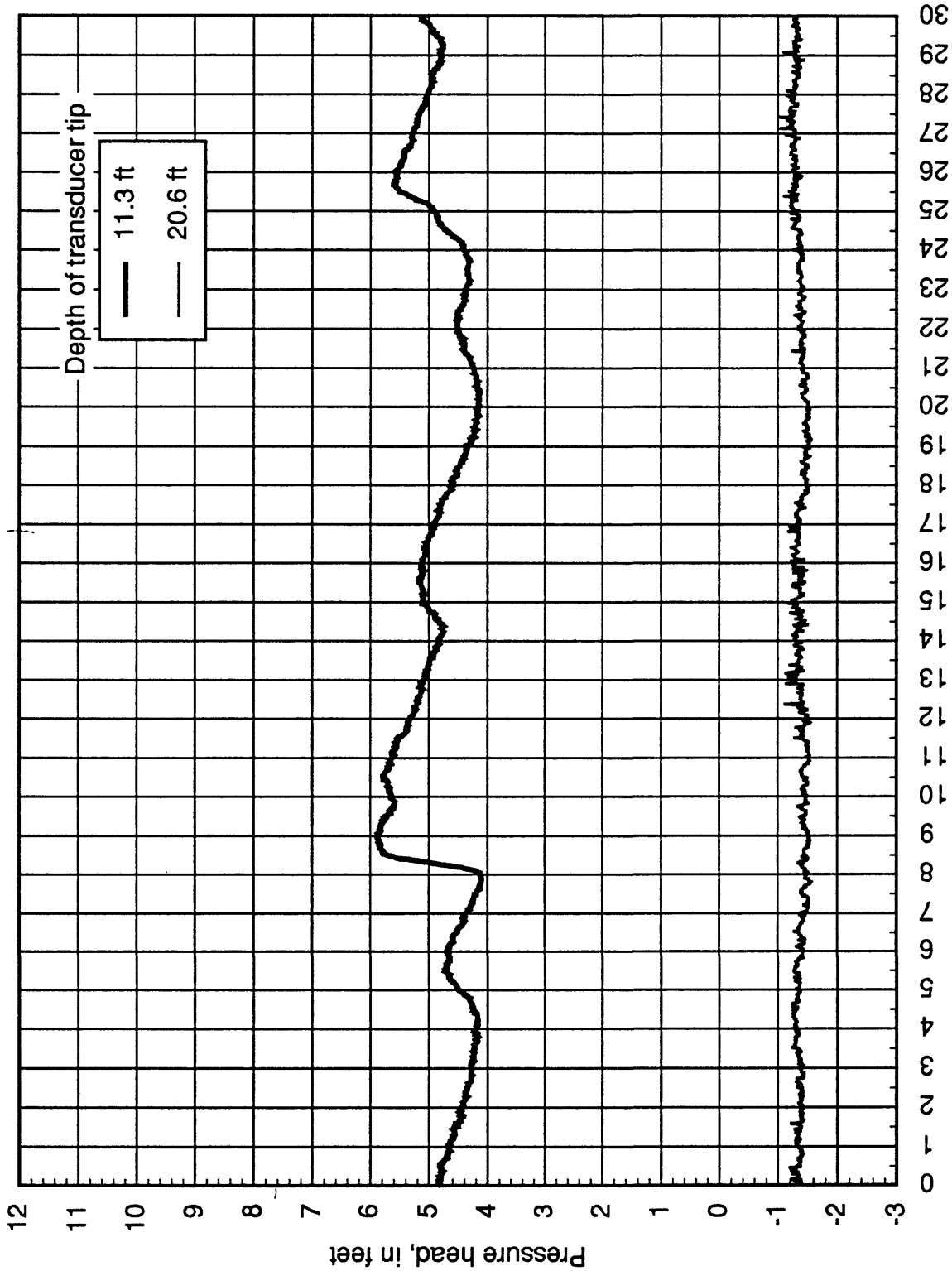

Figure B33. Transducers in boring 22, April 1991

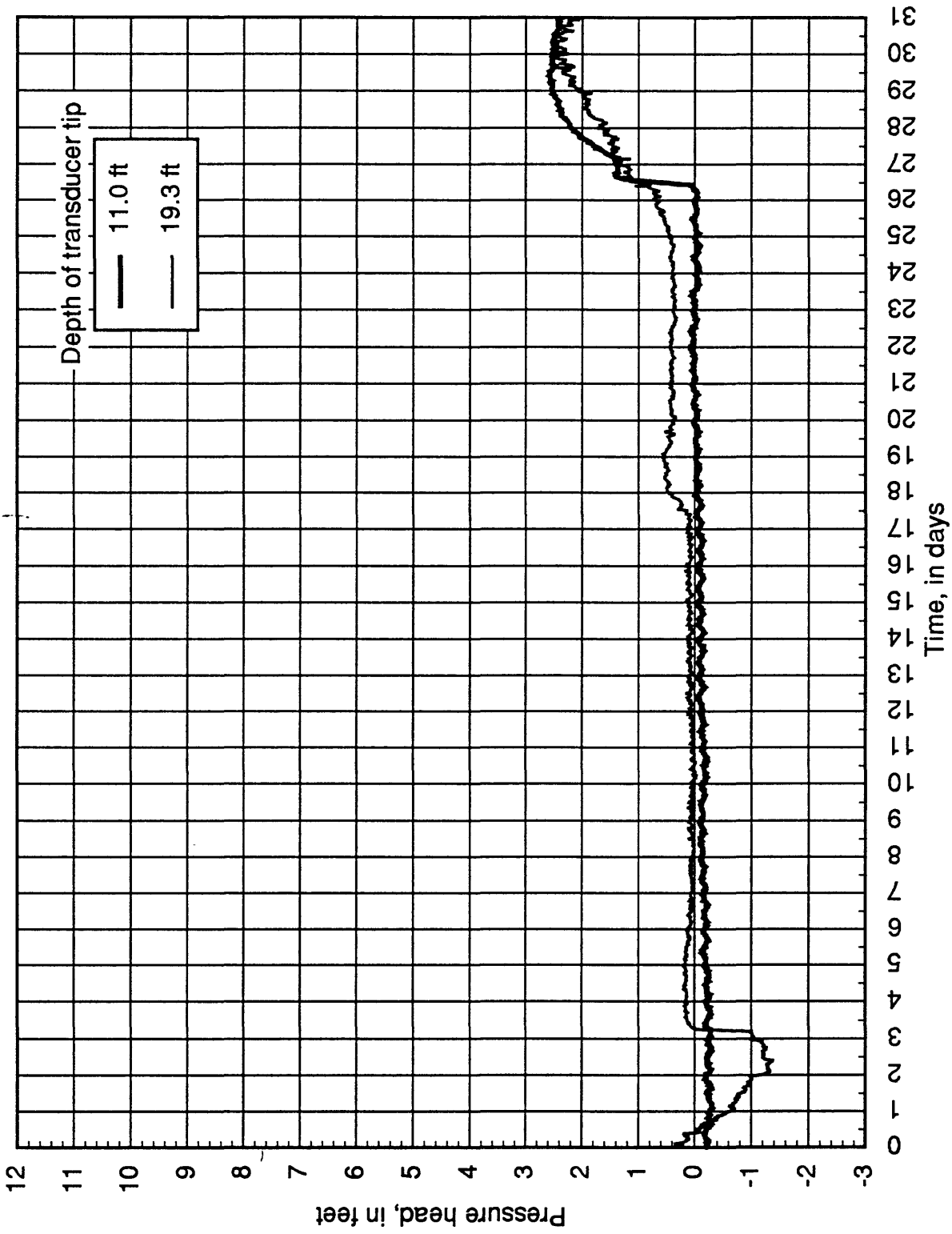

Figure B34. Transducers in boring 24, July 1990

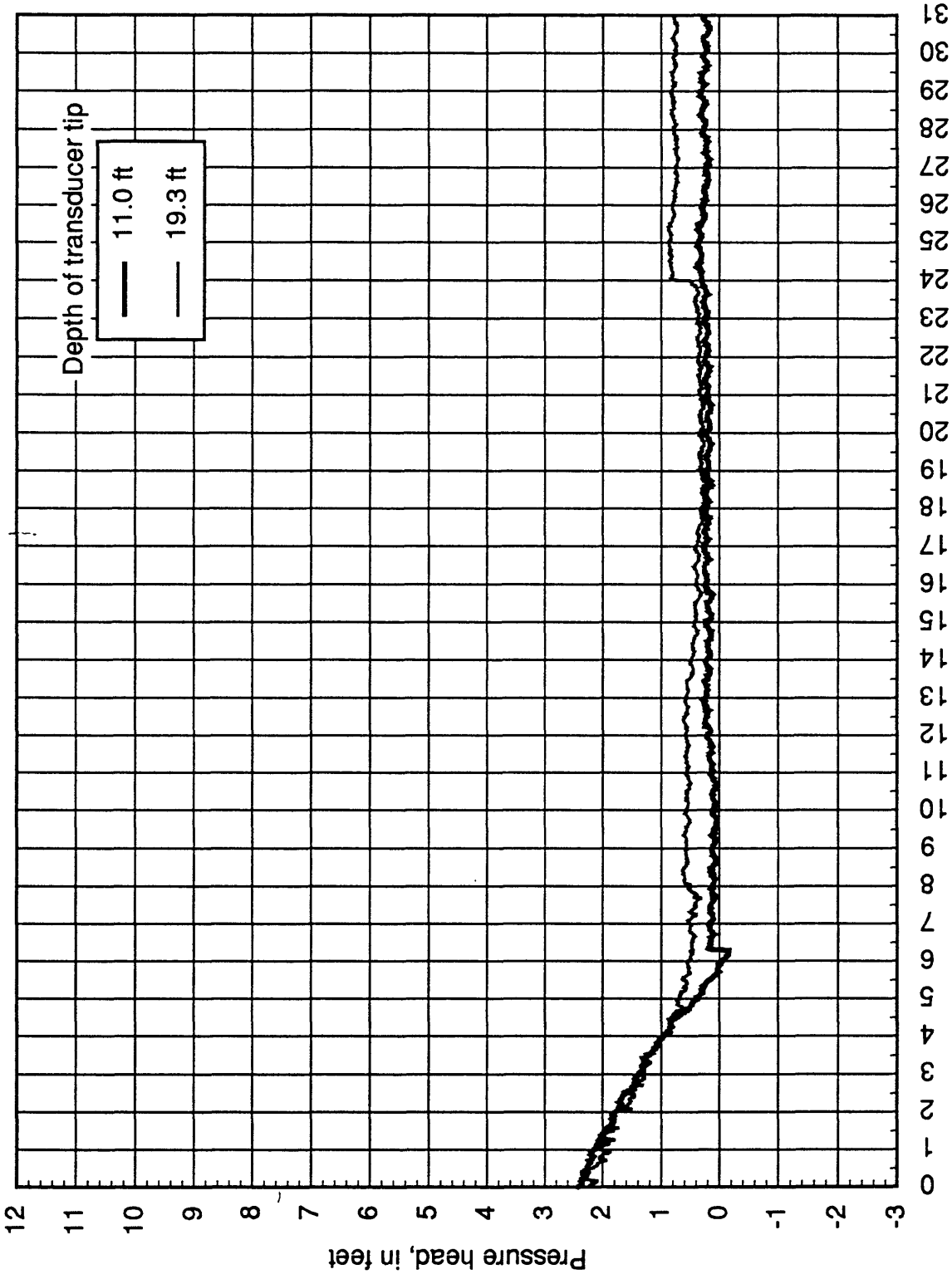

Figure B35. Transducers in boring 24, August 1990

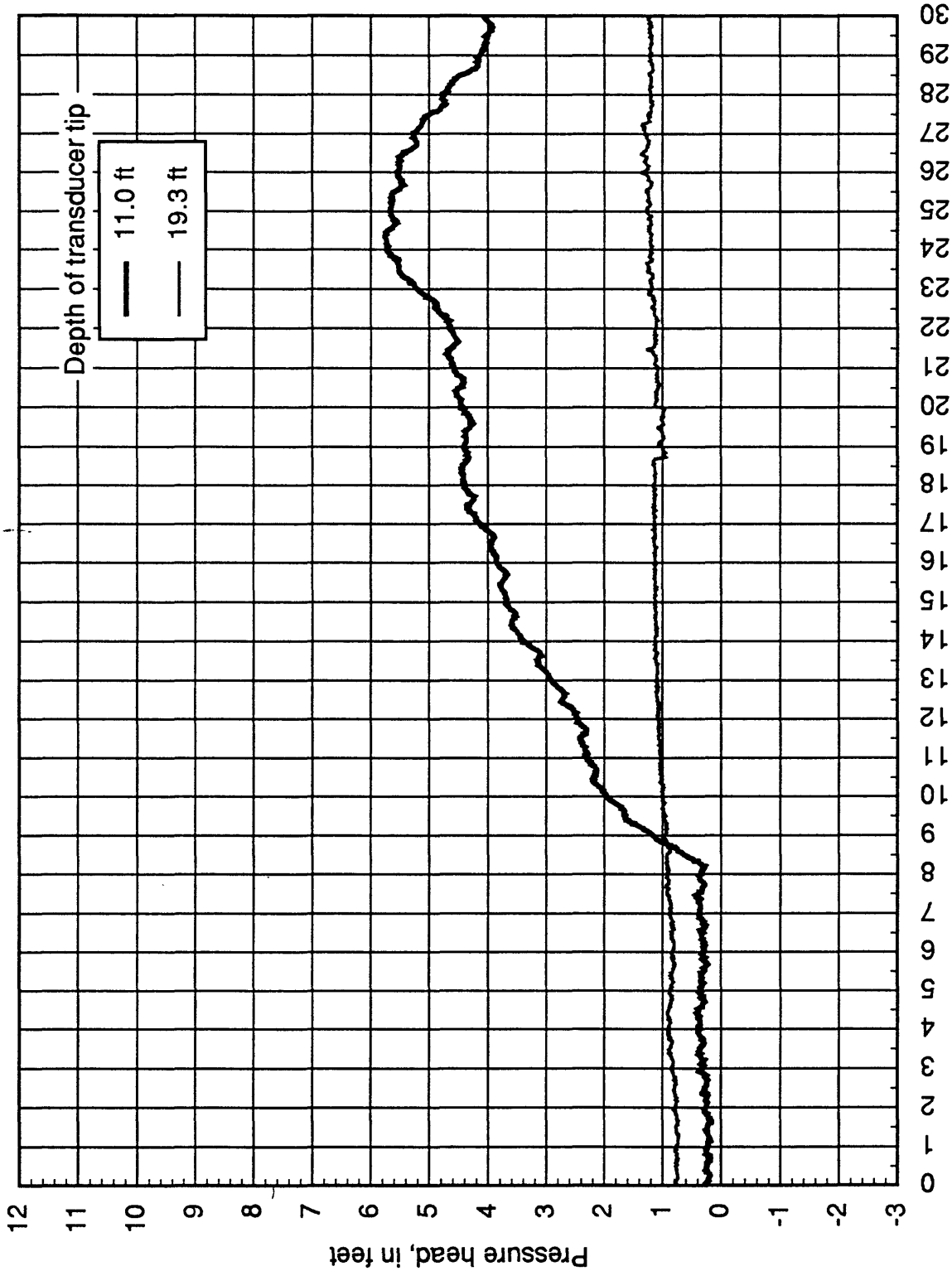

Figure B36. Transducers in boring 24, September 1990

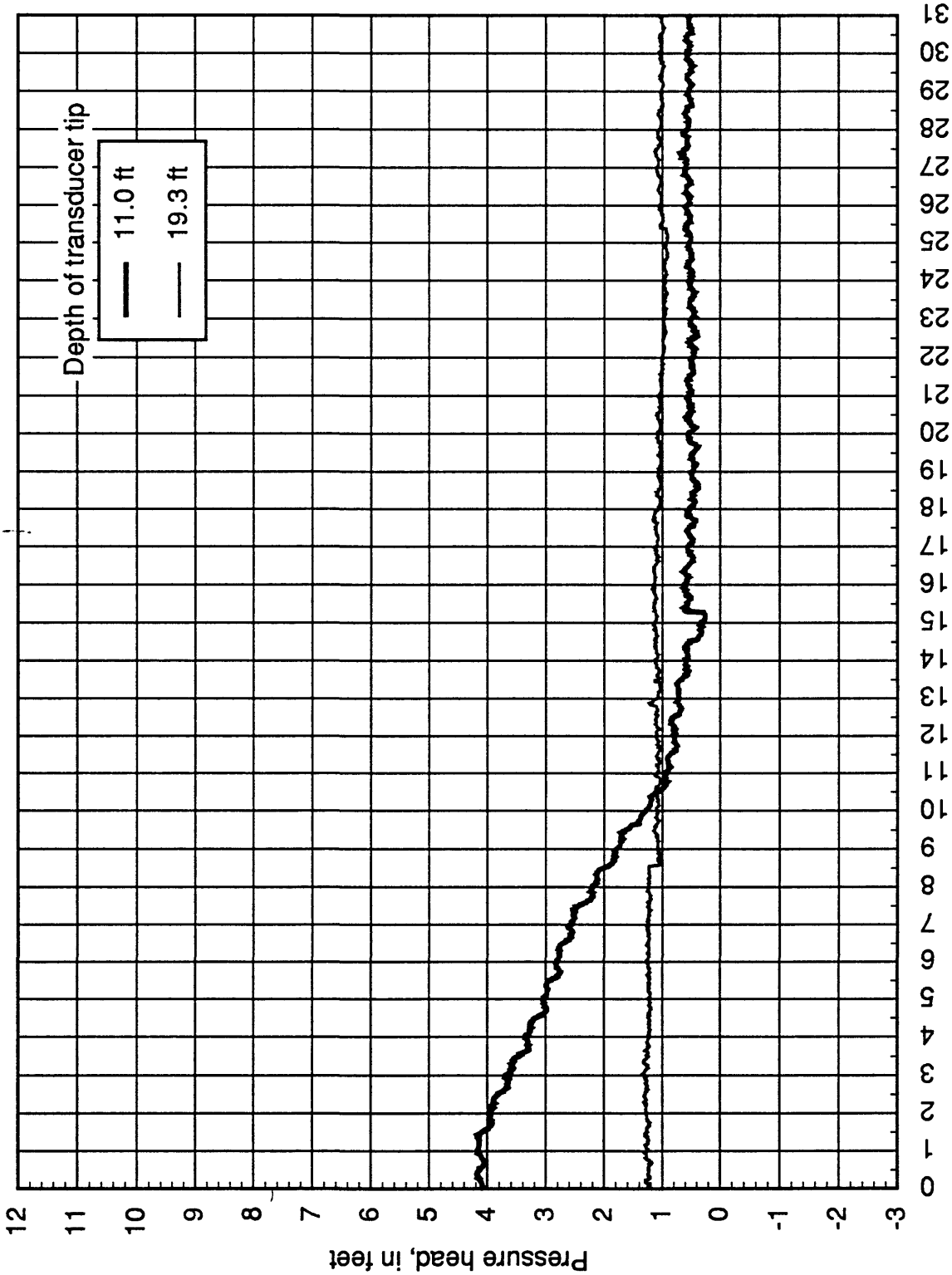

Figure B37. Transducers in boring 24, October 1990

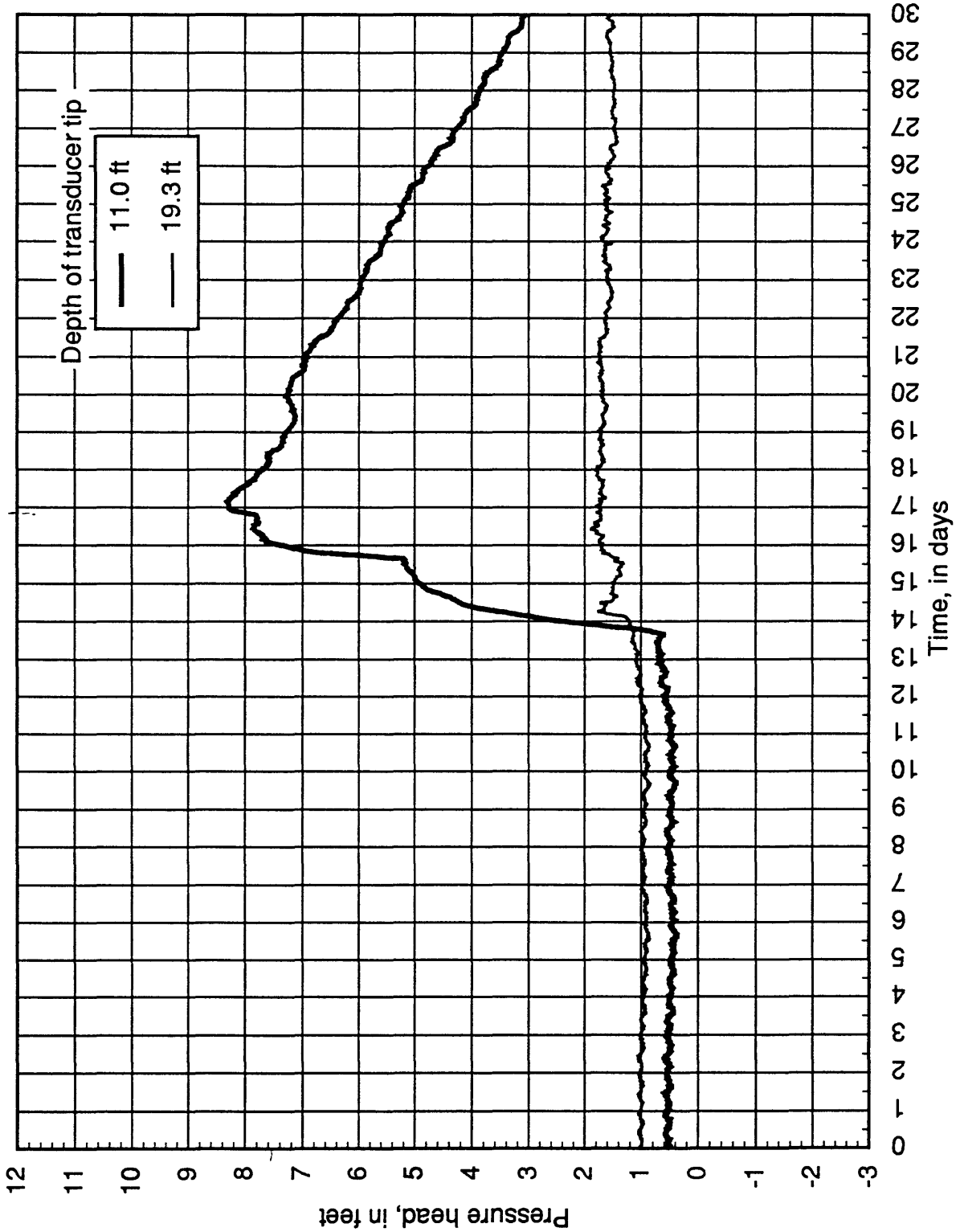

Figure B38. Transducers in boring 24, November 1990

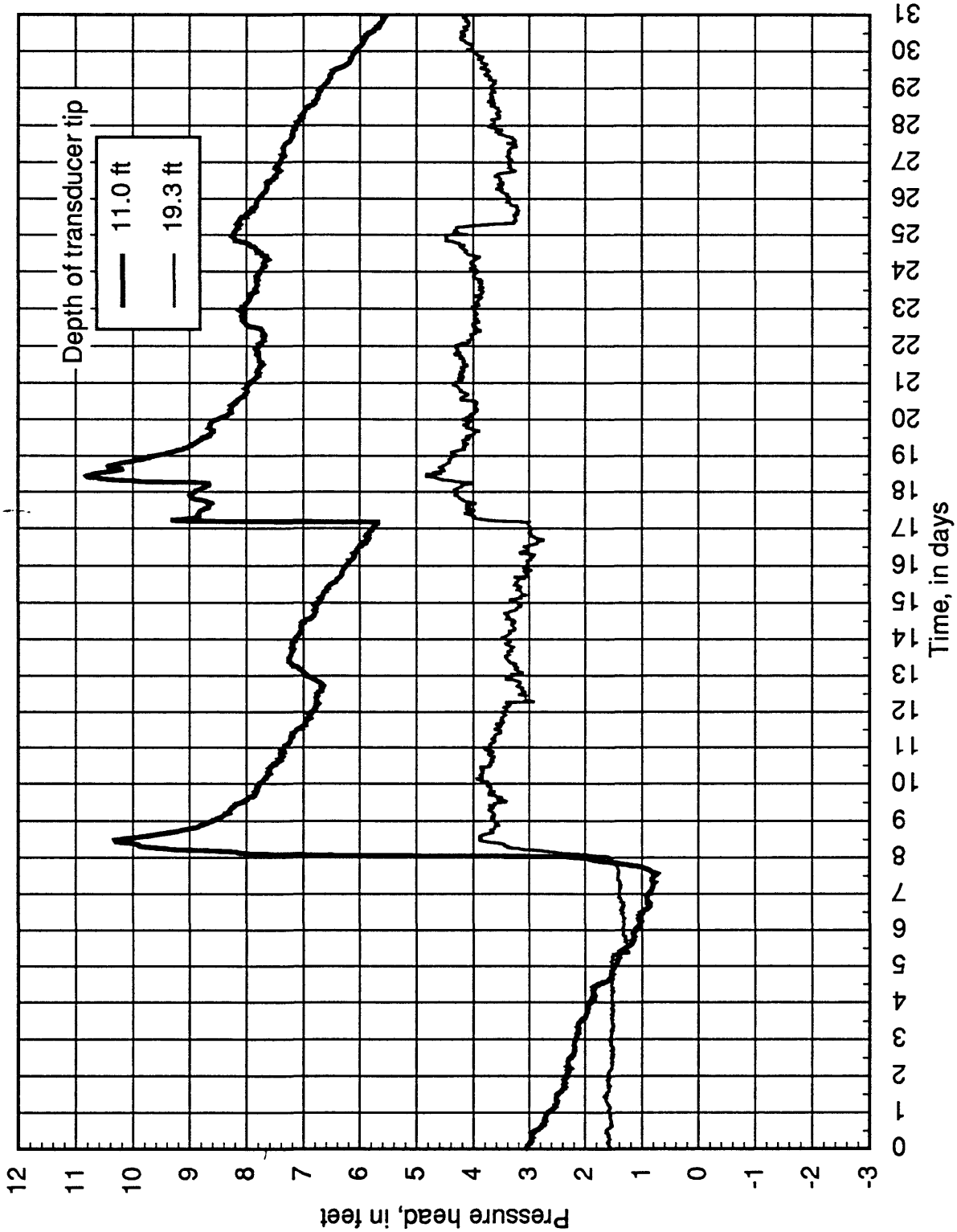

Figure B39. Transducers in boring 24, December 1990

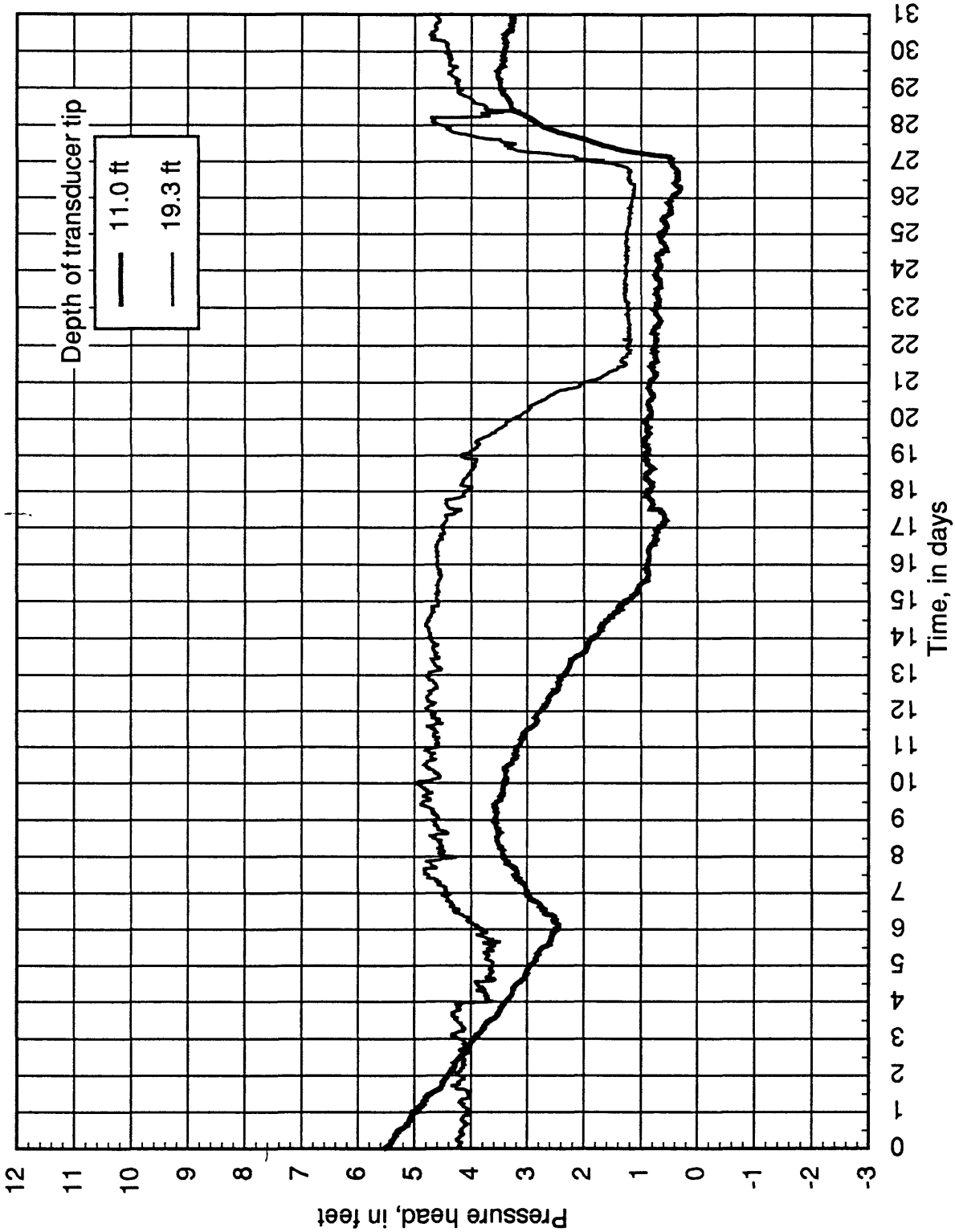

Figure B40. Transducers in boring 24, January 1991

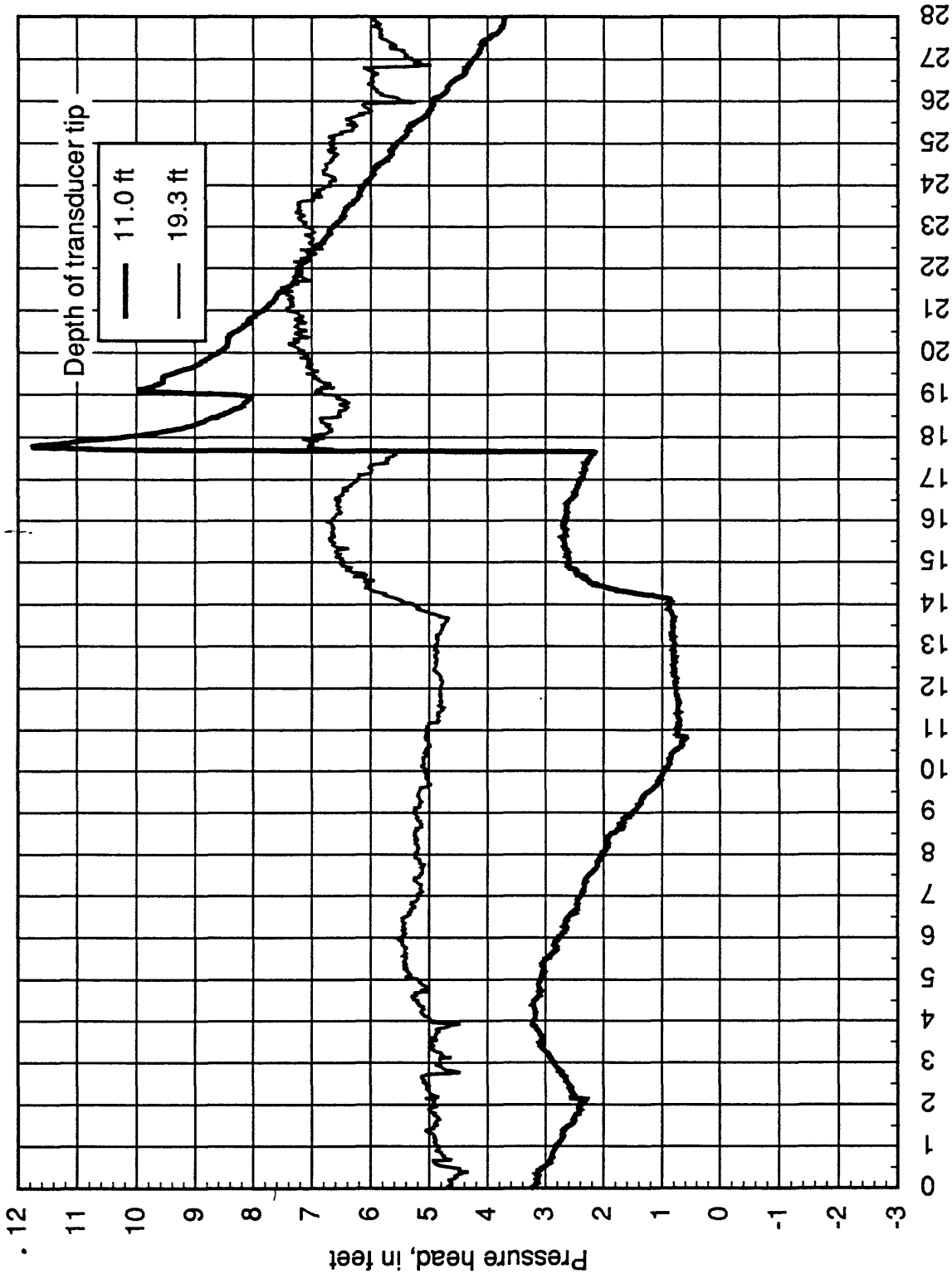

Figure B41. Transducers in boring 24, February 1991

Figure B42. Transducers in boring 24, March 1991

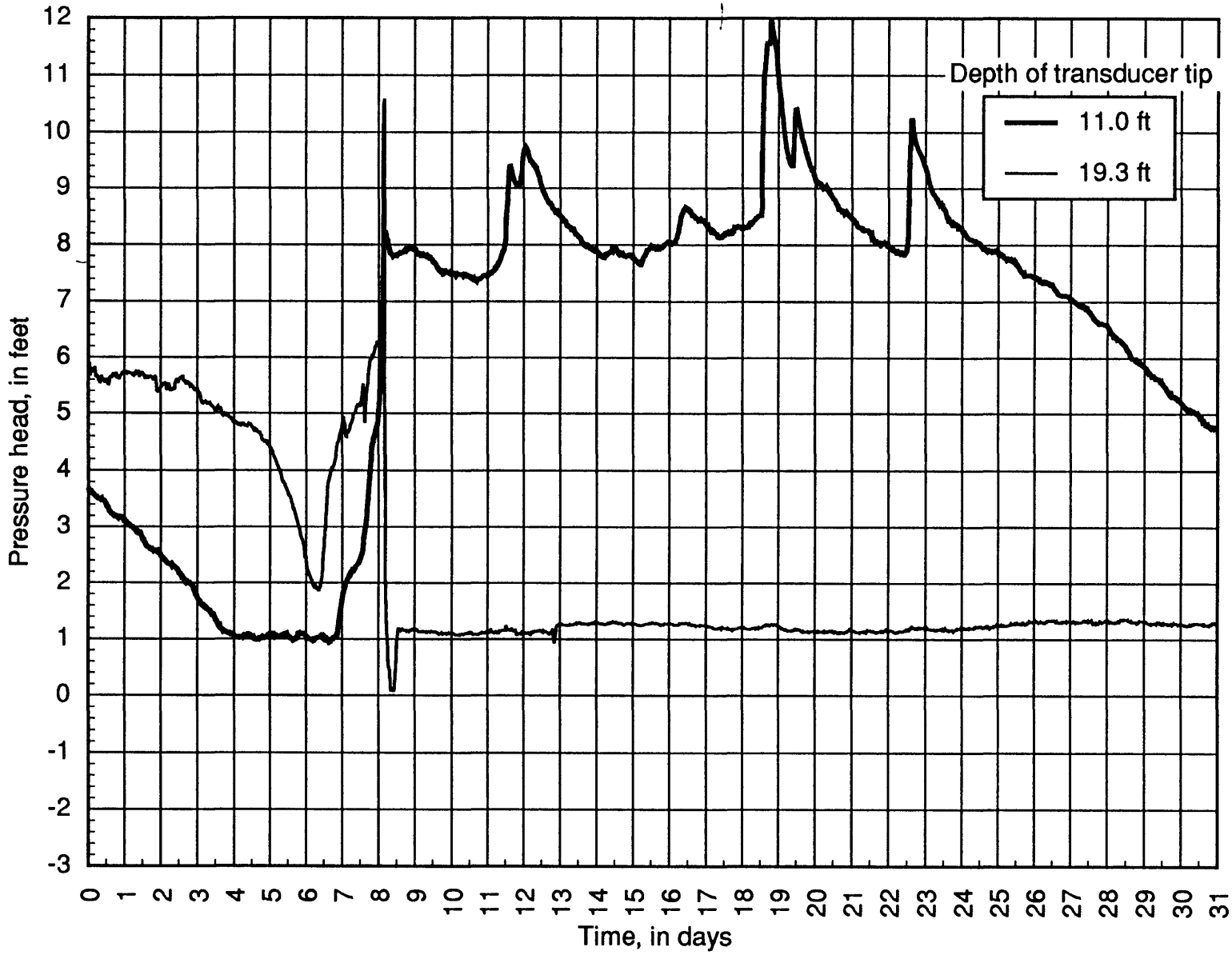

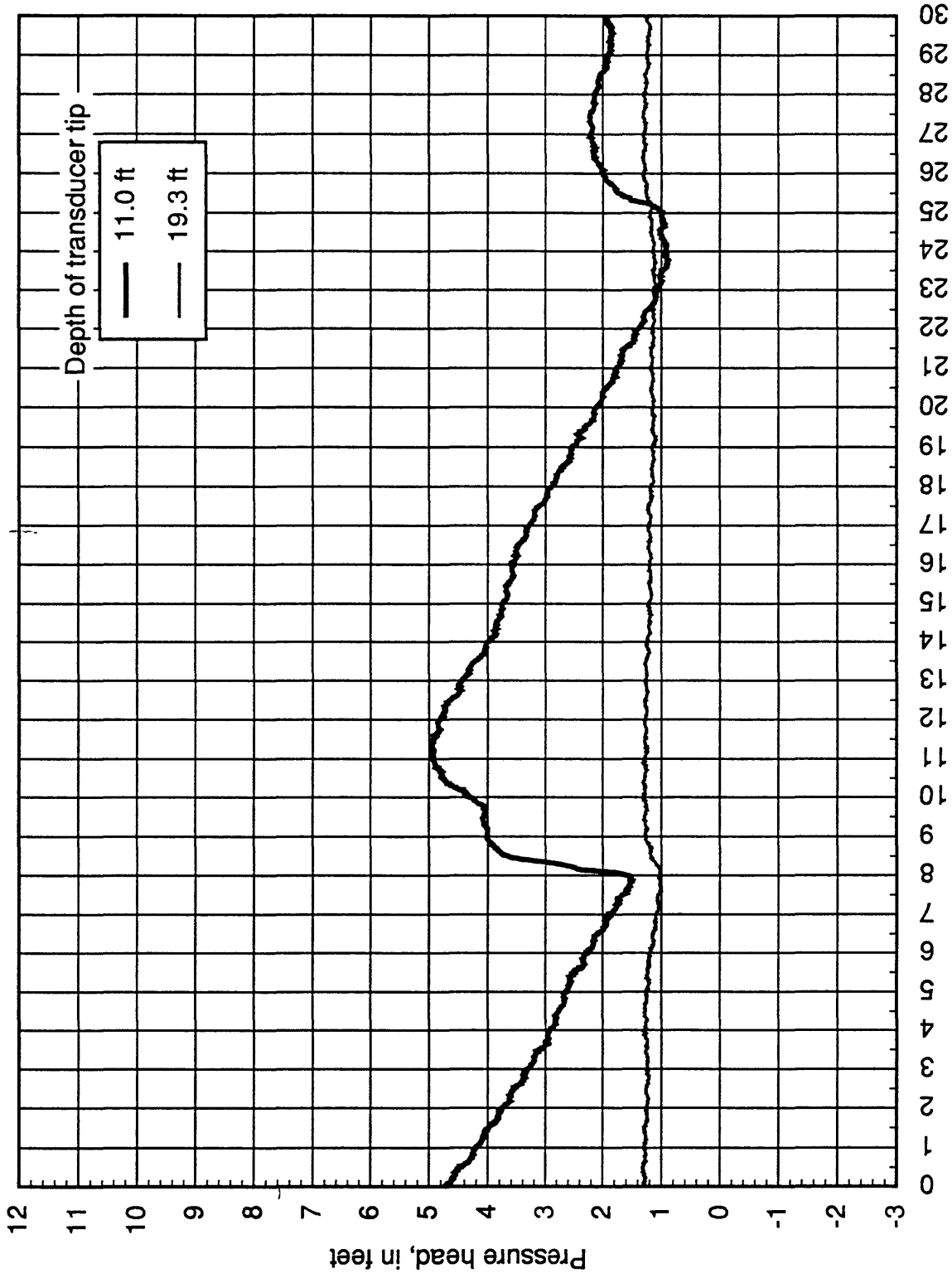

Figure B43. Transducers in boring 24, April 1991

Figure B44. Transducer in boring 29

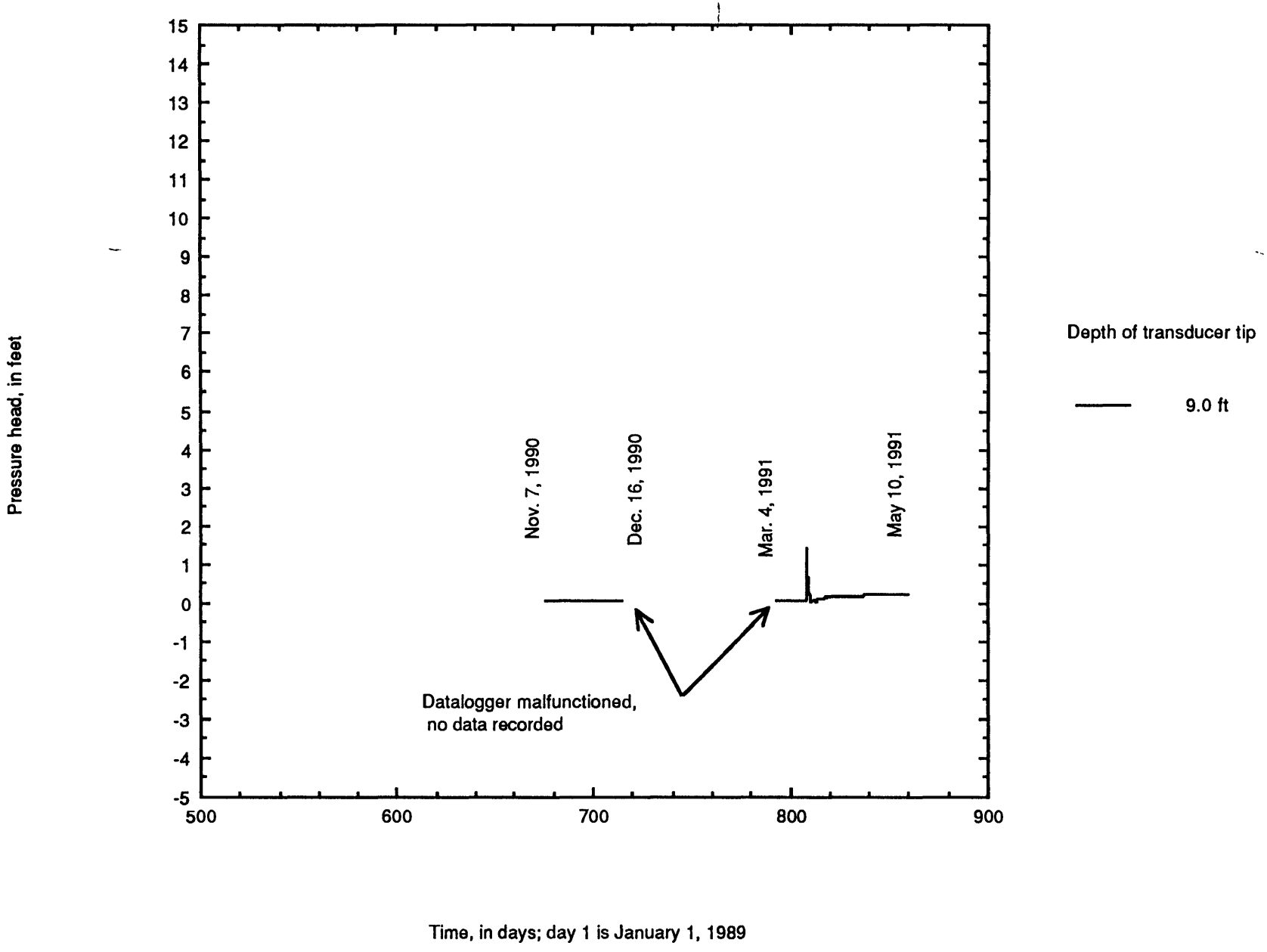

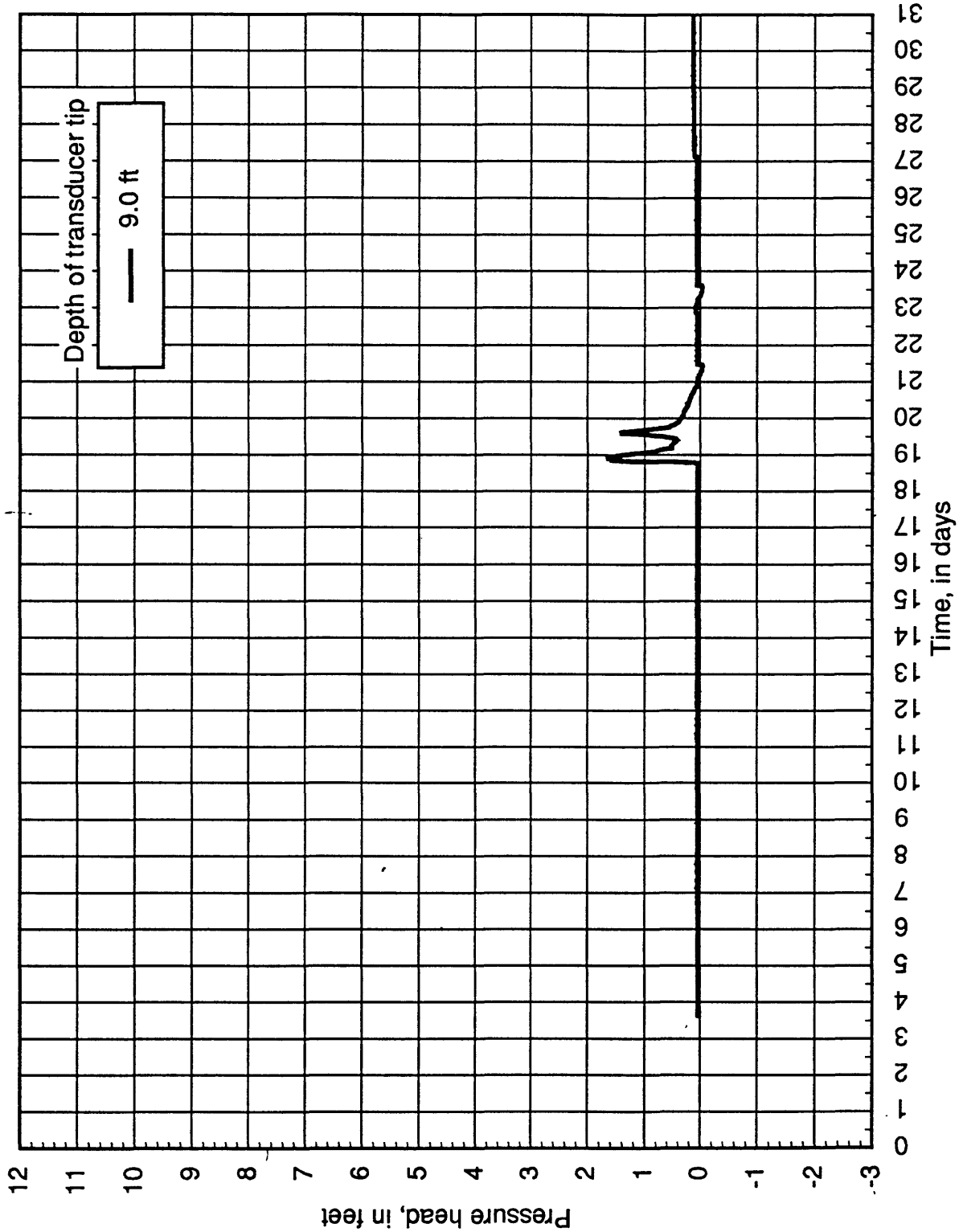

Figure B45. Transducer in boring 29, March 1991

Figure B46. Graph showing response of pore-water pressure in the Alani-Paty landslide to rainfall during November 1990

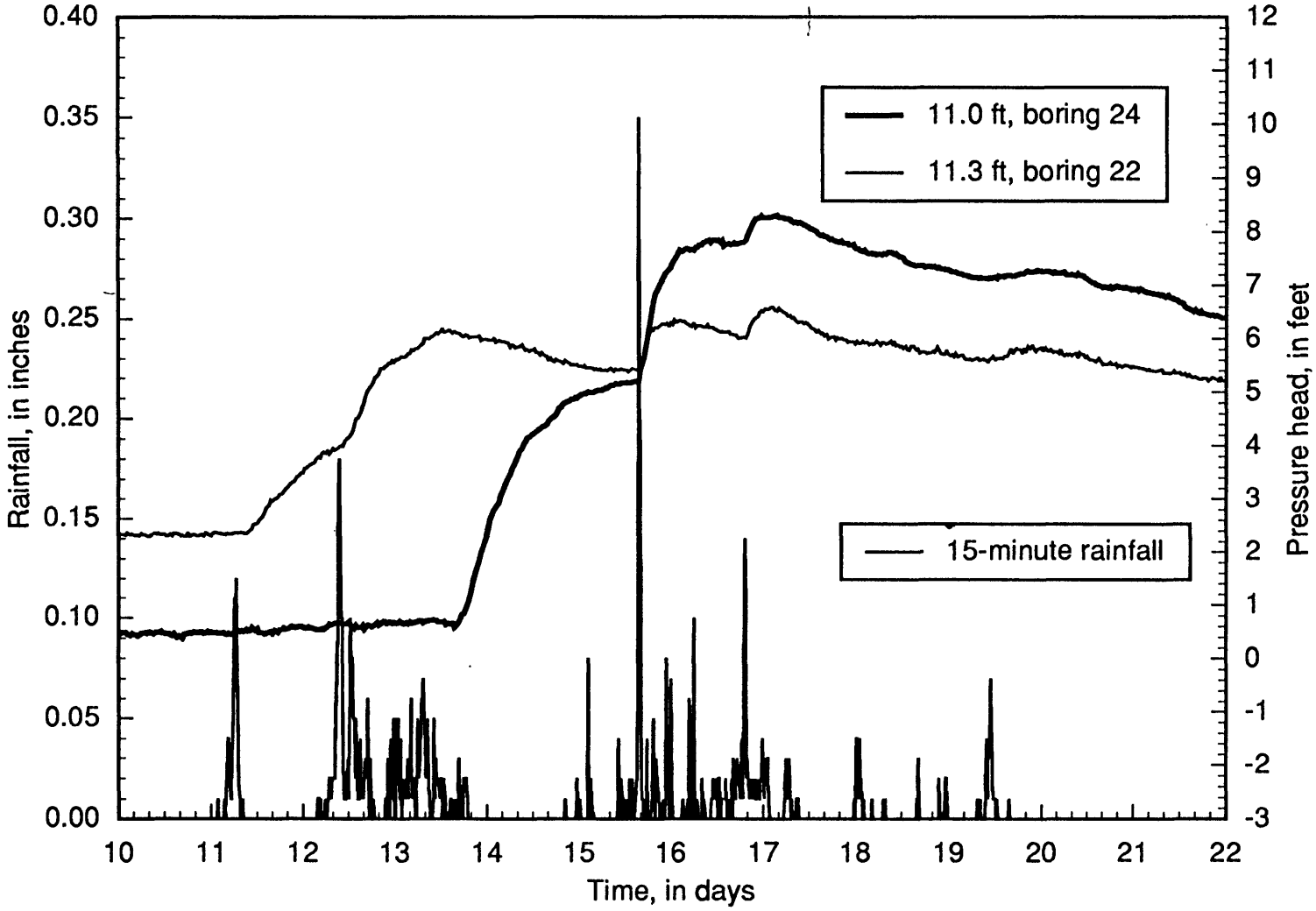

Figure B47. Graph showing response of pore-water pressures in the Alani-Paty landslide to rainfall on December 8 and 9, 1990

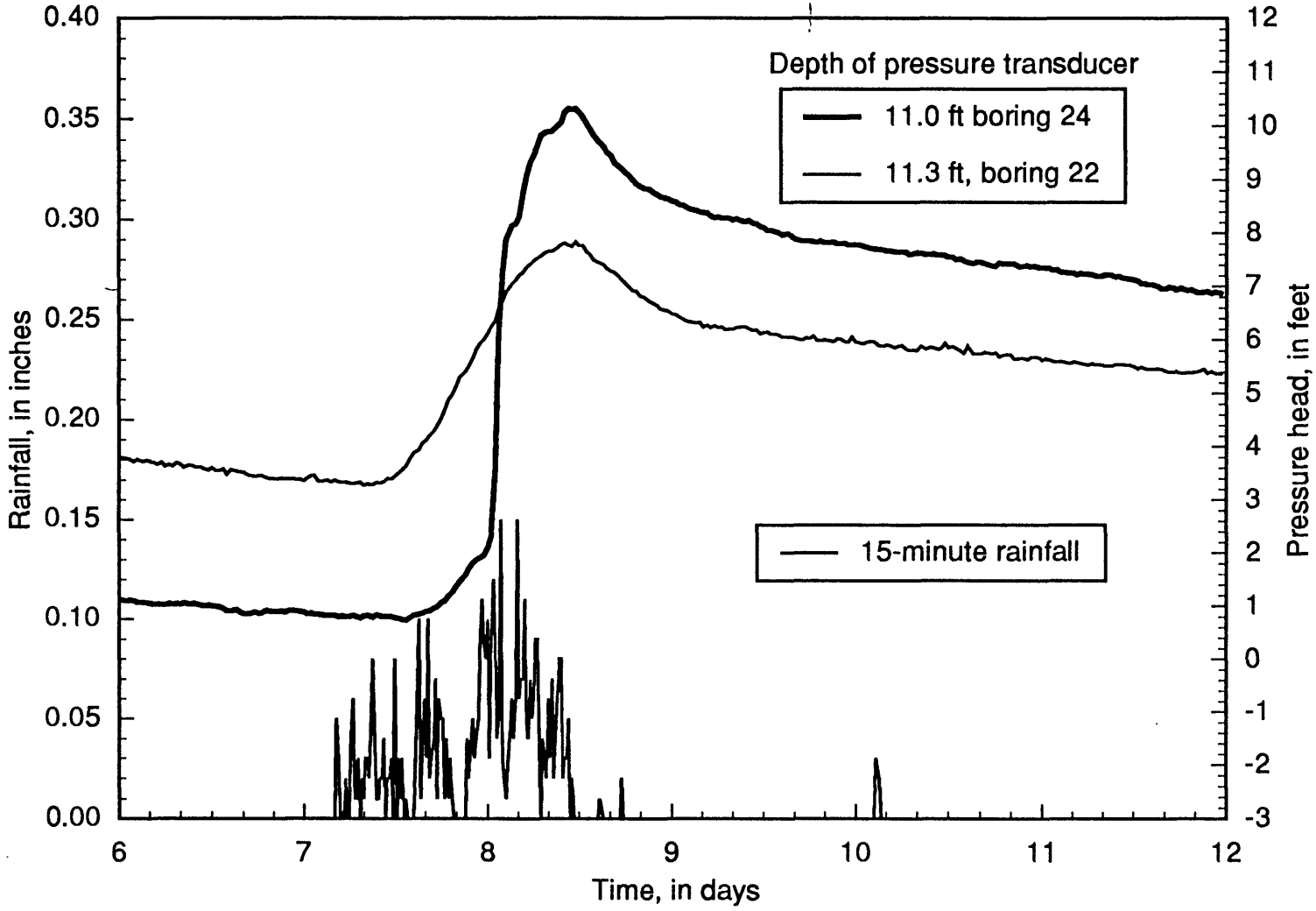

Figure B48. Graph showing response of pore-water pressure in the Alani-Paty landslide to rainfall from March 5 to March 23, 1991

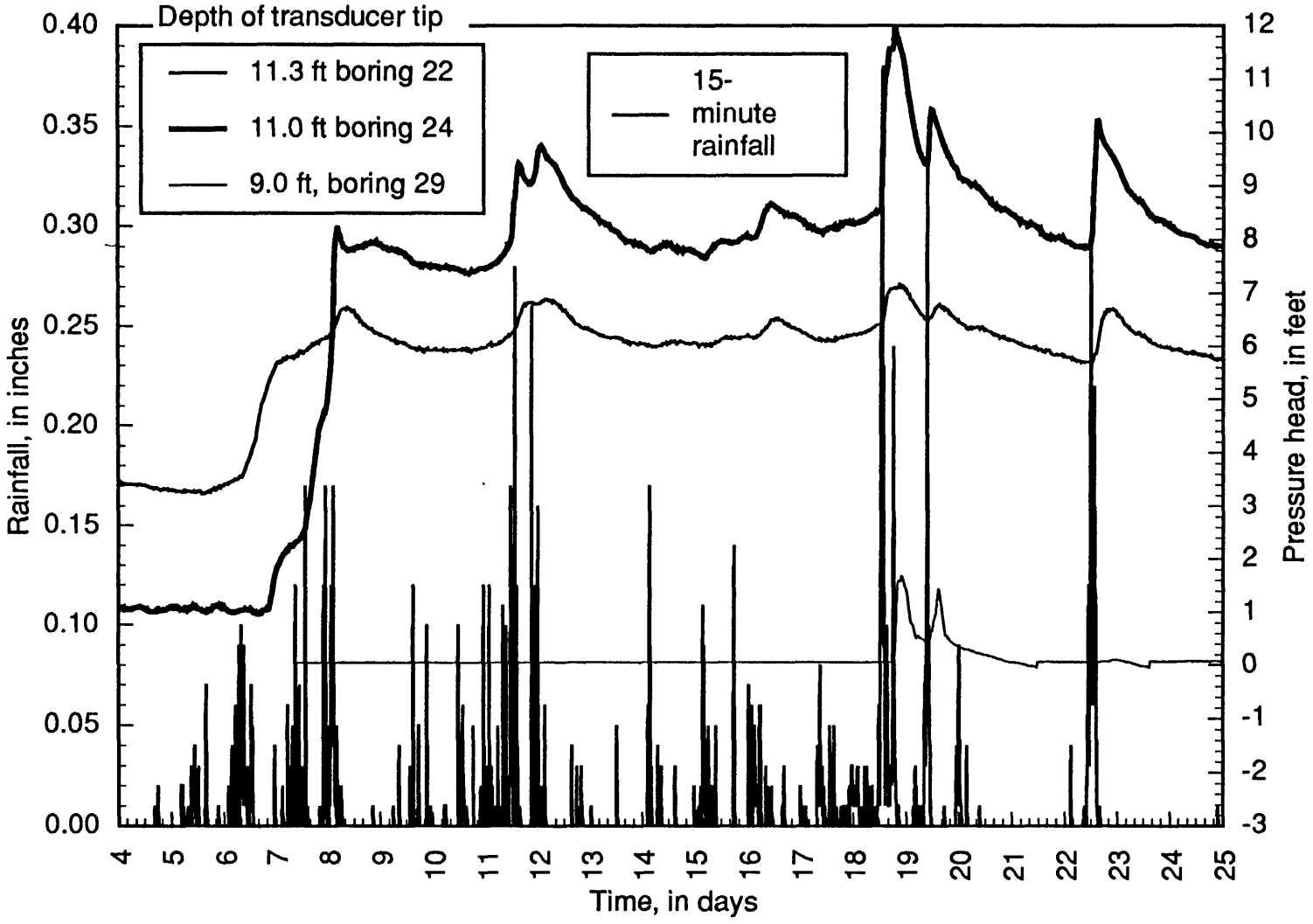

APPENDIX C

Measurement of Precipitation

This appendix contains a map showing locations of rain gauges (figure C1) and graphs of daily rainfall (the only form of precipitation observed during the study period) at 3102 Alani Drive, in the head of the landslide (figs. C2, ..., C13). A tipping-bucket rain gauge (0.01-in.-capacity bucket) at 3102 Alani Drive was monitored continuously by a datalogger that records both 15-minute and daily increments of rainfall. The data logger malfunctioned on February 1, 1991, and no rainfall data were recorded from then until the data logger was replaced at 12:30 p.m. on February 20, 1991.

An estimate of the daily rainfall at 3102 Alani Drive for the first 20 days of February 1991 was constructed by scaling cumulative rainfall measured in a standard 8-in.-diameter gauge at 3102 Alani Drive to the rainfall measured at the University of Hawaii (UH) in Manoa (fig. C14). The estimate has several sources of uncertainty. The amount and timing of rainfall are known to vary spatially in Manoa valley. Rainfall at 3102 Alani was recorded on the following dates: Jan. 25, at 10:00 a.m.; Feb. 1, at 10:49 a.m.; Feb 8, at 10:22 a.m., Feb. 15, at 10:10 a.m., and Feb. 22, at 10:12 a.m. Rainfall at the University of Hawaii was recorded at 7:30 a.m., Monday through Friday. Thus, the Monday reading includes rainfall from the weekend, and readings on other weekday mornings include about 2/3 of the previous day. The tipping bucket rain gauge records daily rainfall at midnight (at days end). In order to compensate for the 7.5 hr difference in timing of measurements at UH and the tipping bucket gauge, our estimates of rainfall are shown one day earlier than the corresponding rainfall measurement at UH (fig. C14). All rainfall between Friday morning and Monday morning was arbitrarily assigned to Sunday.

Cumulative rainfall for approximately a one-year period (From April 24, 1990 to April 26, 1991) at the head of the landslide and at sites on Waahila Ridge is shown in Figure C15. Cumulative rainfall was determined by measuring the accumulation of water in standard 8-in.-diameter rain gauges at intervals of approximately one or two weeks. Two gauges were used at site 1; gauge 1A was on the leeward side of a small ridge protruding from the cliff face of Waahila Ridge, and 1B was on the windward side of the same ridge. Rainfall recorded in gauges 1A and 1B was practically identical. Gauges 1A and 2 were installed on August 10, 1989, gauge 3 was installed on September 12, 1989, and gauge 1B was installed on March 16, 1990. The gauges on Waahila ridge (1A, 1B, and 2) were removed.on April 26, 1991.

Figure C16 is a graph of daily increments of rainfall for the period from September 25, 1989 until April 30, 1991. The time scale on the graph is the same as on the graphs of water levels in piezometers in Appendix B (figures B1, ..., B19).

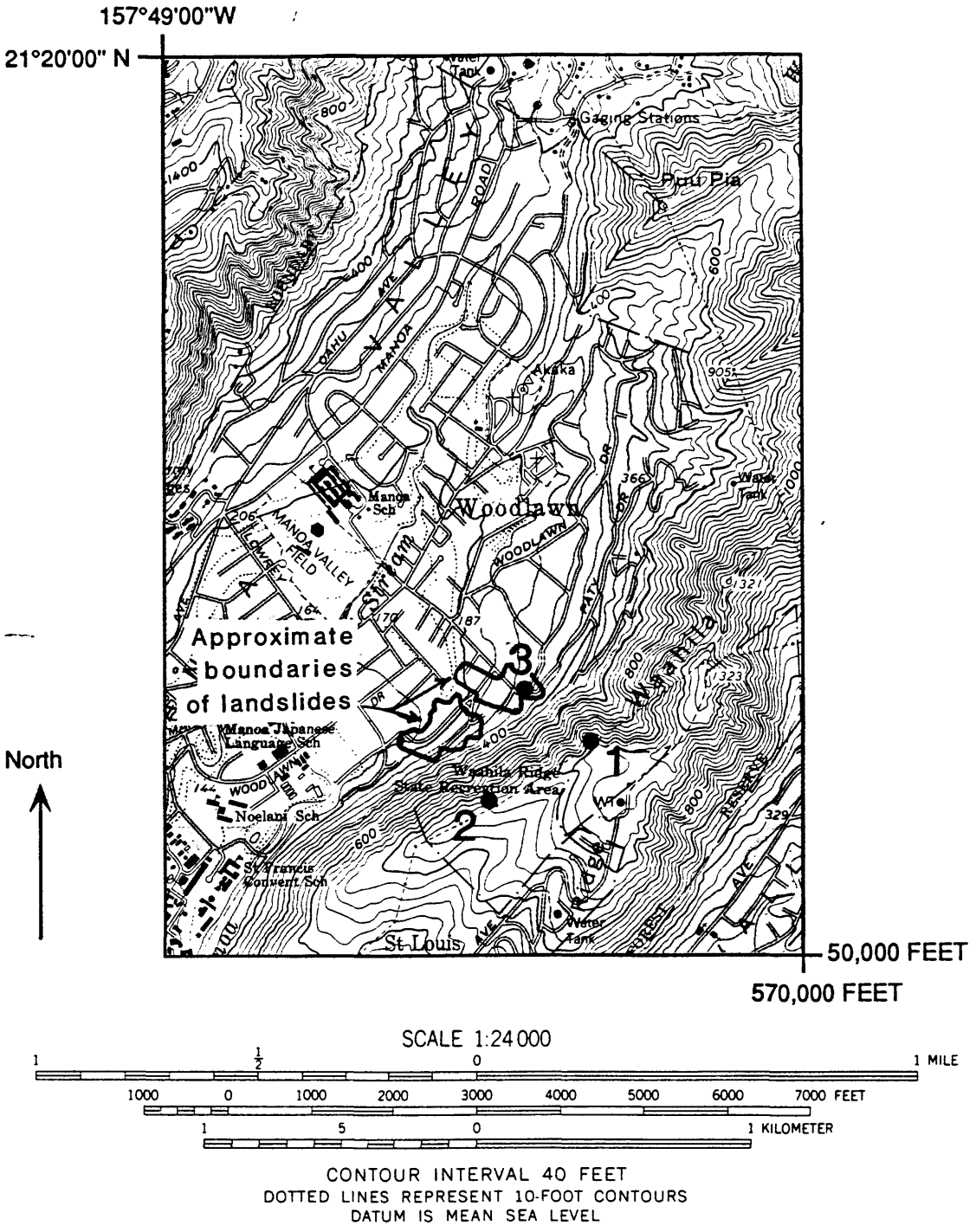

Figure C1. Map showing locations of rain gauges in the study area. Site 1 had two 8-in. cans, site 2 had one 8-in. can, and site 3 had one 8-in. can and one-tipping bucket rain gauge. Base from U.S. Geological Survey, Honolulu, Hawaii, 7-1/2 minute quadrangle, 1983.

Figure C2. Daily rainfall during May 1990

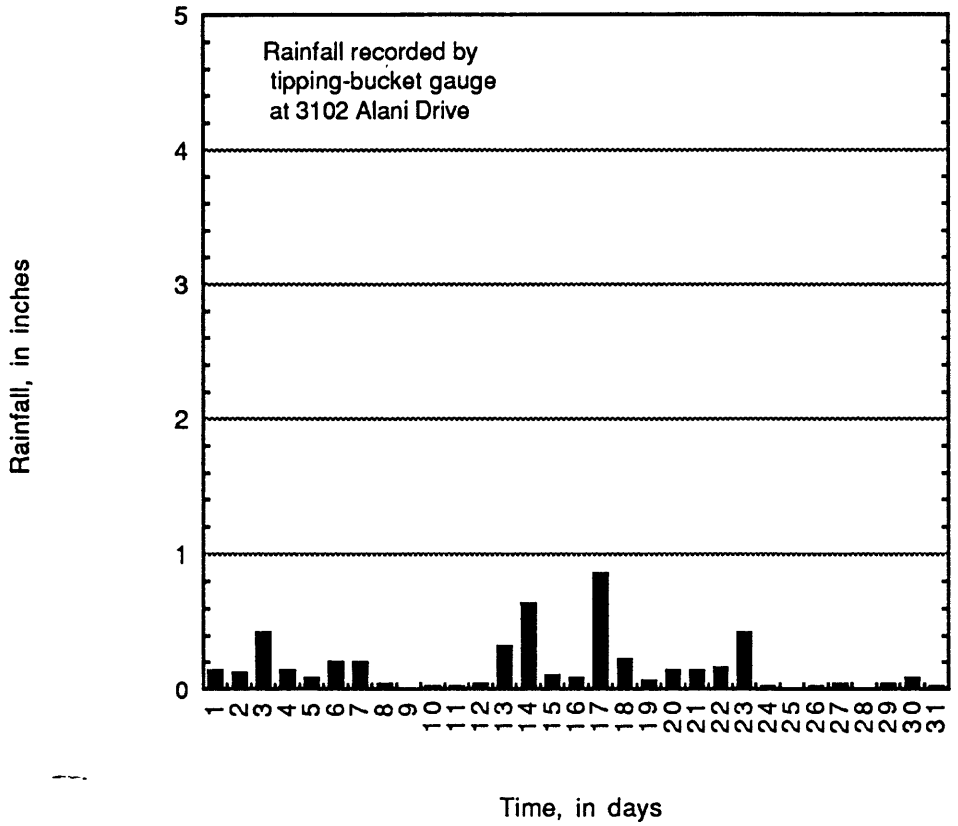

Figure C3. Daily rainfall during June 1990

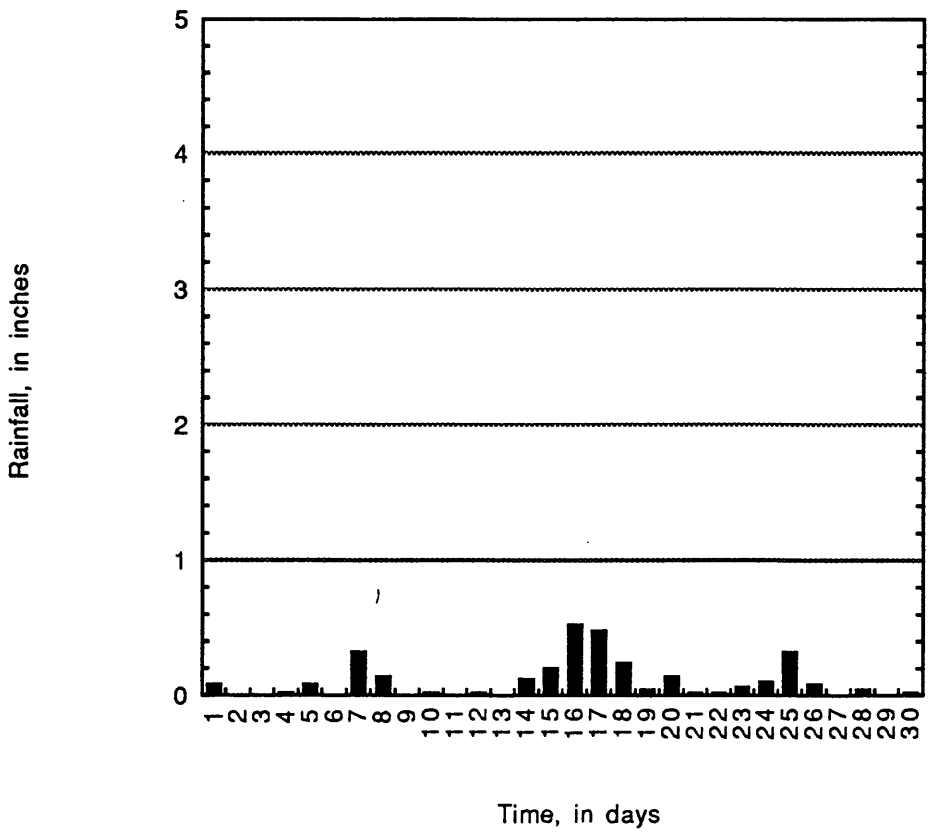

Figure C4. Daily rainfall during July 1990

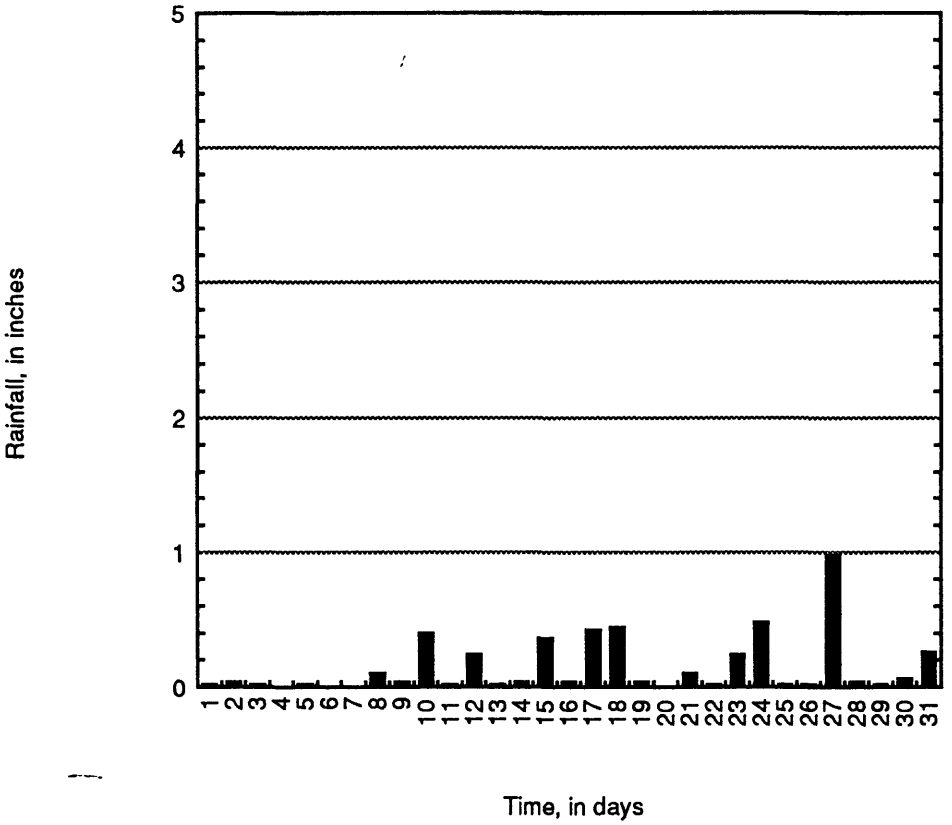

Figure C5. Daily rainfall during August 1990

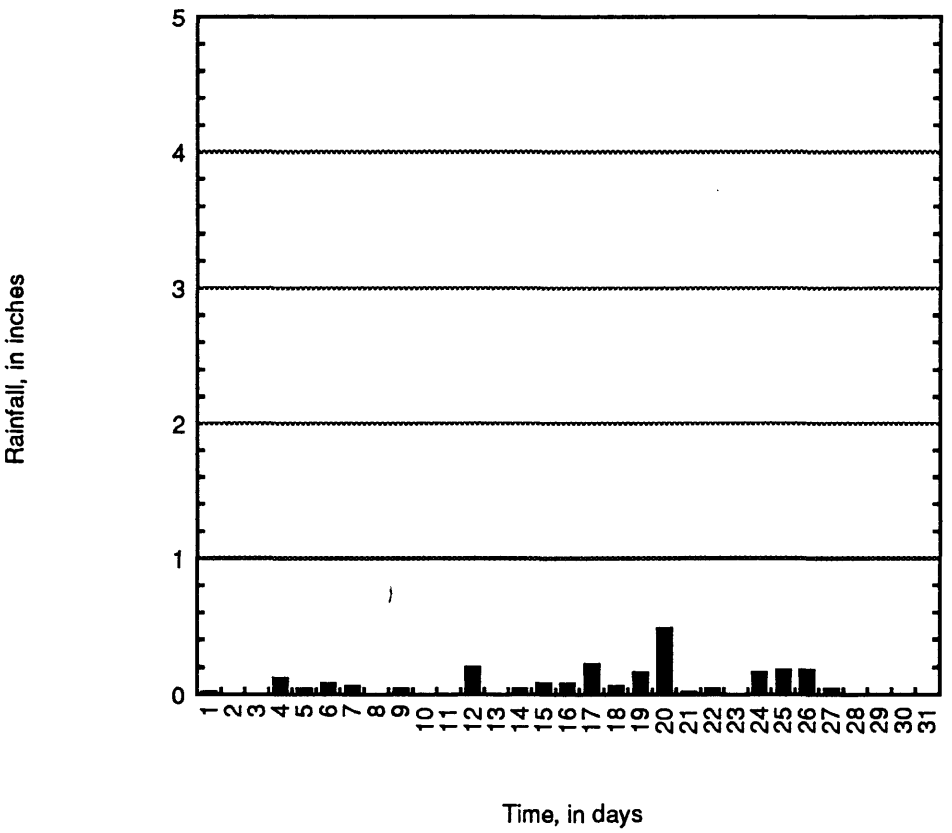

Figure C6. Daily rainfall during September 1990

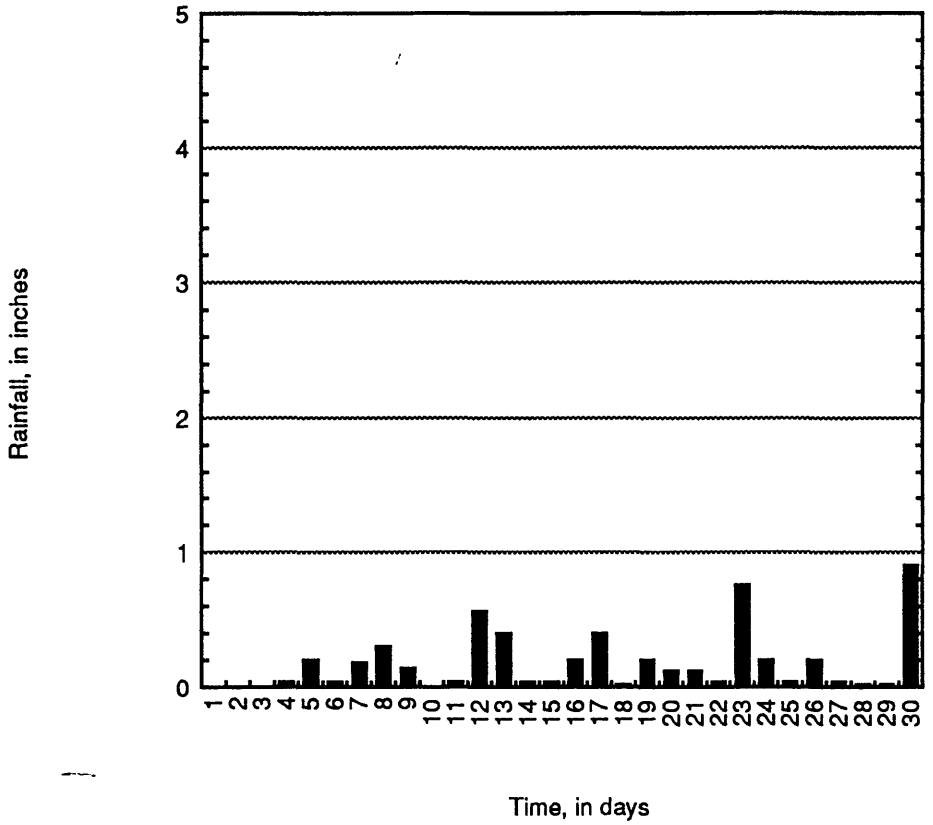

Figure C7. Daily rainfall during October 1990

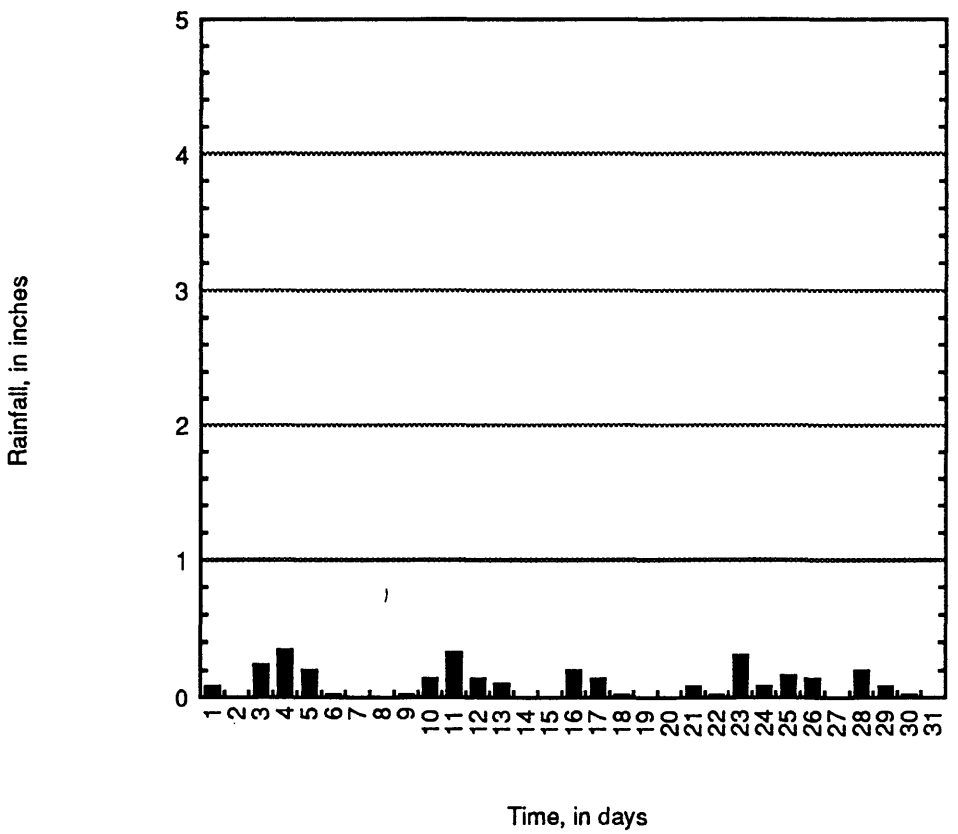

Figure C8. Daily rainfall during November 1990

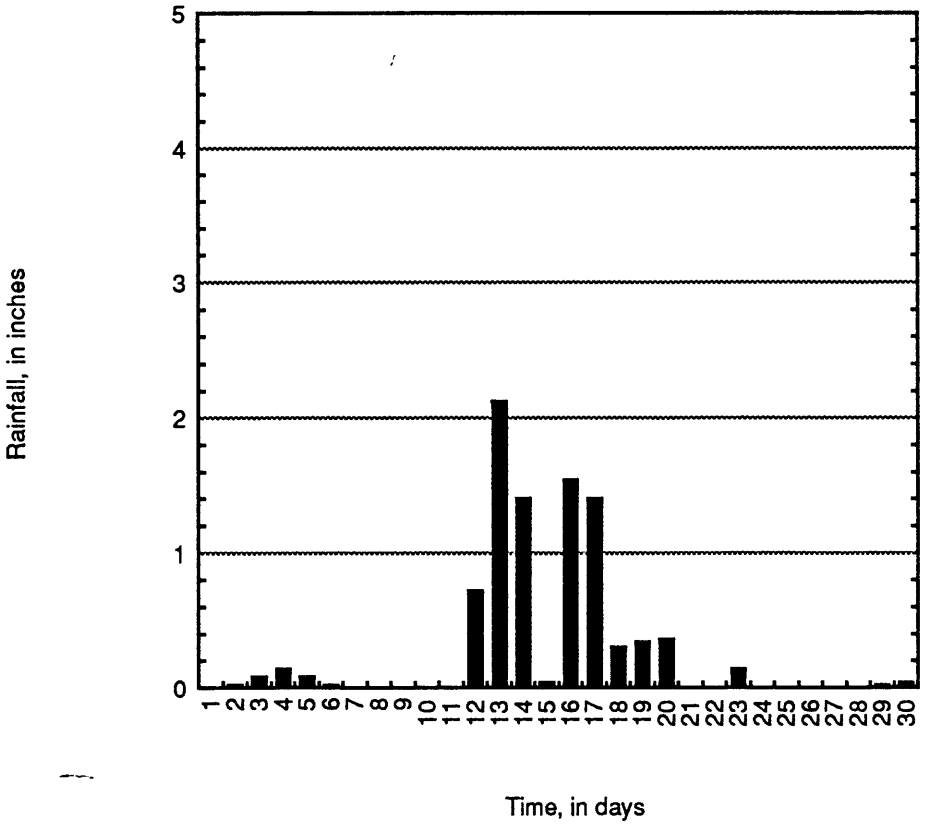

Figure C9. Daily rainfall during December 1990

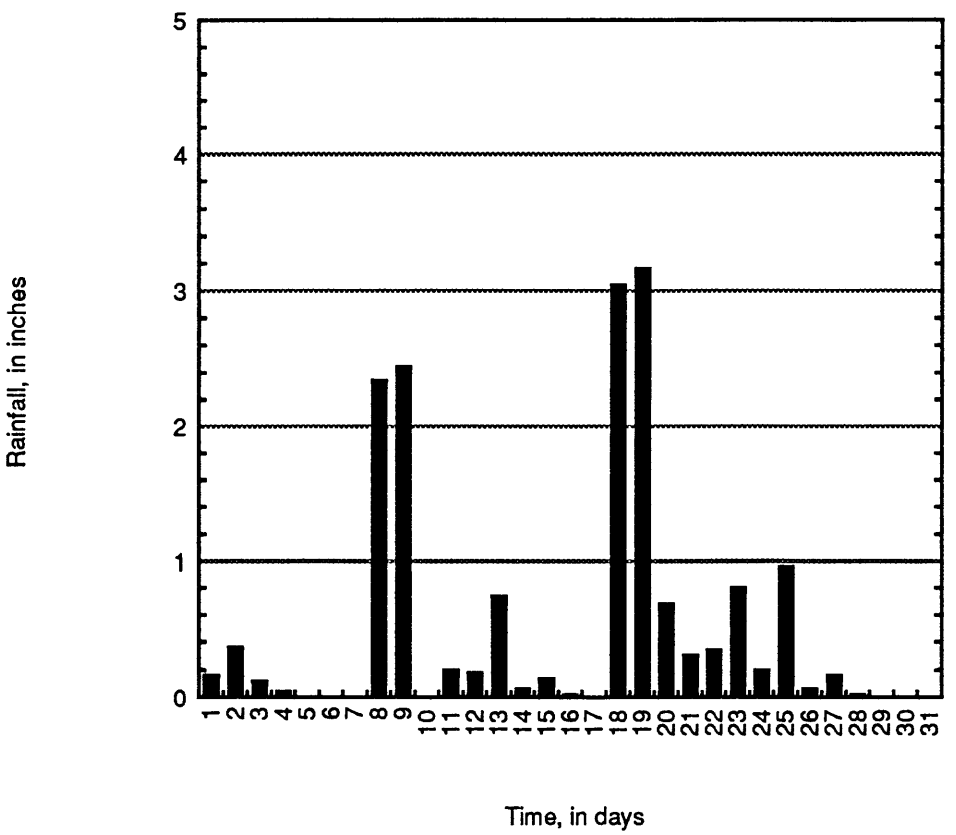

Figure C10. Daily rainfall during January 1991

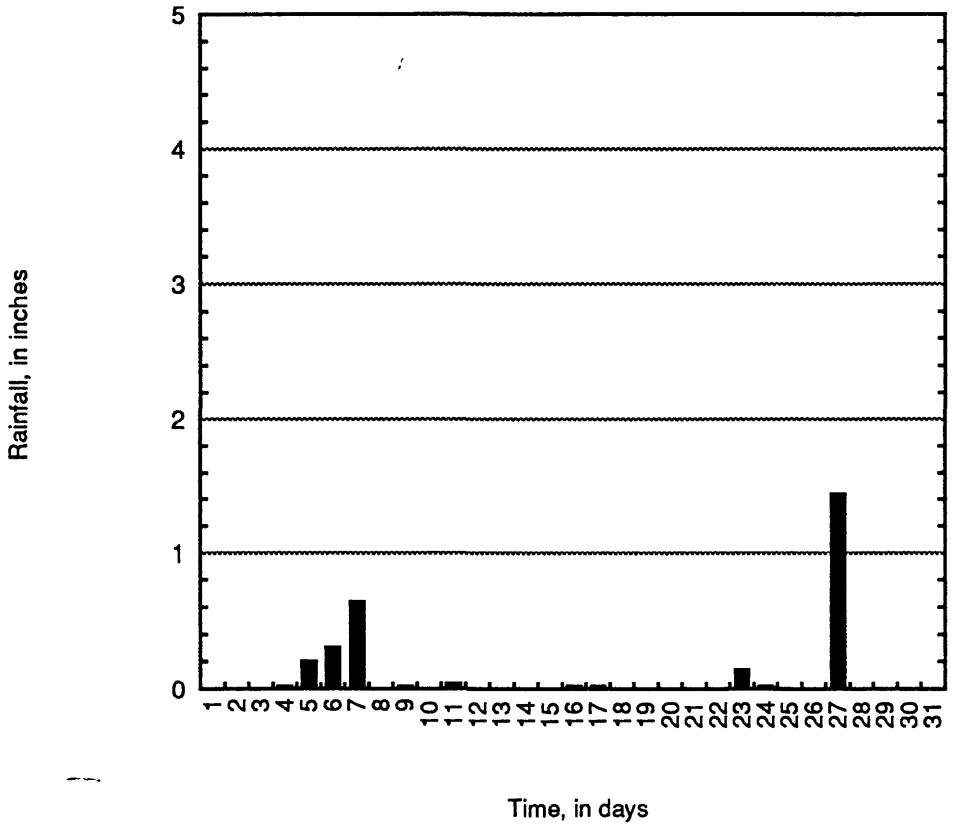

Figure C11. Daily rainfall during February 1991

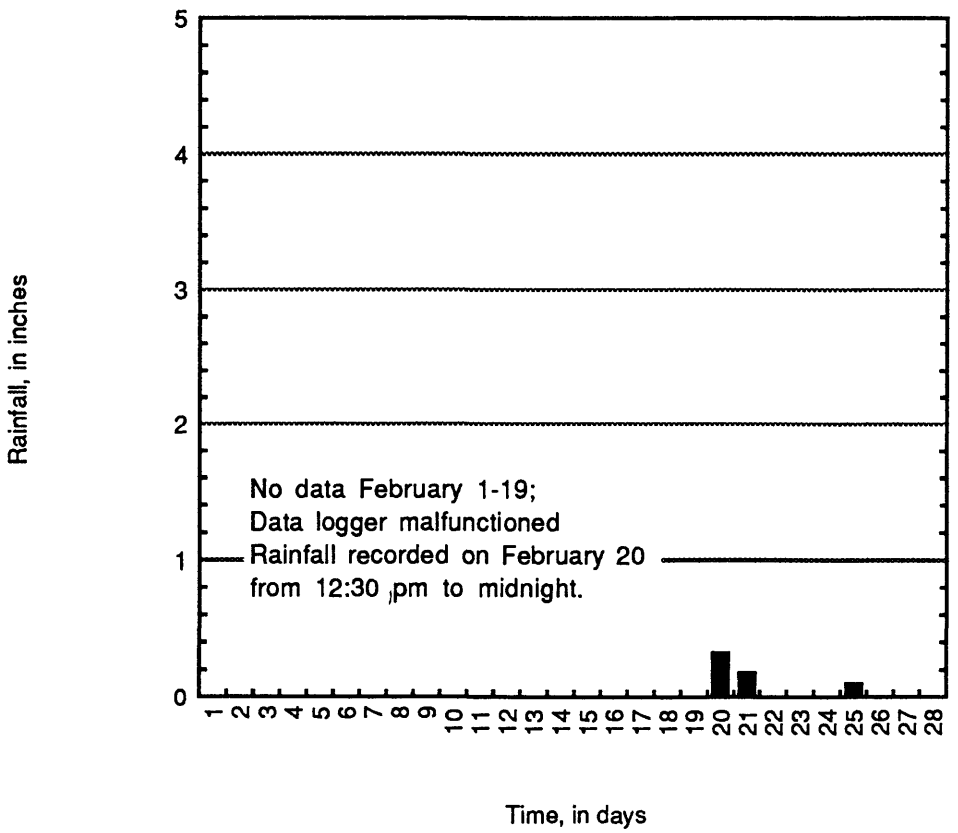

Figure C12. Daily rainfall during March 1991

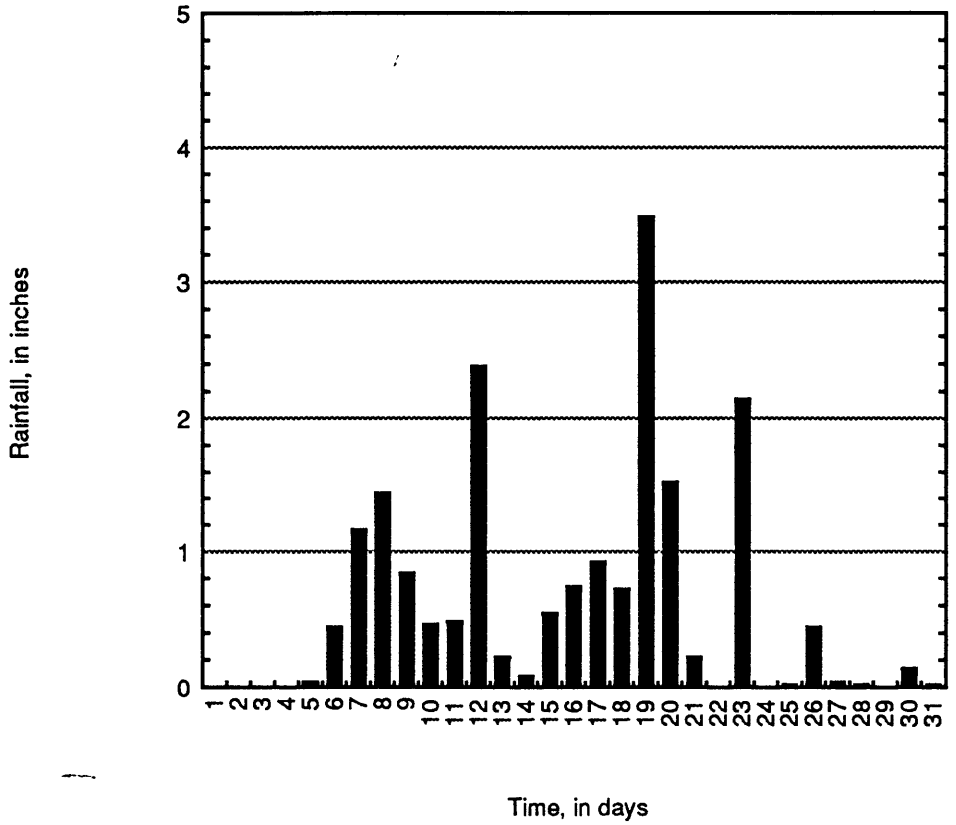

Figure C13. Daily rainfall during April 1991

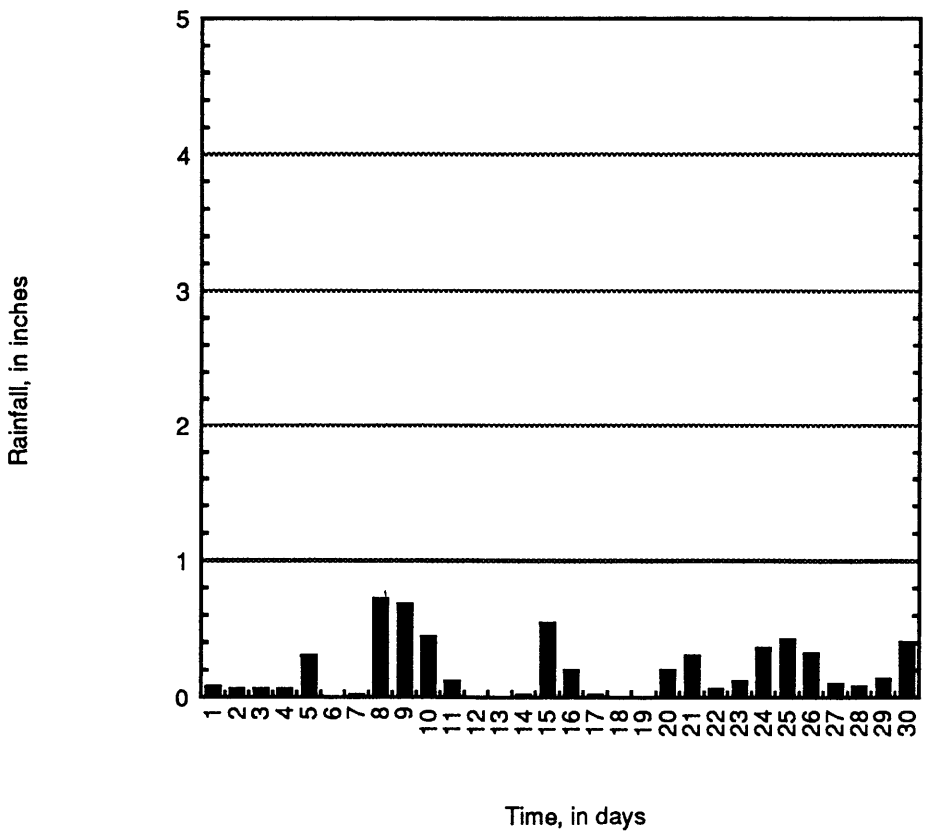

Figure C14. Estimated daily rainfall during February 1991

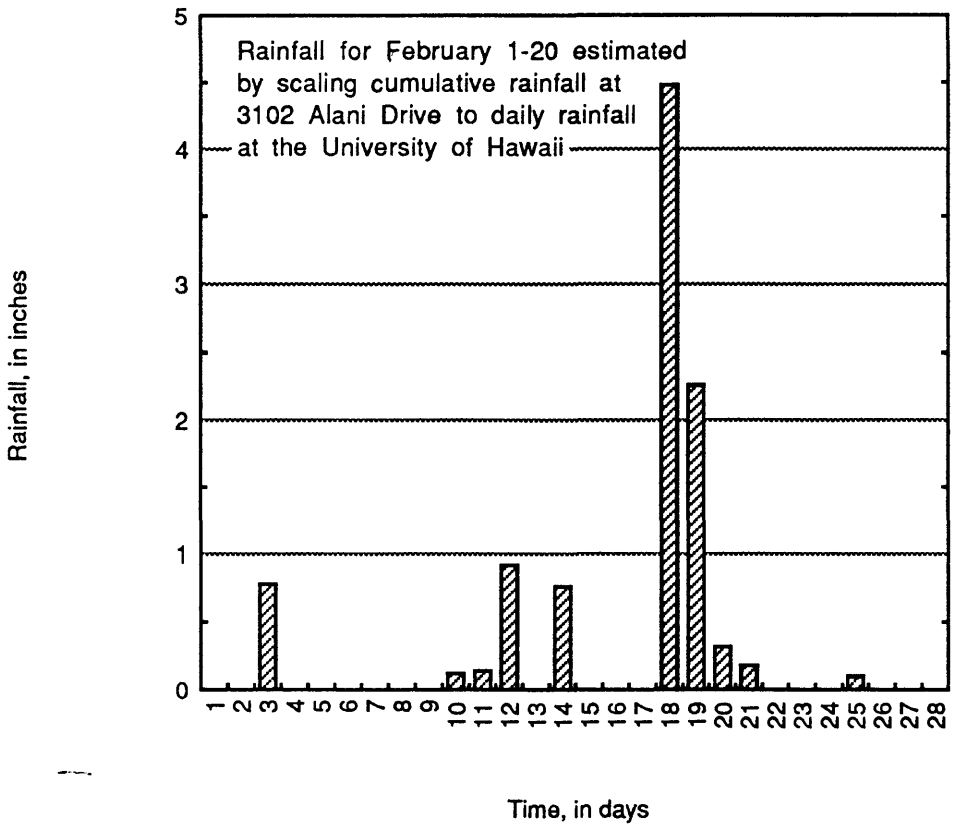

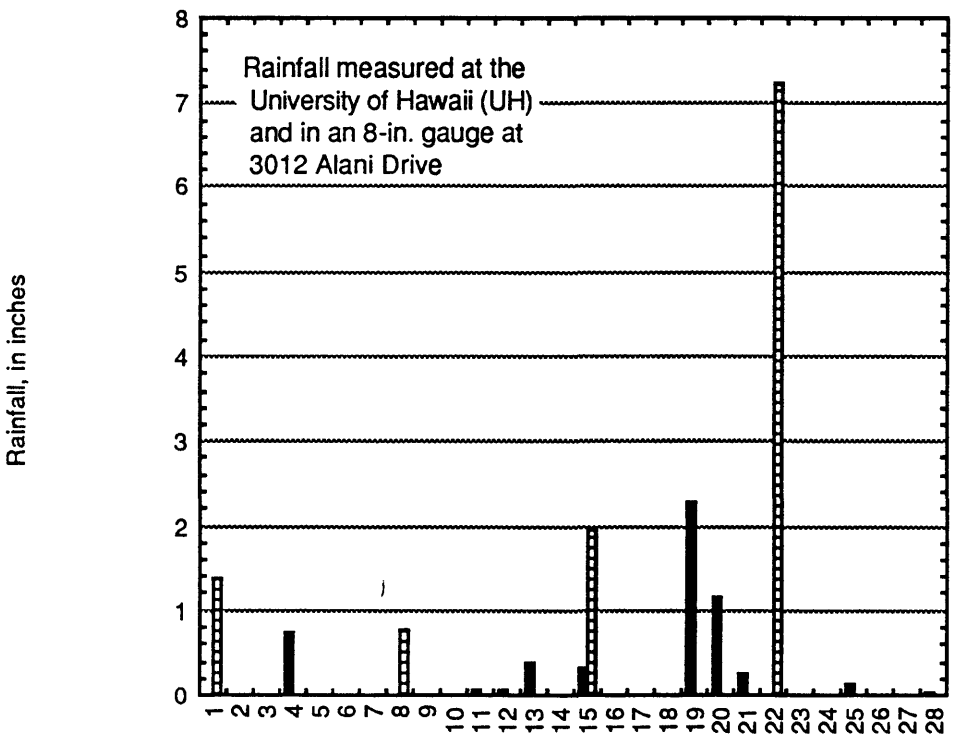

Figure C15. Graph comparing cumulative rainfall at the head of the Alani-Paty landslide with two sites on Waahila Ridge

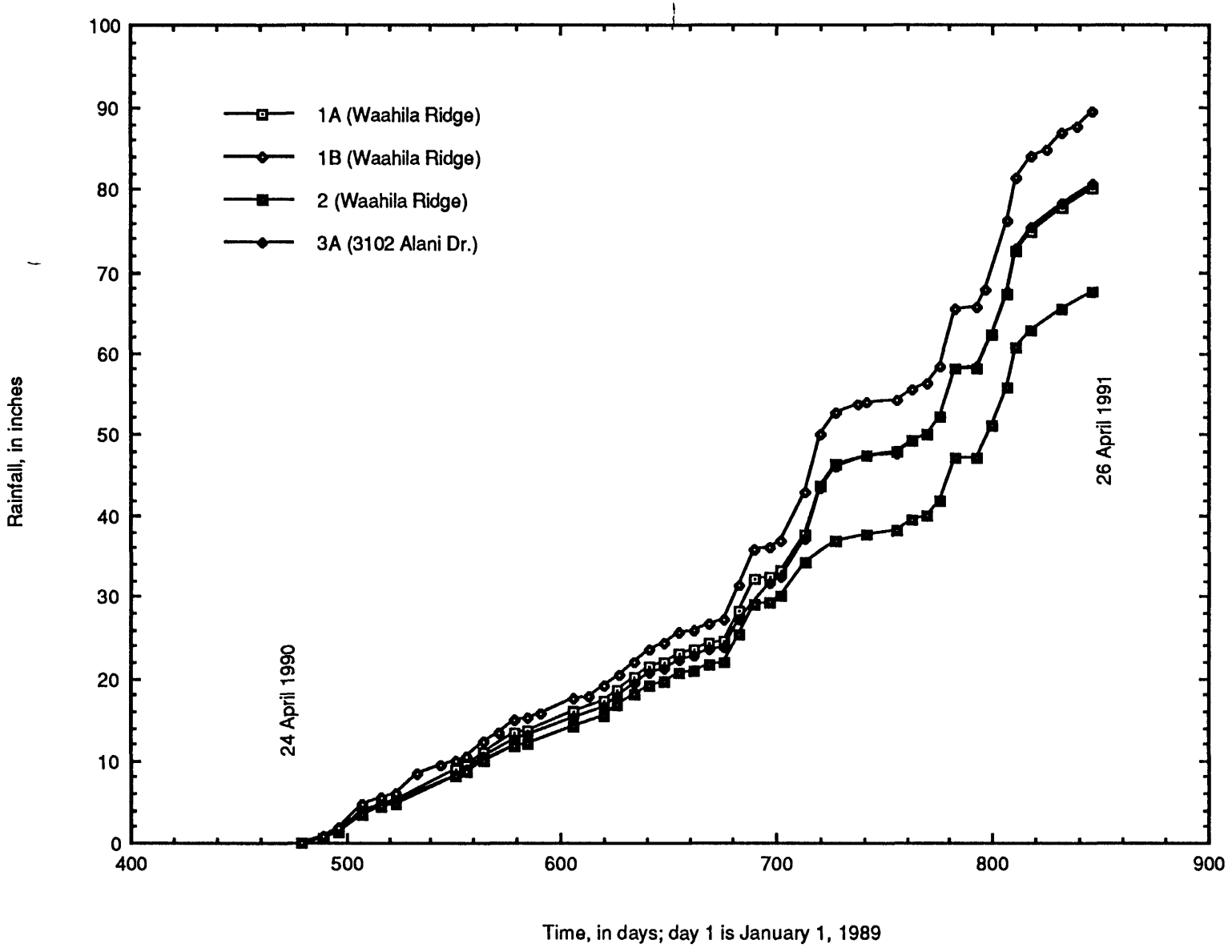

Figure C16. Daily rainfall at 3102 Alani Drive from September 25 1989 through April 30, 1991

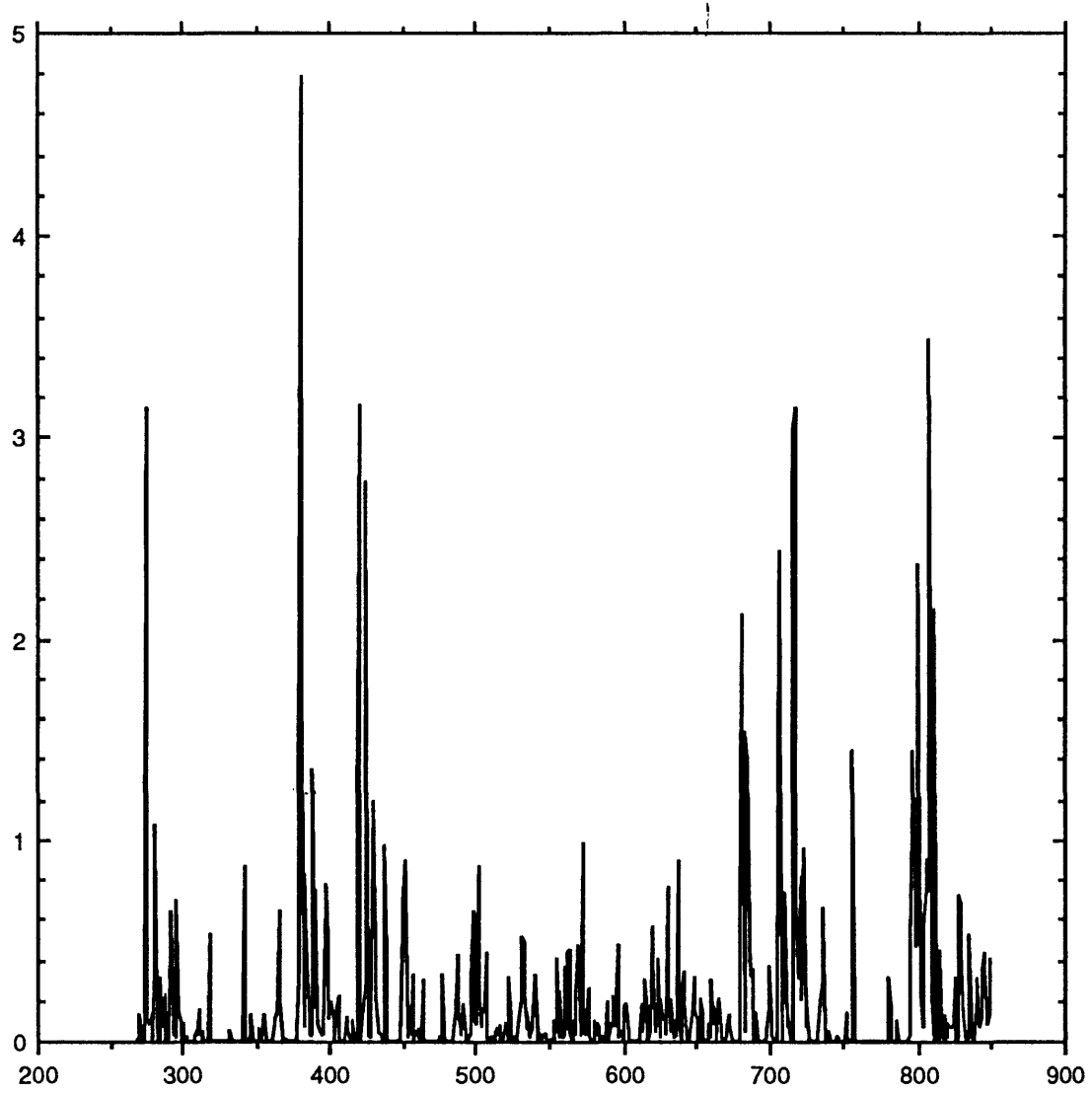

No data Feb. 1-20, 1991
(days 762-781)

APPENDIX D

Displacement of the landslide

This appendix contains a graph of cumulative displacement at the headscarp (from May 1989 through April 1990) superimposed on a graph of cumulative rainfall (fig. D1), a graph of displacement indicated by changes in length of cables anchored below the slip surface from May 1990 to April 1991 (fig. D2), and a map showing crude estimates of total displacement measured in April 1989, April 1990 (Baum and others, 1990), and September 1991 (fig. D3). Plots of the inclinometer measurements are shown in figures D4-D19.

We monitored displacement at the head of the landslide (fig. 2) by means of a simple extensometer consisting of a Stevens digital recorder and a wire cable. The recorder was anchored to a wall upslope from the headscarp of the landslide, on non-moving ground. The wire cable was attached to the trunk of a large tree growing on the head of the landslide. As the distance between the tree and the recorder changes, the cable causes a wheel on the recorder to turn. The recorder mechanism keeps track of position by counting the revolutions of the wheel from an arbitrary zero position. The mechanism records the current position of the wheel once every 15 minutes. Subsequently, the recorded changes in the position of the wheel are converted into displacements.

We made rough estimates of total surface displacement by measuring offsets of curbs and walls where they cross the lateral boundaries of the landslide (fig. D3). We measured the offsets by standing on one side of the boundary and sighting along a curb or wall on the opposite side. We then measured the perpendicular distance from the wall or curb on our side of the boundary to the projection of the wall or curb on the opposite side. Precision of the measurements varies from site to site, but averages about ± 0.5 ft.

Holes for inclinometer measurements were cased with ABS (acrylonitrile--butadiene-styrene) tubing having special grooves to align the inclinometer probe. The casing in borings 6, 10 and 15 was secured by pouring grout down the annular space between the sides of the hole and outside of the casing. The annular space appears to have been incompletely filled, thus allowing the casing to shift and deflect at random. The casing in boring 25 was secured by pumping grout into the annular space through a valve in the bottom of the casing, and the grouting seems to be adequate to prevent random deflections of the casing. The cased holes are surveyed approximately bimonthly using an inclinometer probe (*Digitilt* model 50325M, with *Digitilt indicator*, model 50309M, both manufactured by Slope Indicator Co., Seatle, Washhington). The algebraic signs of the deflections indicated in the graphs follow the convention that positive deflection on the A-axis is upslope and negative is downslope; positive deflection on the B-axis is to the left of an observer looking downslope and negative is to the right. Orientations of the A and B axes are listed in table D1.

Table D1. Orientations of axes of inclinometer casings

Boring	A(-)[1]	A(+)	B(-)	B(+)
6	N79°W	S79°E	N11°E	S11°W
10	N50°W	S50°E	N40°E	S40°W
15	N69°W	S69°E	N21°E	S21°W
25	N52°W	S52°E	N37°E	S37°W

[1](+) and (-) correspond to directions of positive and negative deflection, respectively, indicated on the graphs (Figures D4,..., D19).

Figure D1. Cumulative displacement at the head of the Alani-Paty landslide

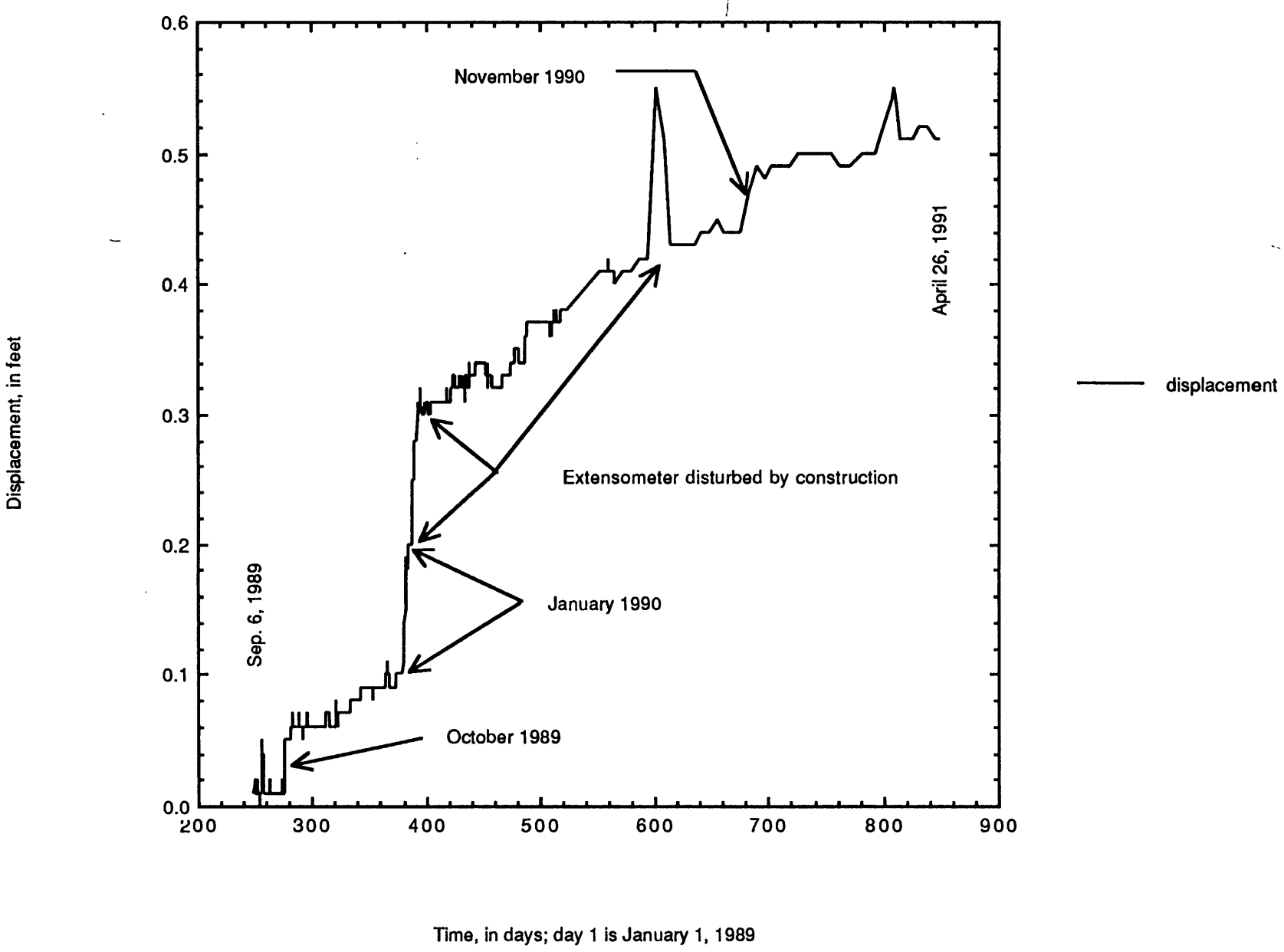

Figure D2. Graph comparing rainfall with displacement at the head of the Alani-Paty landslide

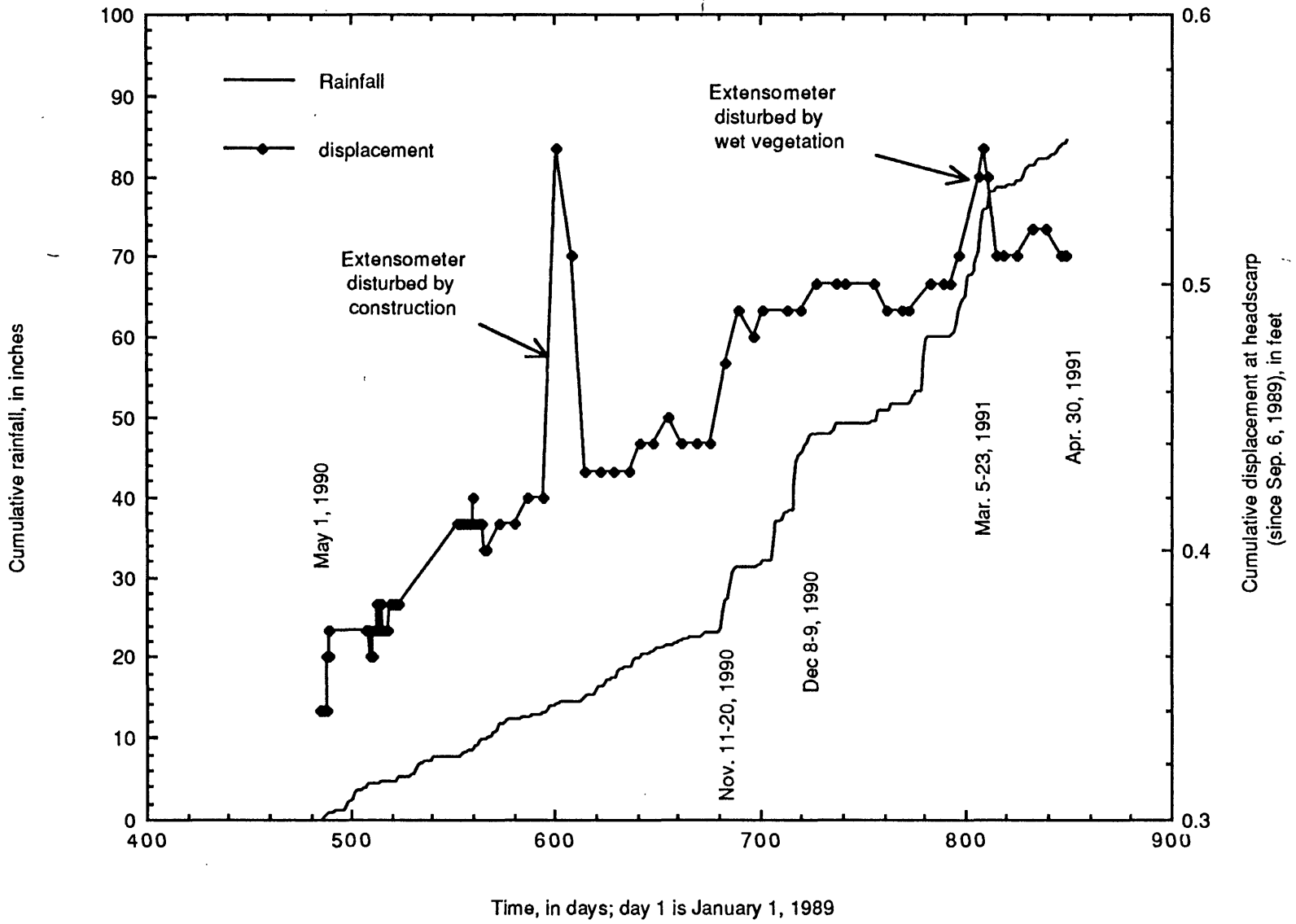

Figure D3. Lengths of cables anchored beneath slip surface in borings

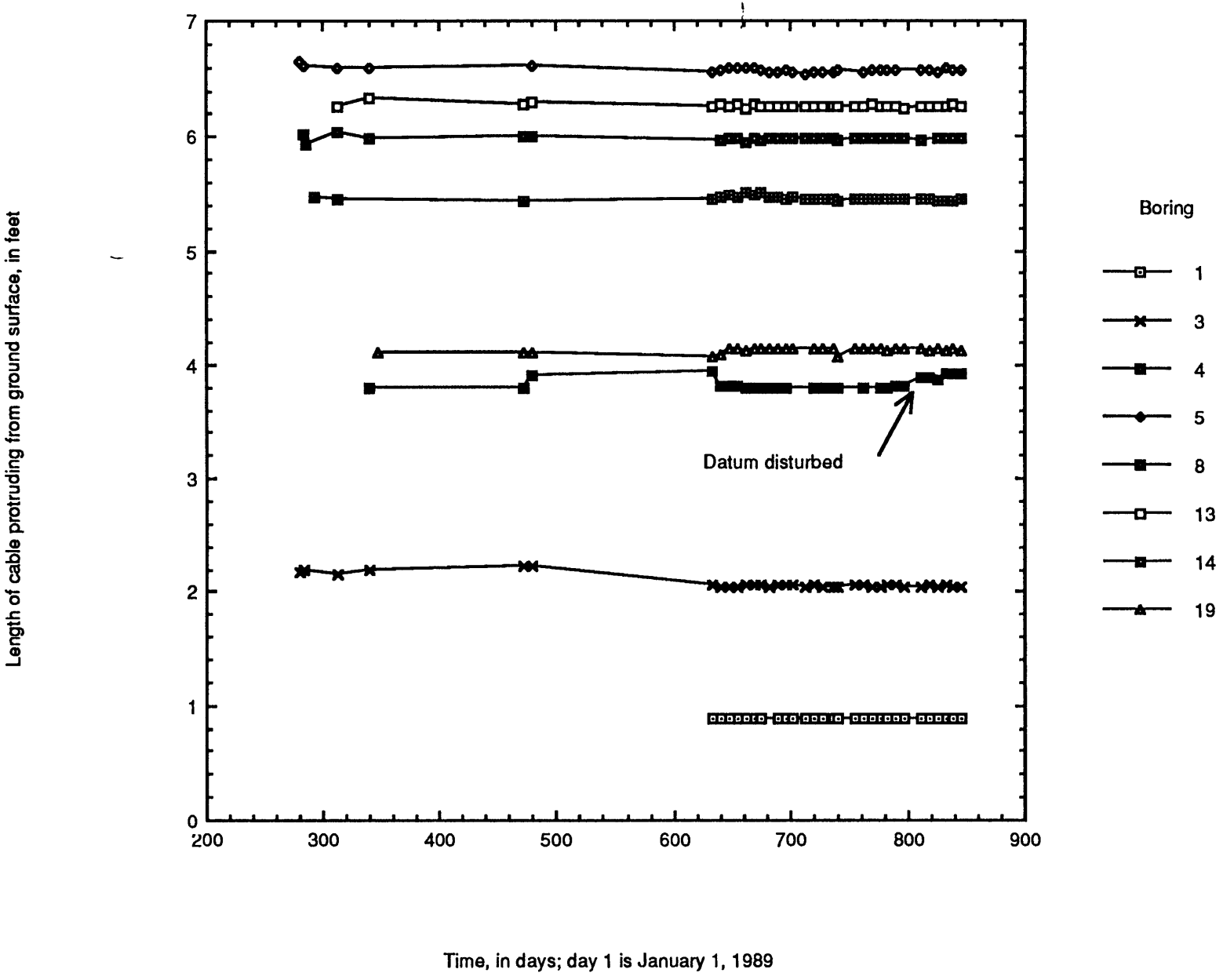

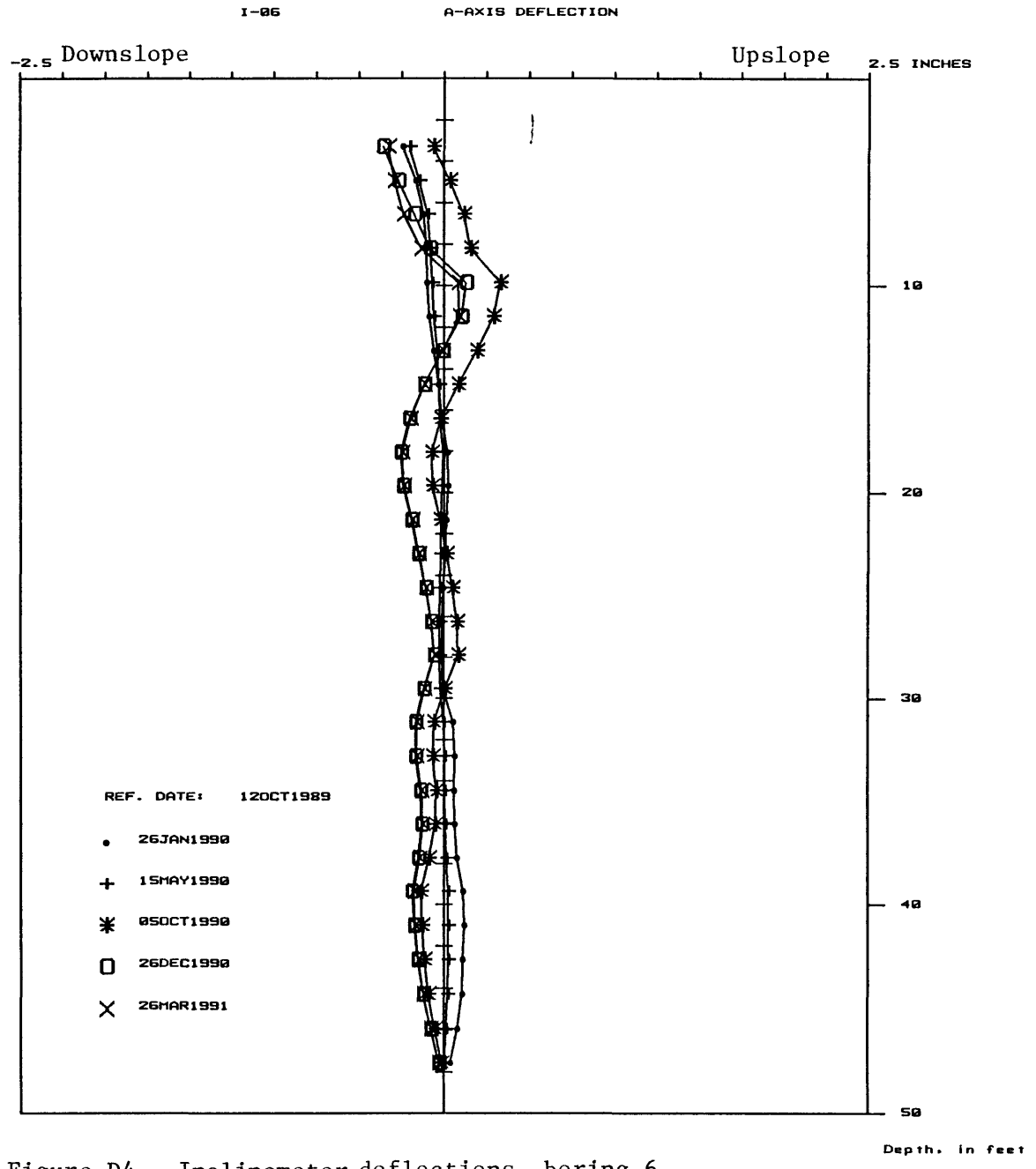

Figure D4. Inclinometer deflections, boring 6

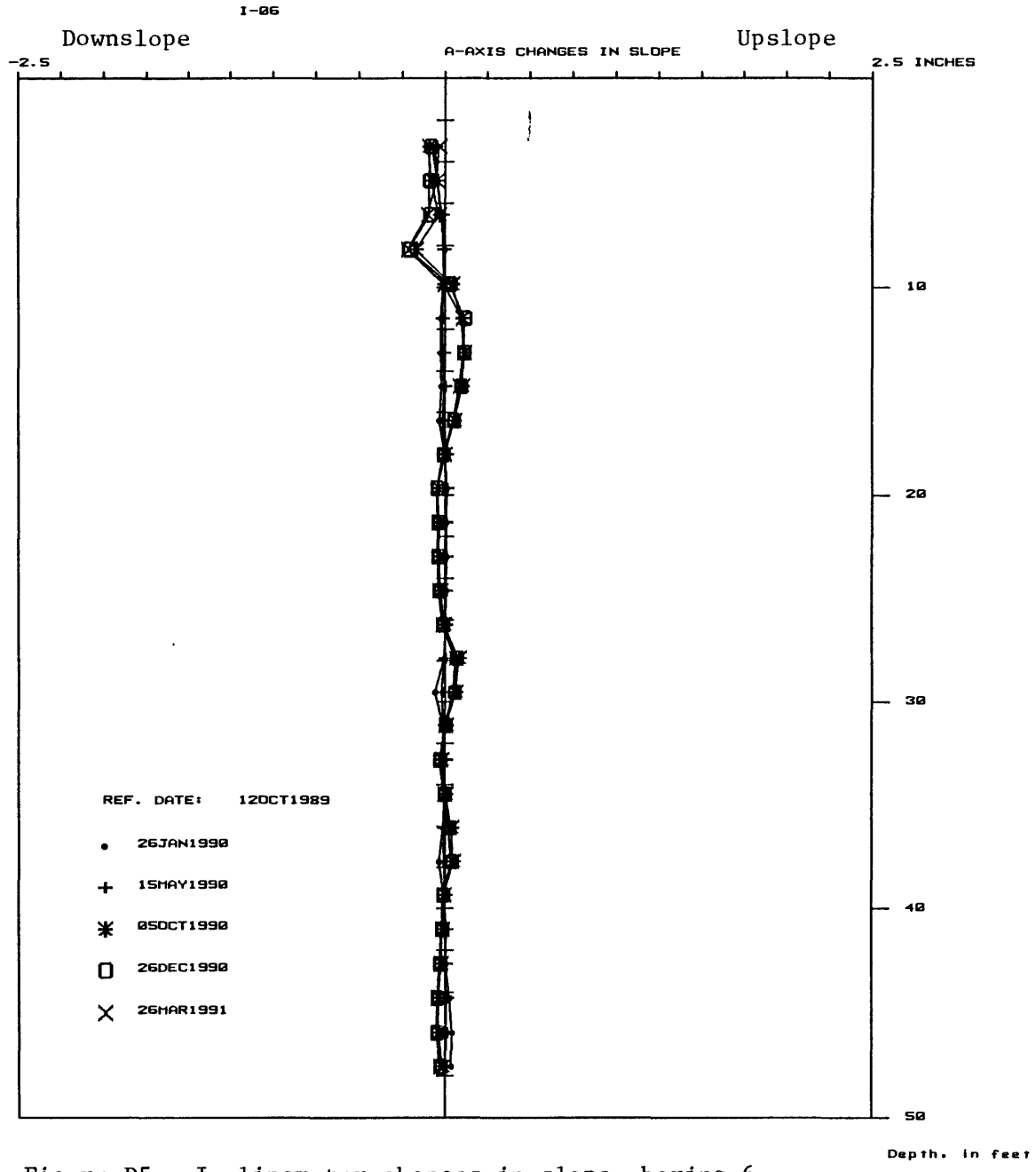

Figure D5. Inclinometer changes in slope, boring 6

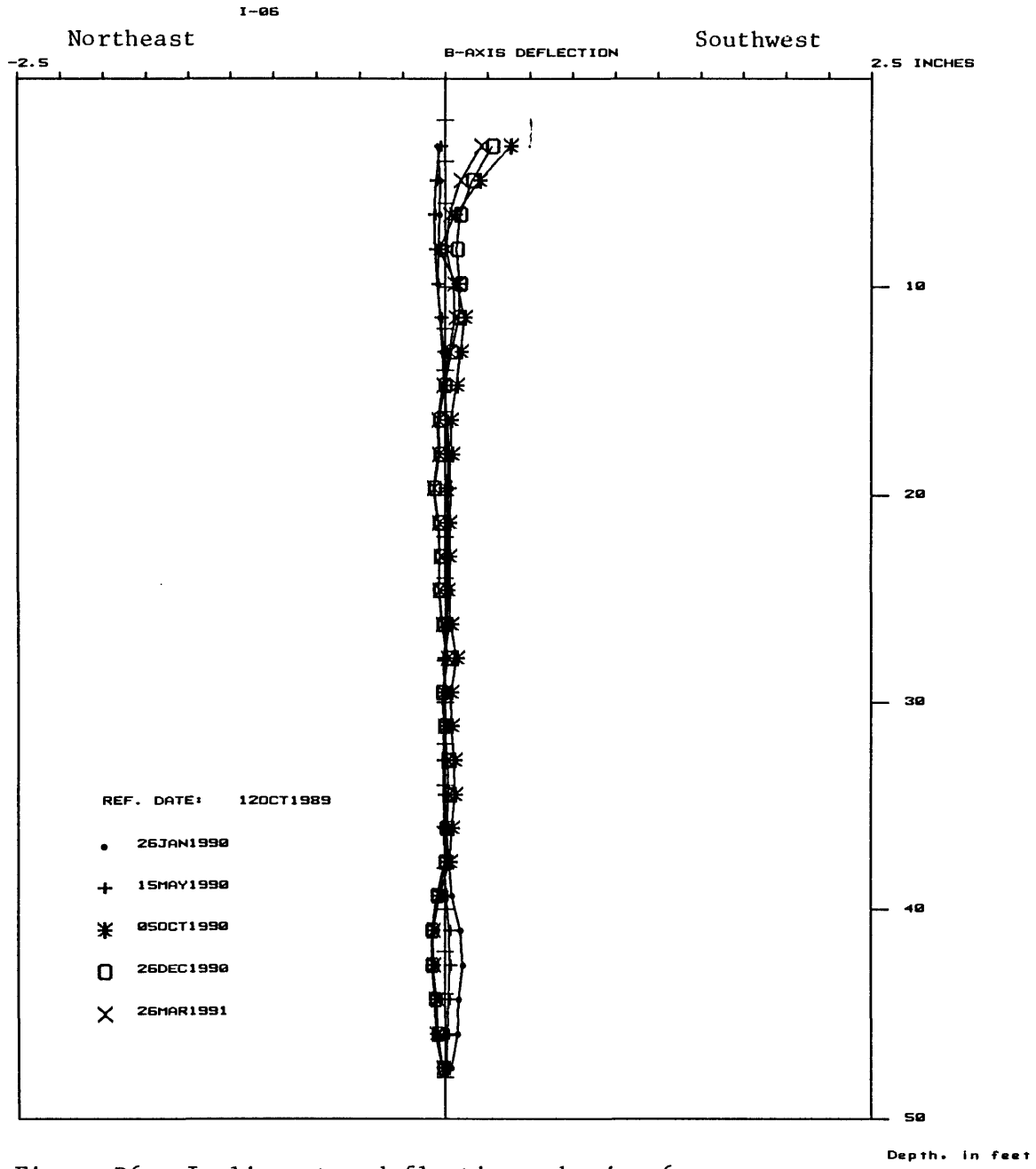

Figure D6. Inclinometer deflections, boring 6

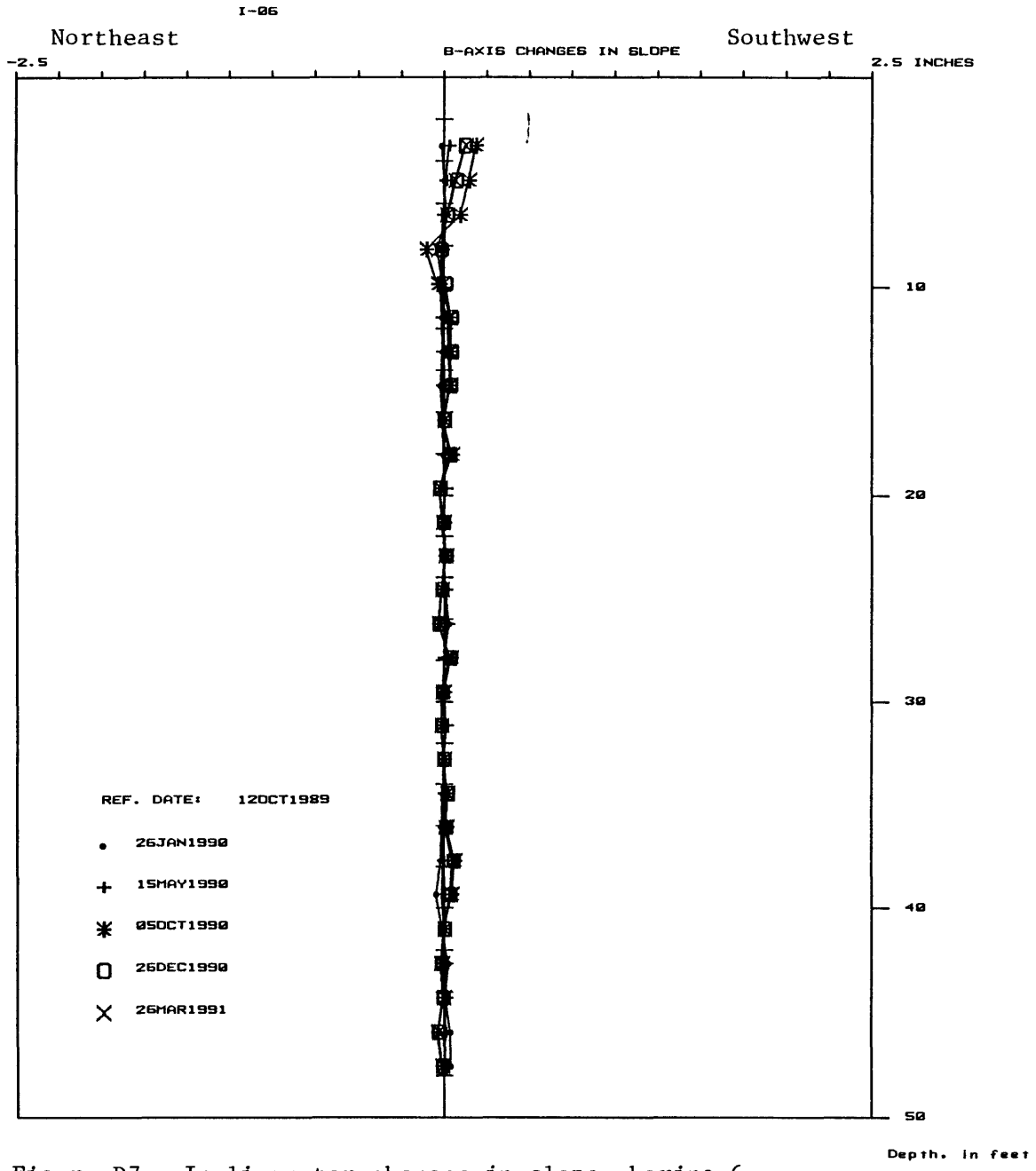

Figure D7. Inclinometer changes in slope, boring 6

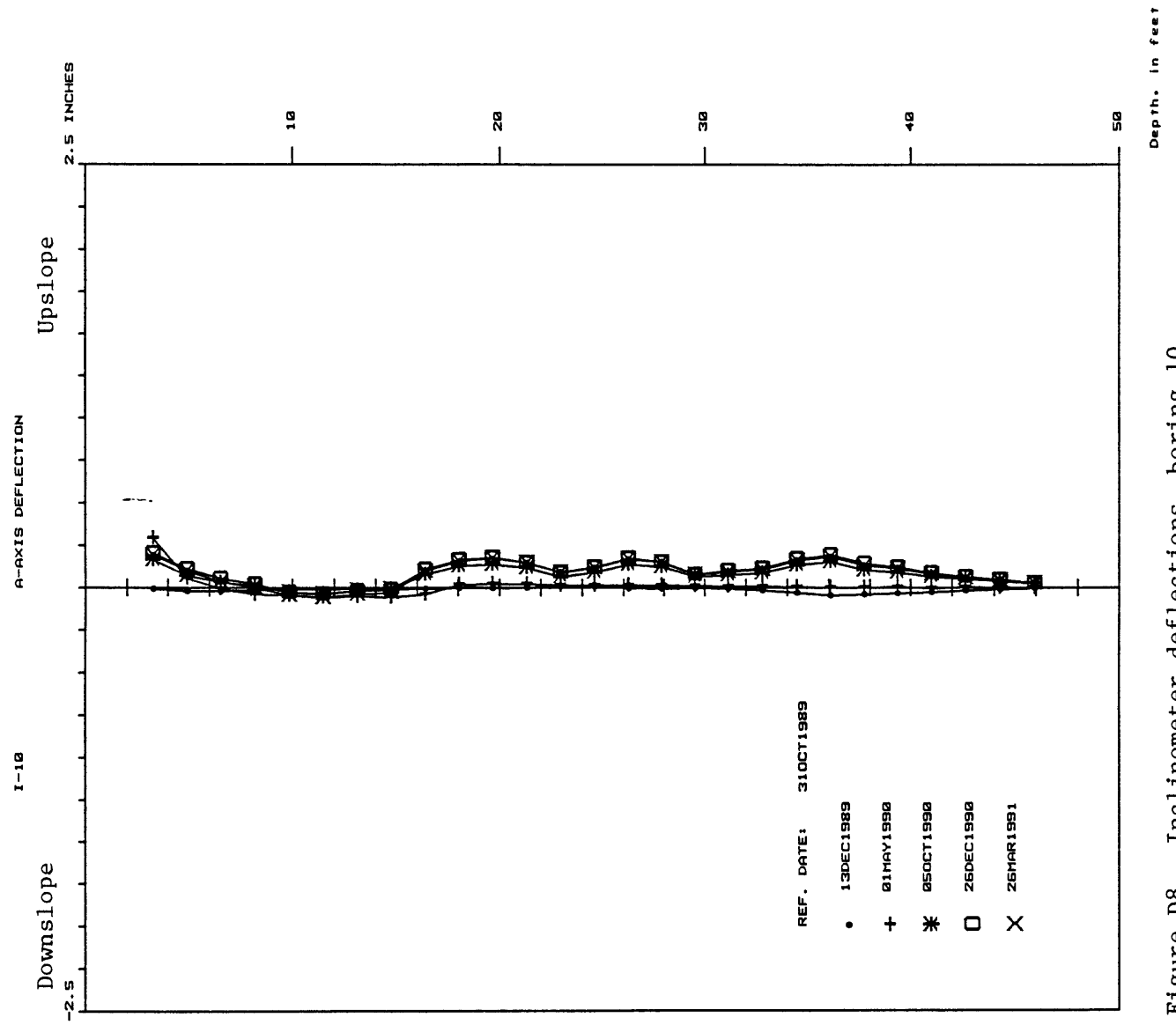

Figure D8. Inclinometer deflections, boring 10

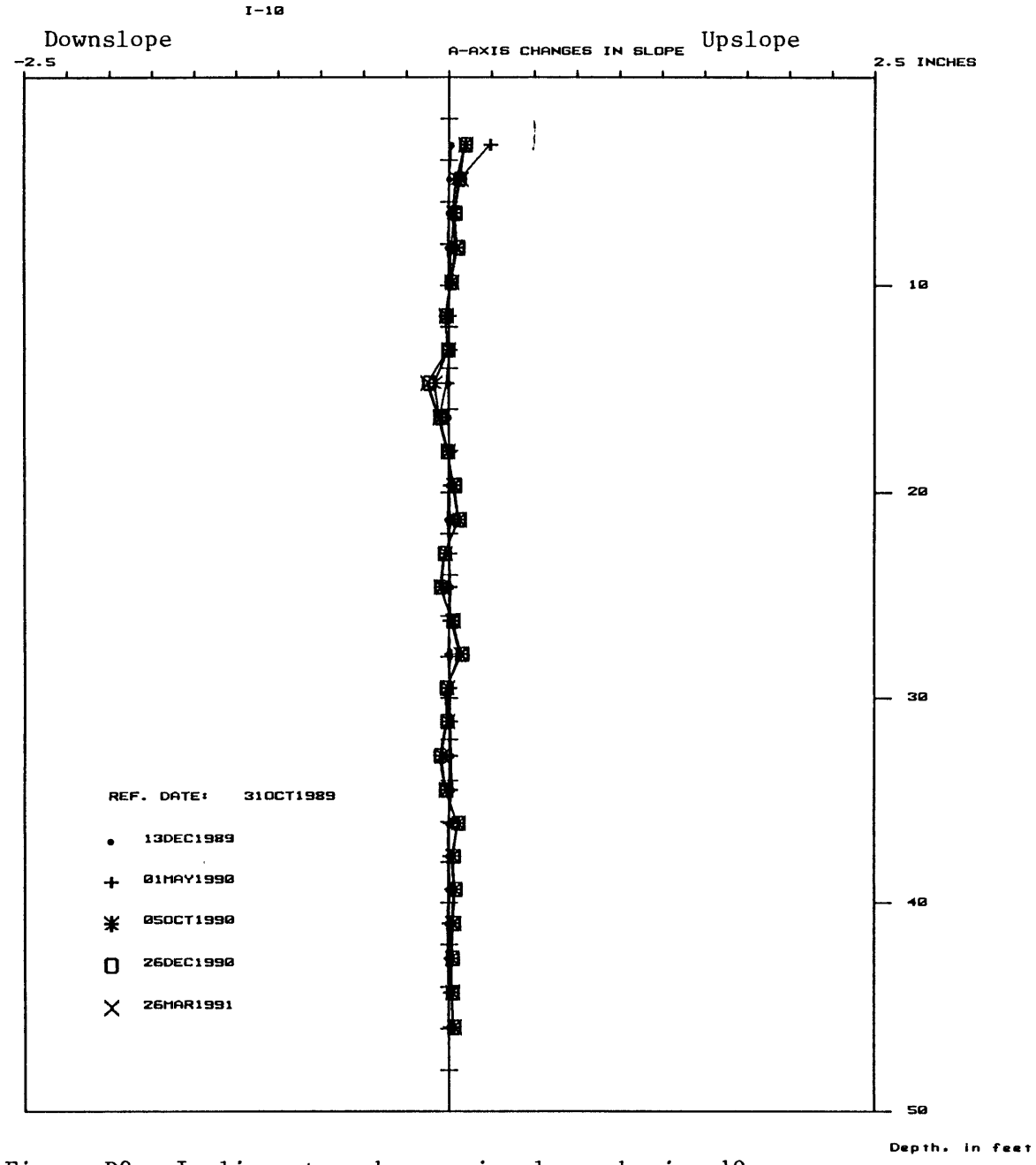

Figure D9. Inclinometer changes in slope, boring 10

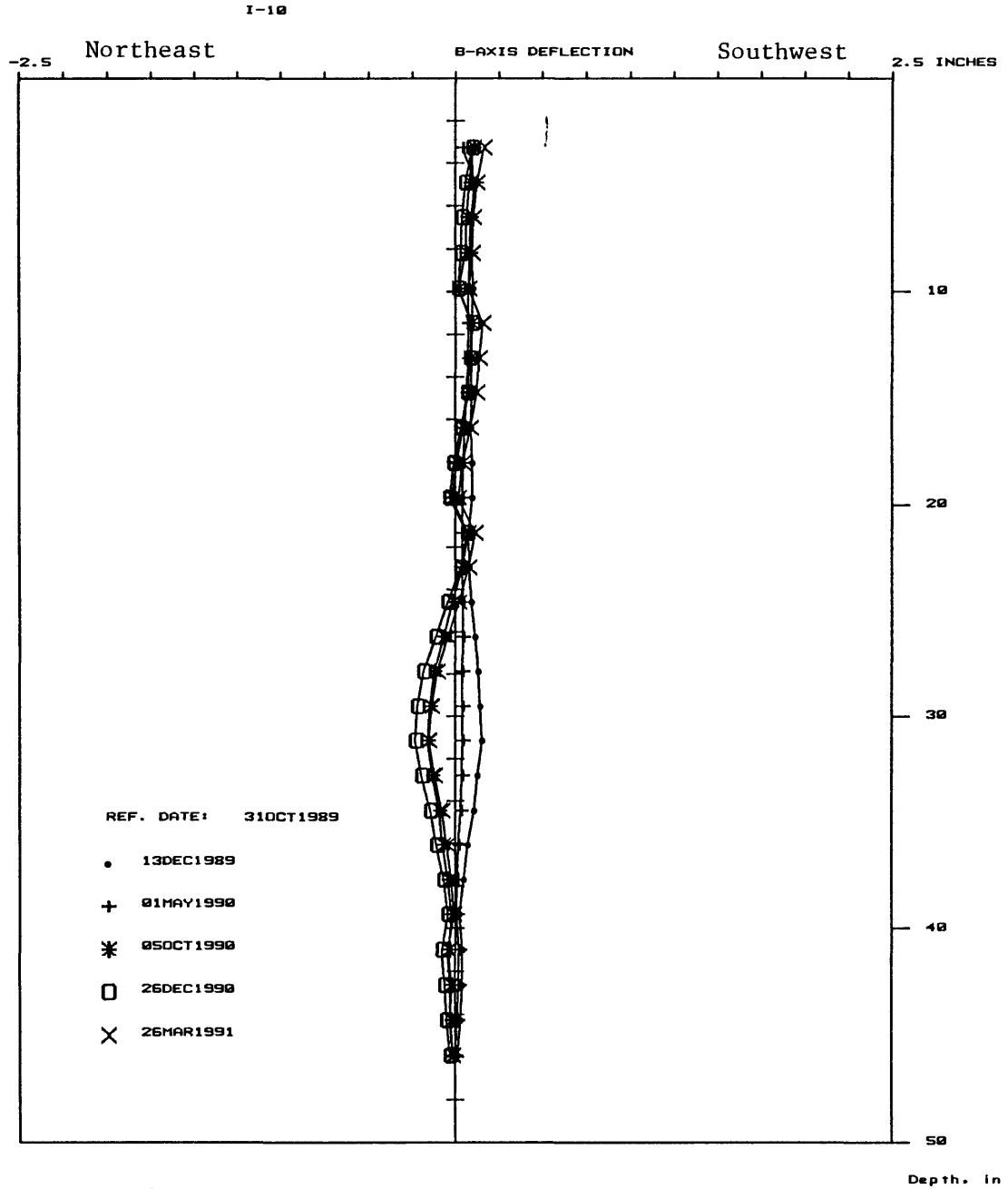

Figure D10. Inclinometer deflections, boring 10

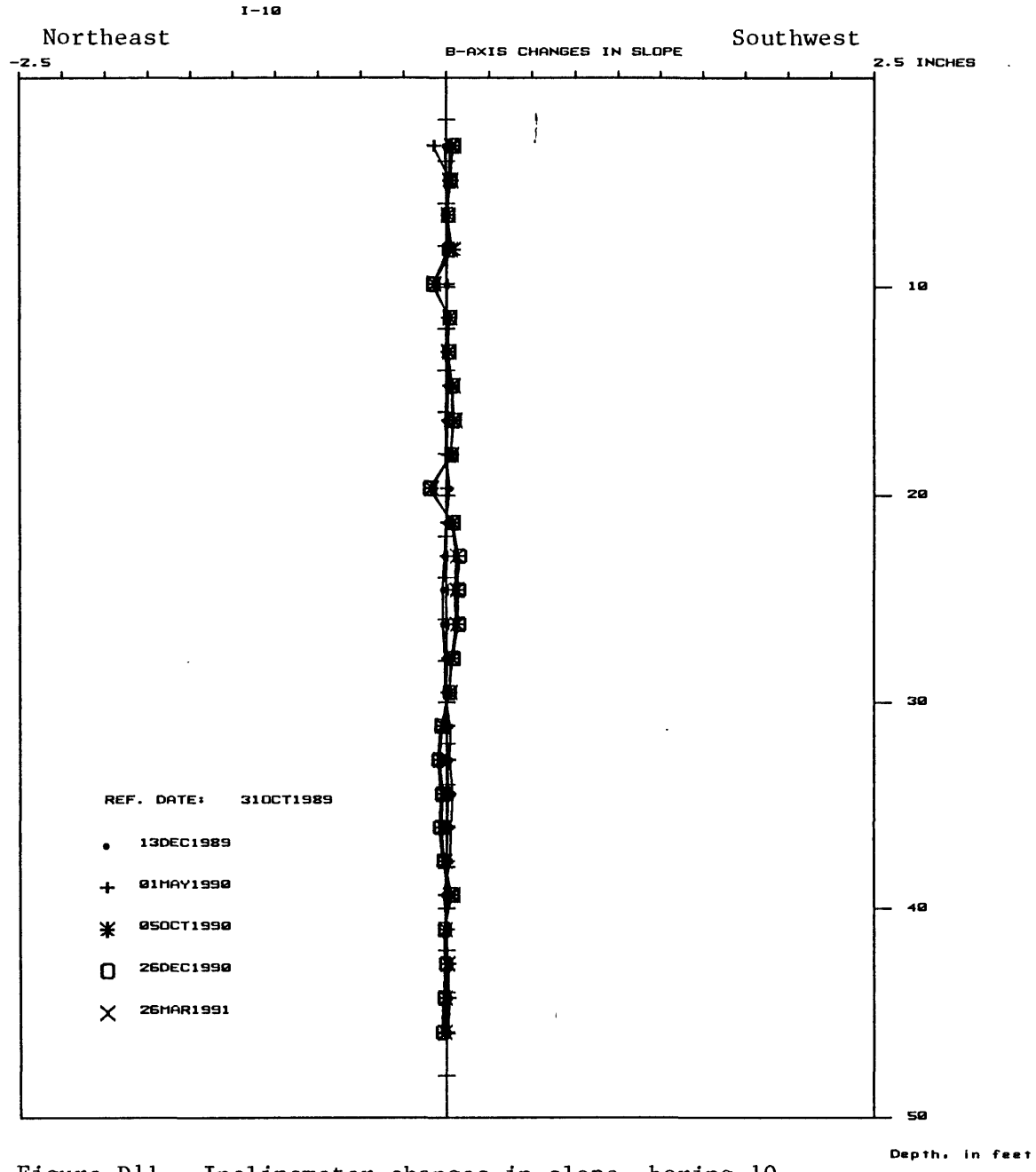

Figure D11. Inclinometer changes in slope, boring 10

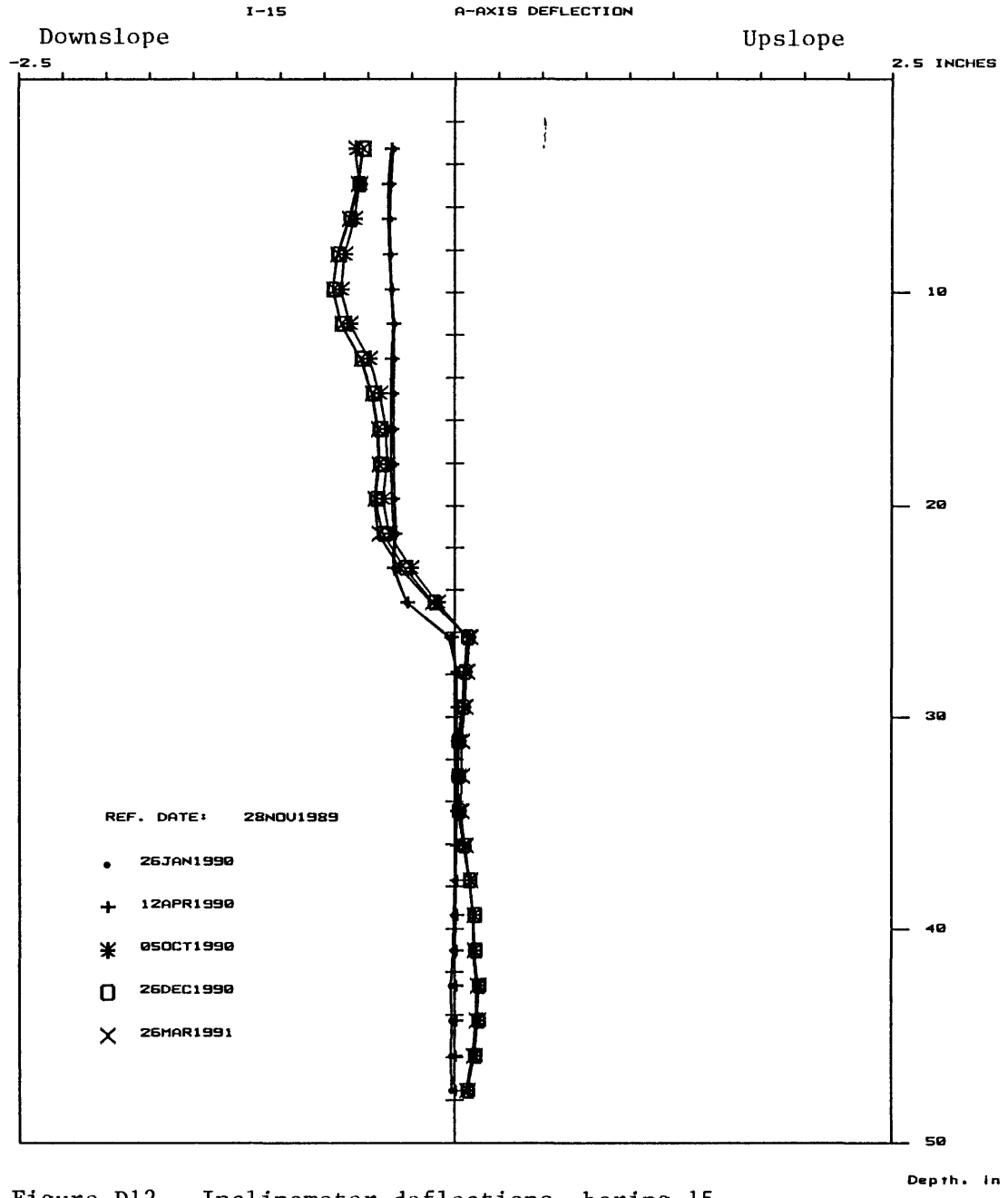

Figure D12. Inclinometer deflections, boring 15

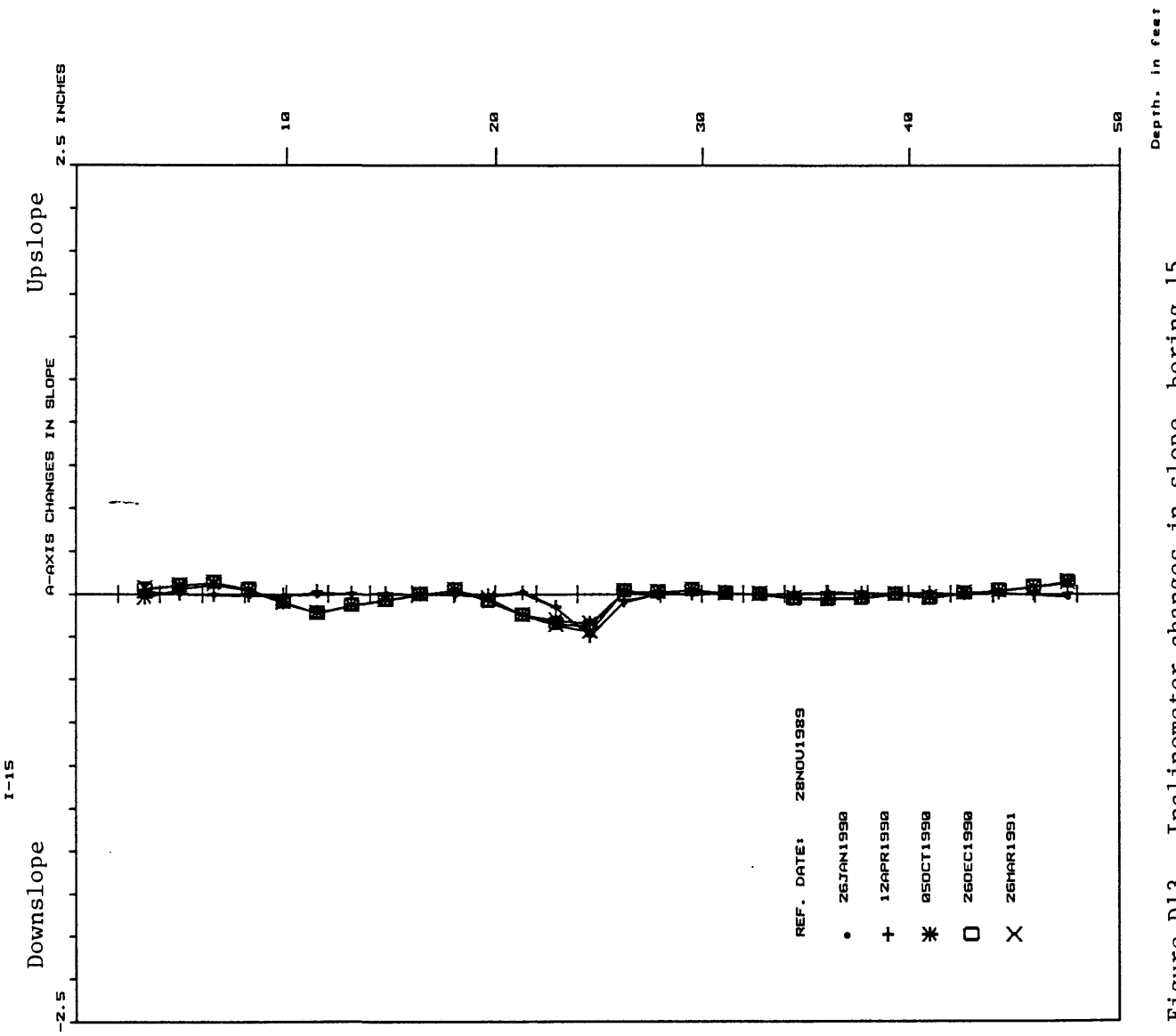

Figure D13. Inclinometer changes in slope, boring 15

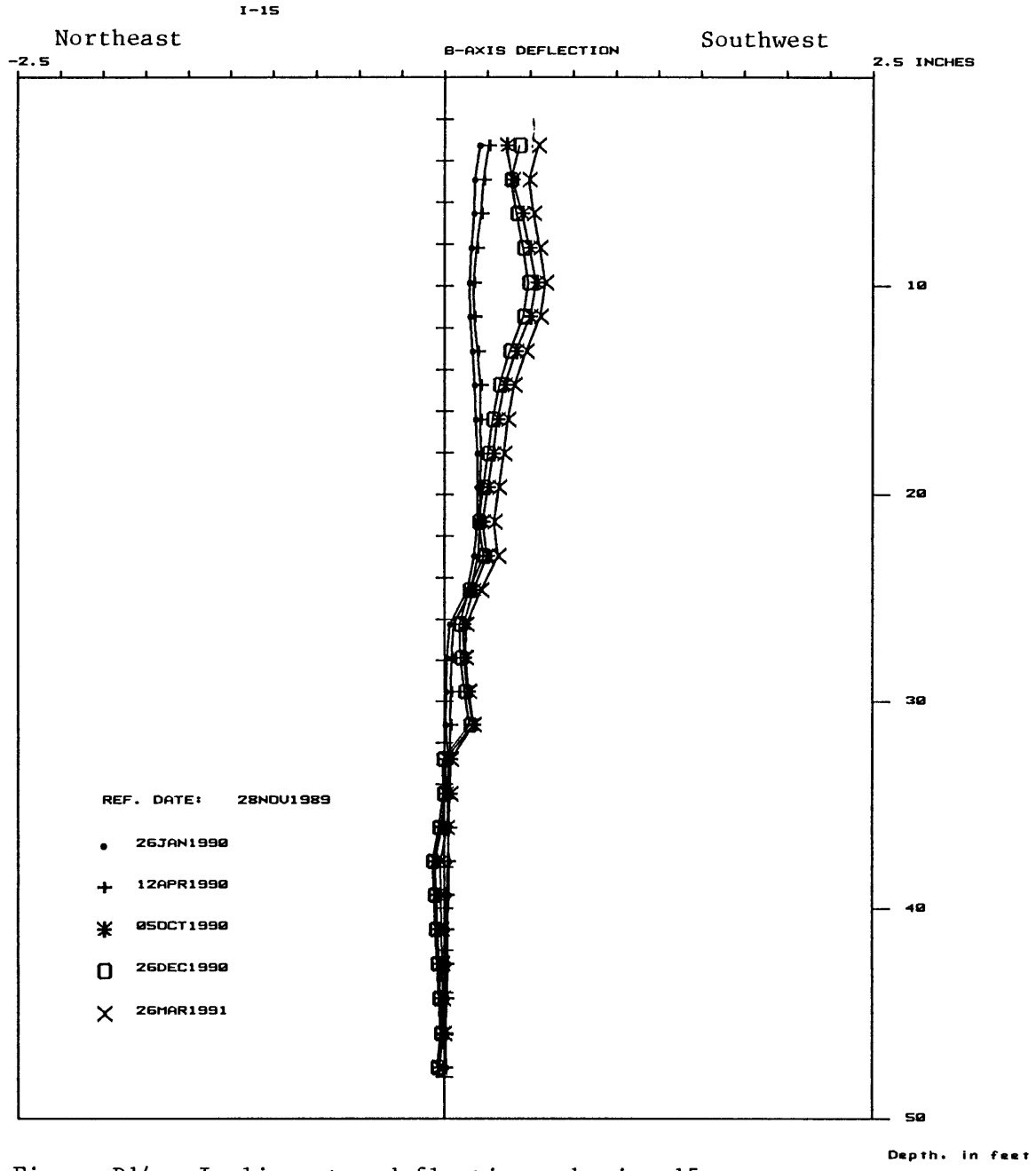

Figure D14. Inclinometer deflections, boring 15

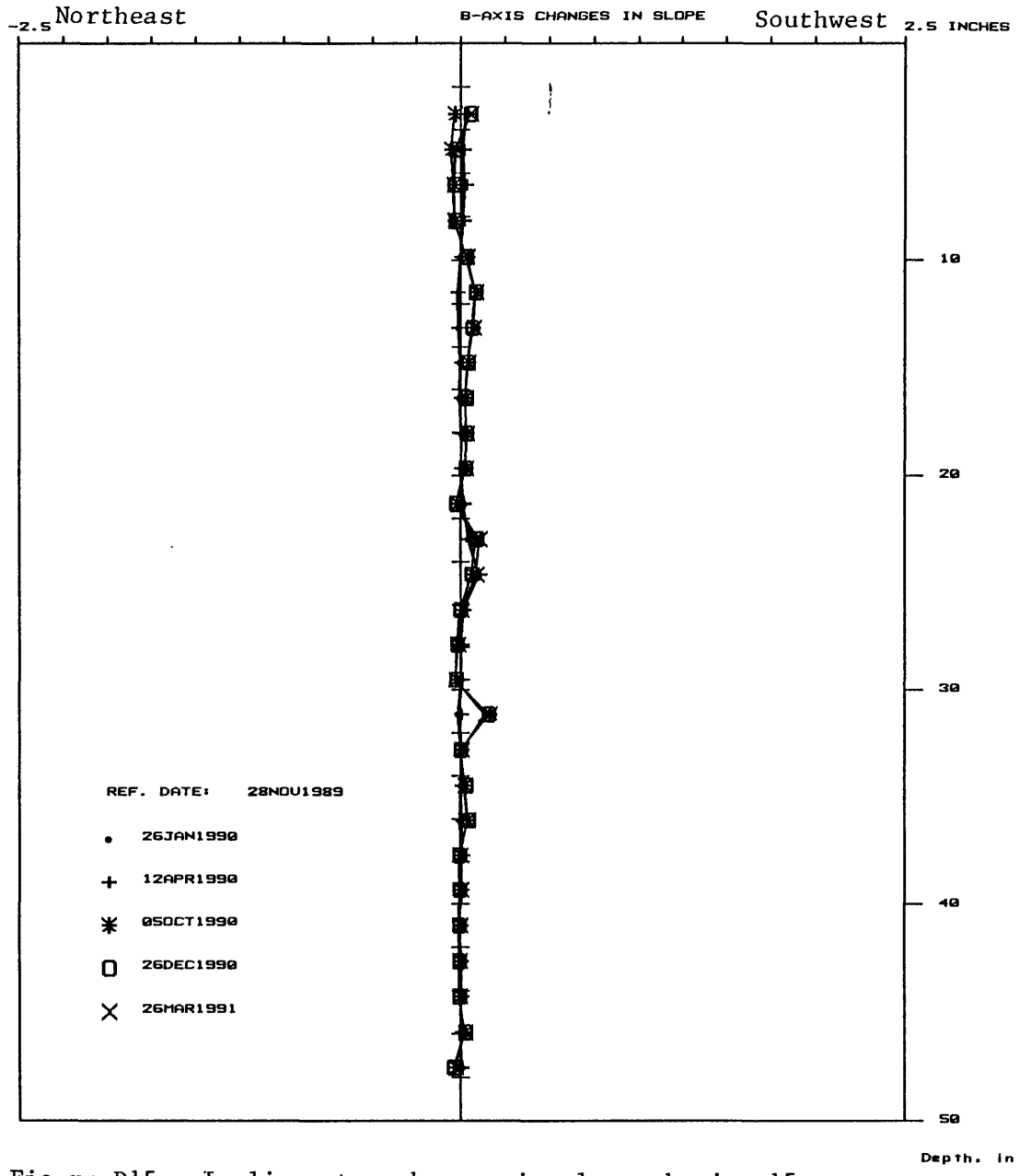

Figure D15. Inclinometer changes in slope, boring 15

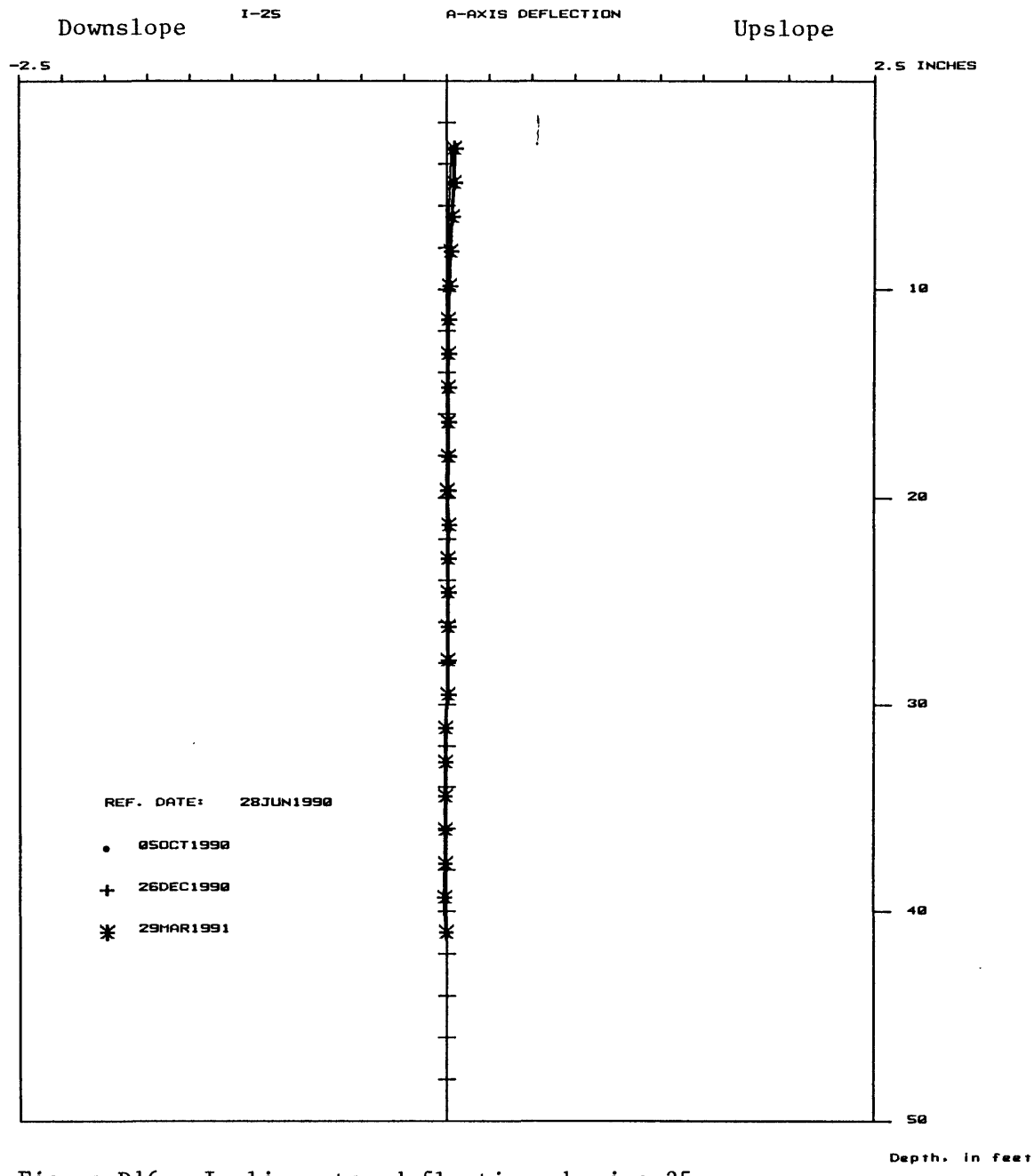

Figure D16. Inclinometer deflection, boring 25

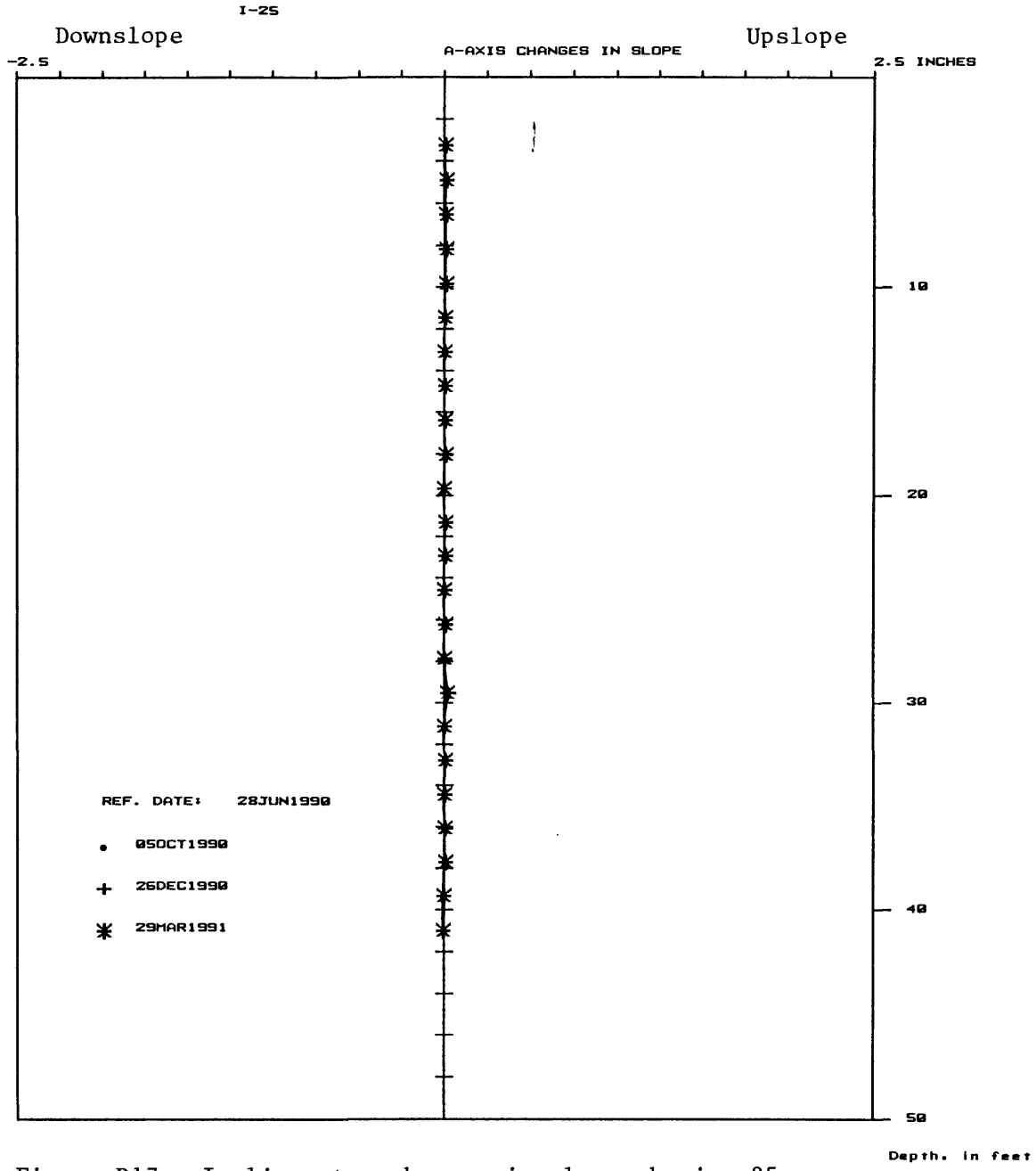

Figure D17. Inclinometer changes in slope, boring 25

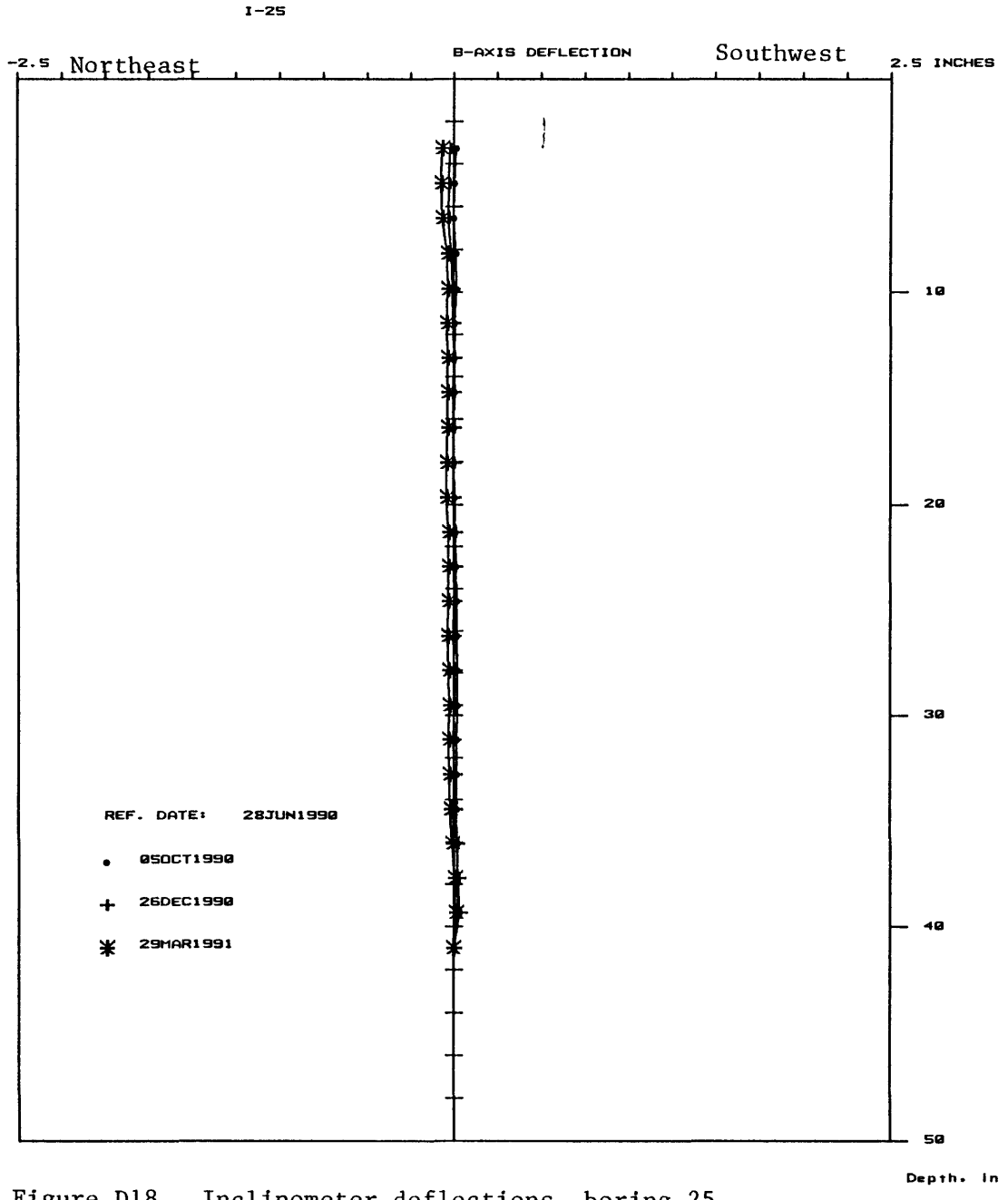

Figure D18. Inclinometer deflections, boring 25

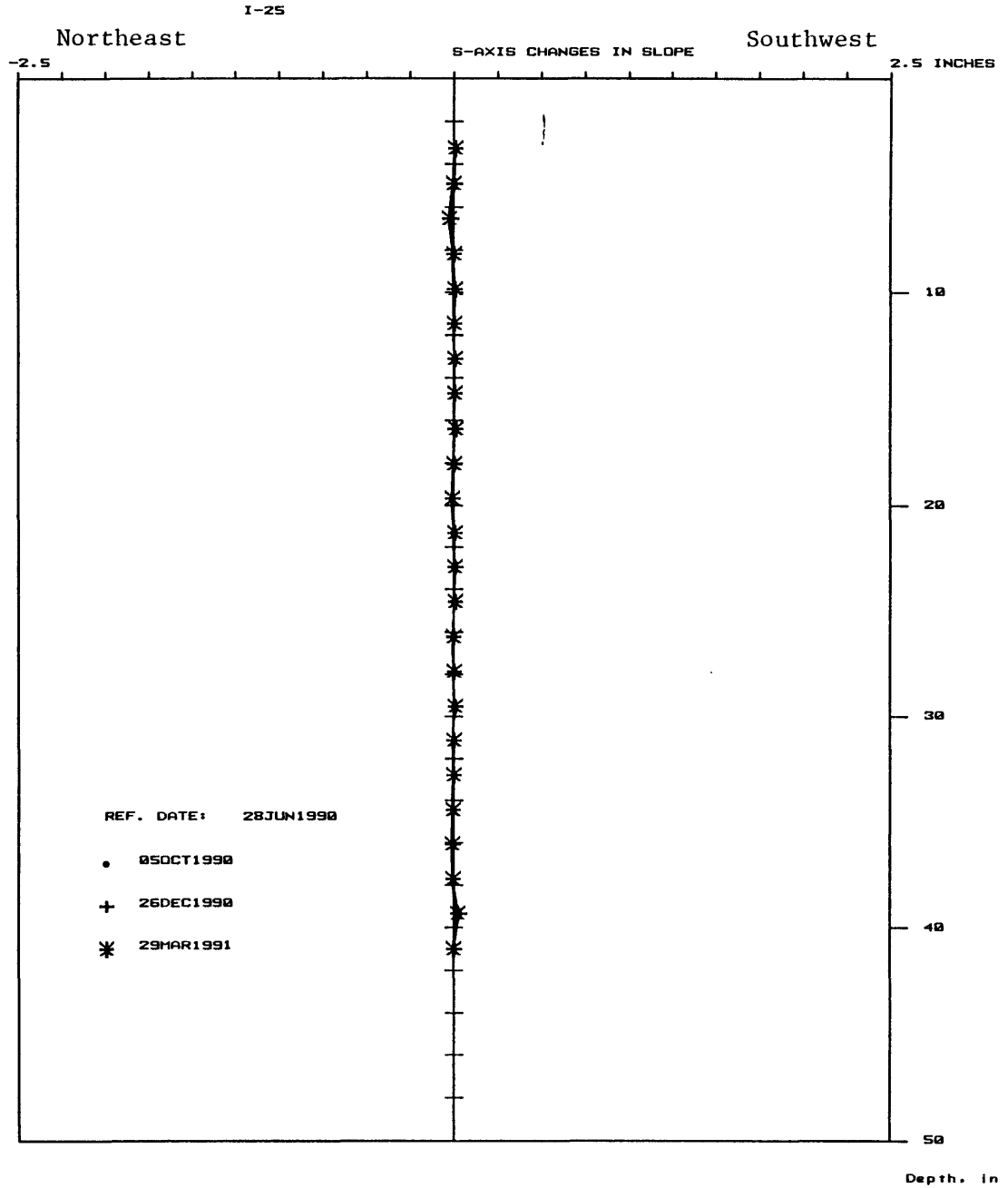

Figure D19. Inclinometer changes in slope, boring 25

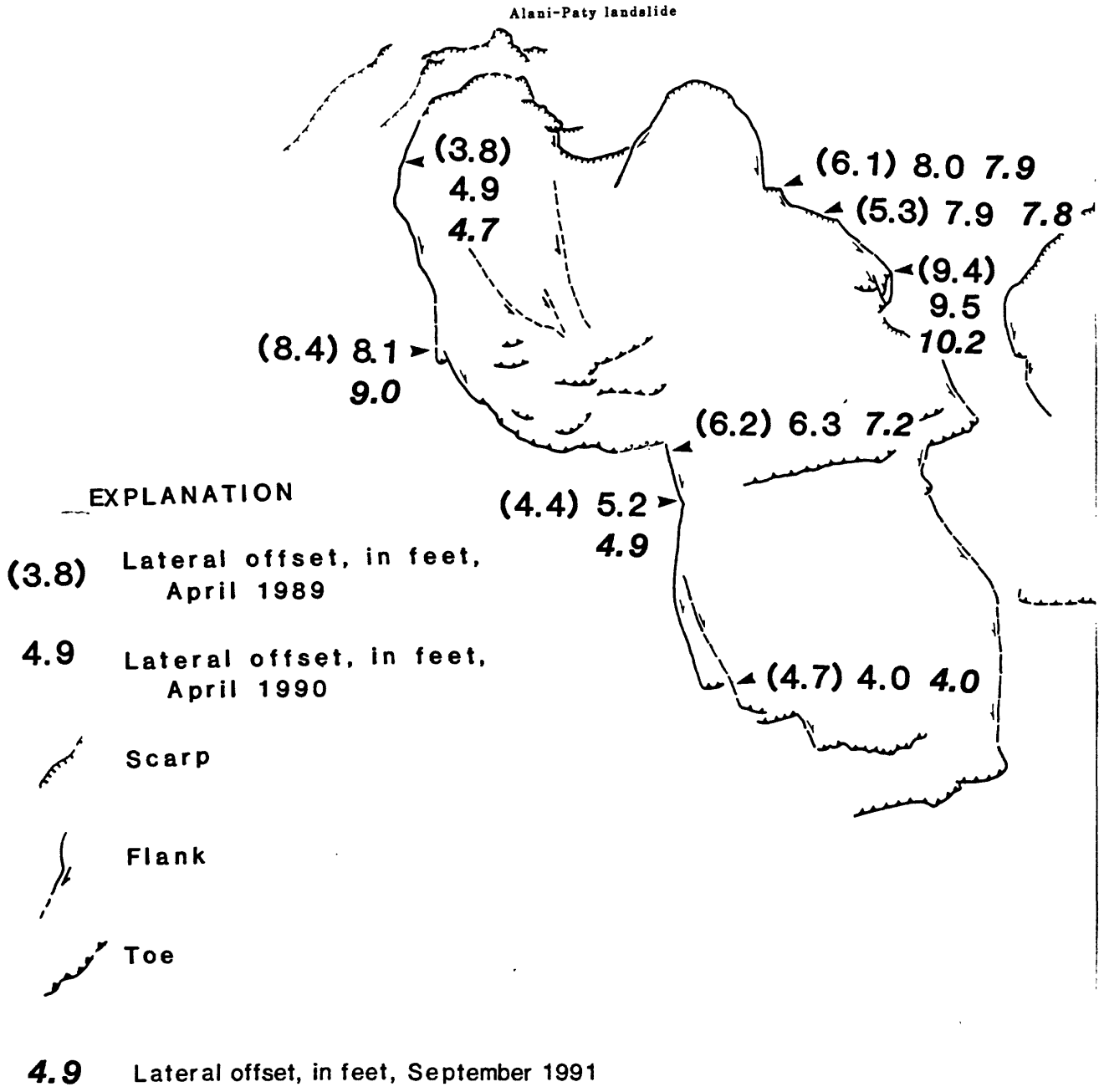

Figure D20. Map showing lateral offsets of curbs and stone walls at boundaries of the Alani-Paty landslide. Base (map of landslide boundaries) from Baum and others (1989).

APPENDIX E

Hydraulic conductivity

We determined the in-situ hydraulic conductivity of saturated earth materials in and near the Alani-Paty landslide by analyzing water-level responses of piezometers to known hydraulic stresses. We conducted and analyzed "slug" tests on several of our open-tube piezometers and we analyzed the slow recovery following initial drilling on some of our other piezometers. Slug tests were performed during the relatively dry month of June 1991. No tests were performed on piezometers with tips in unsaturated materials.

Field procedures -- Each open-tube piezometer that was tested consists of a 1-in.-diameter PVC pipe with a 6-in.-long porous ceramic tip, placed in a 4-in.-diameter borehole. The tip is surrounded by a sand pack, from 1 to 2 ft thick, that is sealed above and below in the borehole with a bentonite layer, also from 1 to 2 ft thick (Baum and others, 1990, p. 58). Prior to each slug test, we placed a small-diameter pressure transducer in the piezometer casing below the water surface. We recorded the water pressure at one minute intervals for at least several hours following transducer submergence to allow the water level to re-equilibrate and to identify any trends in the water level response caused by other hydraulic stresses. The transducer can measure pressures ranging from 0 to 6 lbf/in.^{2}; a Campbell Scientific Inc., model CR10 datalogger was used to record the pressures. After the water level had stabilized, we quickly added about 15 in.^{3} (250 ml) of water to the piezometer casing and recorded the transducer pressure response at 15 second intervals until the elevated pressure decreased substantially. For the piezometers with slow recovery following drilling, we measured water levels in the piezometer casing at irregular intervals for several months after drilling. This data is shown in Appendix B.

Analysis methods -- We used the method described by Bouwer and Rice (1976) and Bouwer (1989) to analyze both the slug tests and the drilling recovery tests. This method can be used to determine hydraulic conductivity in confined or unconfined aquifers with fully or partially penetrating wells. Using this method,

$$K = \frac{r_c^2 \ln(R_e/r_w)}{2L_e} \frac{1}{t} \ln\frac{y_0}{y_t}$$

where:
K = saturated hydraulic conductivity
r_c = radius of well
R_e = effective radius over which the hydraulic stress is dissipated
r_w = radius of borehole
L_e = length of tip
y_0, y_t = pressure displacement at time = 0 and time = t
t = time.

Our slug tests affect only the area near the piezometer tip and the materials there are stratified and at least partially confined. Therefore, we

assume that the tip fully penetrates the strata being tested (so L_e equals both the thickness of the water table and the aquifer). Given this assumption,

$$\ln(R_e/r_w) = \left(\frac{1.1}{\ln(L_w/r_w)} + \frac{C}{L_e/R_w}\right)^{-1}$$

where L_w is the height of the water table above the piezometer tip. C is a shape factor, in this case it equals 0.75. Thus for all piezometers, r_c = 1.25 cm; r_w = 5 cm; L_e = 15 cm; $\ln(R_e/r_w)$ = 0.799; and L_w = 15 cm. The results obtained using this method are very similar (within a factor of two) to those obtained using Hvorslev's piezometer method described in Freeze and Cherry (1979, p. 339-341).

Example -- Figure E1 shows the pressure response to an added slug of water in the shallow piezometer in borehole 9. A semi-log plot of the displacement from the initial pressure is shown in Figure E2. The straight line portion of this plot can be used to evaluate $(1/t)\ln(y_0/y_t)$; in this example it equals 1.5 X 10^{-5} cm/s. Thus, using the parameters above, K = 6.2 X 10^{-7} cm/s (1.8 X 10^{-3} ft/day).

Results -- Table E1 lists the saturated hydraulic conductivities determined from the open-tube piezometers. These values represent an estimate of the saturated hydraulic conductivity near the borehole at the tip depth.

Figure E1. Graph showing response of water level in boring 9 to the sudden addition of water during a slug test.

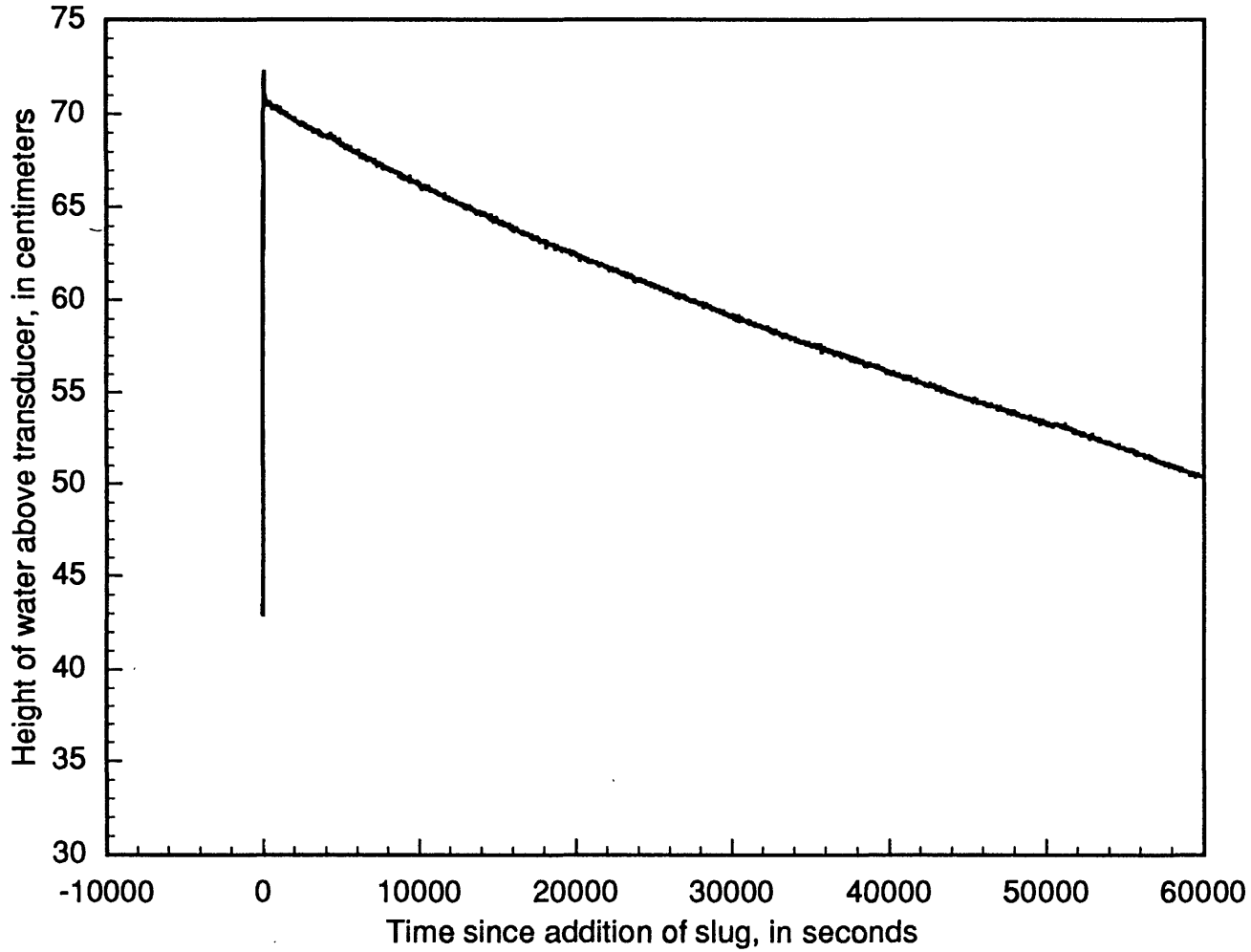

Figure E2. Graph showing displacement of the water level from its original position during the slug test in boring 9.

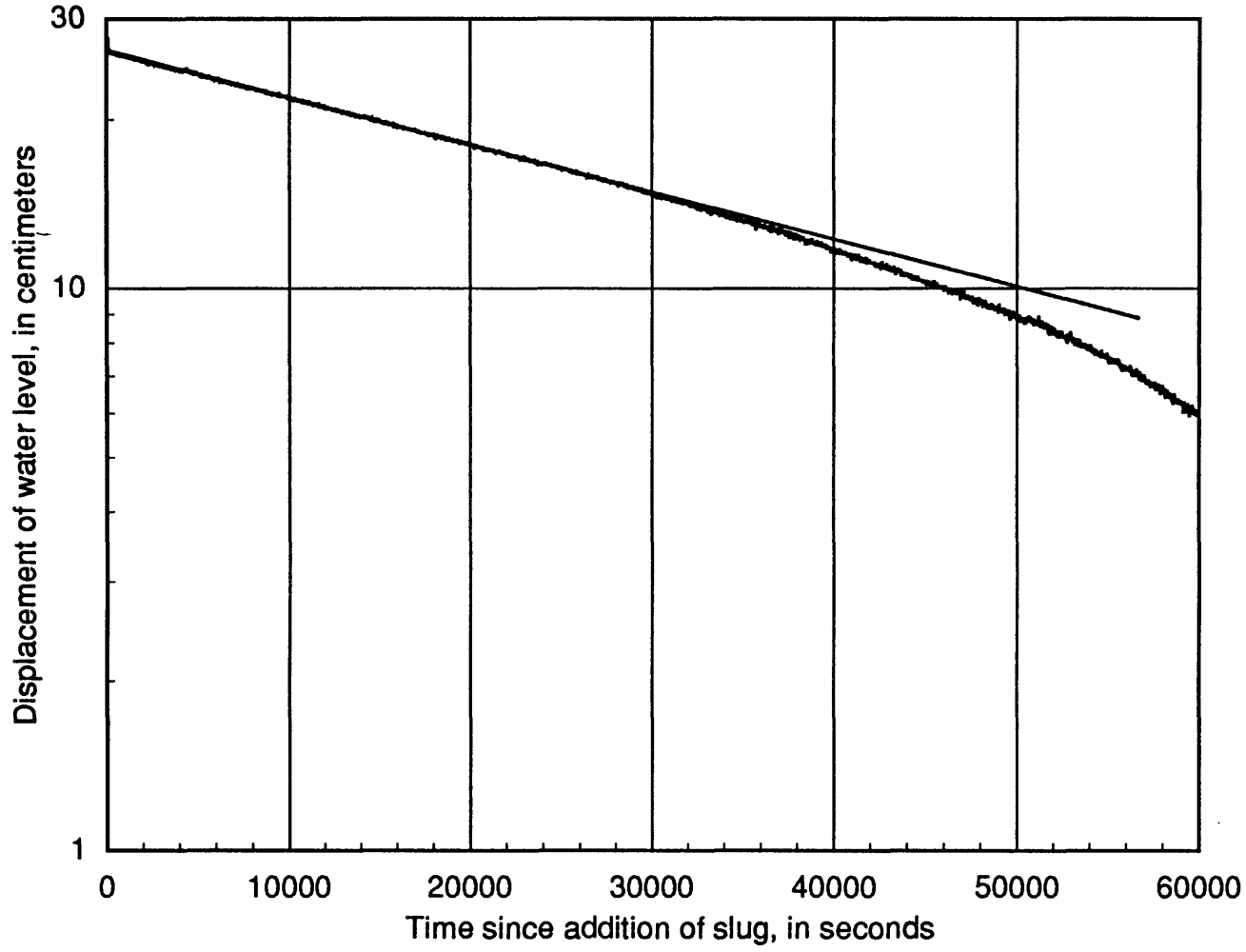

Table E1. Hydraulic conductivity of materials in and near the Alani-Paty landslide as determined from slug tests and recovery of water levels following drilling

Boring	Depth to tip (ft)	Test Method S = slug test R = recovery from drilling	K (cm/s)	K (ft/day)
1	13.2	S	4.2×10^{-6}	1.2×10^{-2}
1	25.5	S	1.5×10^{-5}	4.3×10^{-2}
3	30.0	R	3.8×10^{-9}	1.1×10^{-5}
4	20.2	S	5.0×10^{-8}	1.4×10^{-4}
7	37.3	S	1.3×10^{-6}	3.7×10^{-3}
9	8.6	S	6.2×10^{-7}	1.8×10^{-3}
9	25.1	R	4.8×10^{-9}	1.4×10^{-5}
12	18.0	S	1.8×10^{-6}	5.1×10^{-3}
13	12.0	S	2.5×10^{-5}	7.1×10^{-2}
14	9.4	S	1.4×10^{-6}	4.0×10^{-3}
14	21.9	R	1.7×10^{-8}	4.8×10^{-5}
16	20.7	R	1.7×10^{-8}	4.8×10^{-5}
19	14.4	R	1.4×10^{-7}	4.0×10^{-4}